MATURATION OF THE HEART: THE ROLE OF PGC1 IN CARDIOMYOCYTE MATURATION AT THE SINGLE CELL LEVEL

by
Sean Murphy

A dissertation submitted to The Johns Hopkins University in conformity with the requirements for the degree of Doctor of Philosophy

Baltimore, Maryland
February 2021

Abstract

Stem cells can be efficiently differentiated into cardiomyocytes for use in disease modeling and therapeutics. However, their development does not progress beyond the late embryonic stage when cultured in the dish. To identify regulators of maturation, we used large-particle sorting and single cell RNA-seq to analyze cardiomyocytes from neonatal to adult mice. Analysis predicted PGC1α as a top target. A conditional mosaic knockout was used to determine the cell autonomous effect of PGC1. PGC1 is both required for cardiomyocyte maturation and is able to promote stem cell-derived cardiomyocyte maturation in vitro. An siRNA screen found that YAP1 and SF3B2 mediate the effects on maturation through regulating hypertrophic growth and calcium handling. This work provides insights into the complex gene regulatory network behind cardiomyocyte maturation.

Thesis Readers

Dr. Chulan Kwon (Primary Advisor)
Associate Professor
Department of Cardiology
Johns Hopkins University

Dr. David Kass (Chair)
Professor
Department of Cardiology, Biomedical Engineering
Johns Hopkins University

Dr. Leslie Tung
Professor

Department of Biomedical Engineering
Johns Hopkins University

Dr. Kenneth Boheler
Professor
Department of Biomedical Engineering
Johns Hopkins University

Dr. Deok-Ho Kim
Associate Professor
Department of Biomedical Engineering
Johns Hopkins University

Dedicated to my grandfather.

He taught me that anything is possible.

Acknowledgements

First and foremost, I would like to express my deepest appreciation for my thesis advisor, Dr. Chulan Kwon, for his guidance and kindness. It was a pleasure to work in an environment that fosters creativity. I would like to thank Dr. Leslie Tung for mentoring me in my first rotation and the rest of my PhD study. I thank Dr. Kass for his support and insightful conversations. I would like to thank Dr. Kenneth Boheler for his encouragement along the way. I thank Dr. Deok-Ho Kim for collaborative effort and probing questions. This work would not have been possible without help from my collaborators Dr. Alex Colas and Dr. Anais Kervadec. I am appreciative of Dr. Dong-ik Lee for believing in me and guiding me through the PhD process.

The support of members from the Heart Generation and Regeneration Lab was invaluable to this work. I am grateful to Sandeep Kambhampati and Danielle Rigau who were excellent students that greatly contributed to this work. I am particularly thankful for Matthew Miyamoto's contributions, which were innumerable, and his wisdom. I received outstanding support and mentorship from the senior members of the Kwon Lab. Dr. Peter Andersen was instrumental in planning this work and troubleshooting along the way. Dr. Emmanouil Tampakakis provided critical support with experimental design and execution. I am extremely thankful for Dr. Hideki Uosaki's commitment to training me and patience. Dr. Renjun Zhu was crucial in thinking through the data and providing a new viewpoint. I am grateful for the opportunity Dr. Gunsik Cho gave me in allowing me to join his study and learn to analyze single cell RNA-seq data. I would like to thank Suraj Kannan for helping with

the single cell RNA-seq work. Brian Lin was essential in teaching me the langendorff isolation and assessing dissociated CMs.

Finally, I wish to thank my family and friends for their support. My parents, Michael and Annette, have always been supportive of my dreams. Jackson, my brother, was helpful in overcoming challenges and even helped out in the lab for a week while visiting Baltimore. I would like to thank others who were supportive including Gus, Bill, Max, Carly, and Gerry.

Contents

List of Tables

List of Figures

Chapter 1

Introduction

Clinical Significance

Heart disease is the leading cause of death worldwide.[1] Heart failure can result from a slide in global heart function following myocardial infarction. Up to 25% of heart muscle can be lost in an ischemic event.[2] While diet and exercise changes along with cholesterol-reducing statins can lower the risk of an arterial blockage, the heart is not a regenerative organ.[3] Over the course of 6 weeks, the infarcted region will have an inflammatory response that activates myofibroblasts to secrete collagen and form scar tissue.[4] This heart remodeling can lead to thinning of the wall and dilation of the heart in an effort to maintain blood flow to other organs.[4] There is a clinical need for replacing the lost beating heart muscle. One method of cardiac regeneration is to grow cardiomyocytes in vitro then graft them into the heart as single cells or an engineered heart tissue patch.[5] However, pluripotent stem cell-derived cardiomyocytes (PSC-CMs) are immature leading to arrhythmias.[6]

Another application of PSC-CMs is in drug discovery and pharmacological testing. Drugs in development are flagged for possible off target effects on cardiomyocytes.[7] However, the primary test for this is in animal models, which differ from human CMs. For example, the mouse has a resting heart rate 10x that of humans and lacks key ion channels.[8] In addition, the predominant isoform for key contractile proteins is

different. In the past, drugs have been falsely rejected that have no effect on the human heart and drugs have passed screening that did have effects on heart function.[4] Therefore, there is a need for a screening method that accurately predicts how a drug will affect human cardiomyocytes.[9] Organoids and engineered heart tissues provide a platform for testing, but immature PSC-CMs may create false positives. Maturation is an obstacle limiting the translational potential of PSC-CMs.

Stem cell-derived cardiomyocytes

Pluripotent stem cells have been derived from embryonic origin. More recently, it was found that somatic cells, such as dermal fibroblasts, can be reprogrammed into pluripotent stem cells (iPSC).[10] Both types are able to differentiate into endodermal, mesodermal, and ectodermal lineages.[11] Cardiomyocytes were initially found to be present in embryonic cell aggregates called embryoid bodies at very low levels.[2] PSCs can be efficiently differentiated by sequentially treating PSCs with recombinant protein cytokines that were found during heart development.[2] Further, small molecule differentiations have been found to yield 90%+ differentiations by activating and inhibiting the Wnt pathway.[3]

Development and Maturation

Embryonic heart development

In development, the heart is the first organ to form and grows from two populations, the first and second heart field.[10] These mesodermal progenitors begin looping and form four separate chambers at E8.5 and E14.5, respectively. The CMs have already committed to their cell fate by E10.5, but they are unlike their neonatal and adult selves. Maturation is the individual cell transformation where cardiomyocytes undergo morphological, functional and transcriptomic changes.[12] Here, I will describe the

various hallmarks of maturation.

Morphology

PSC-CMs are visibly different from adult CMs. As CMs mature, they increase in volume 30-40 fold, elongate into a rectangular structure.[13,14] The sarcomeres are parallel to each other and align with the long axis of the CM. Transverse-tubules form as invaginations of the plasma membrane to allow the action potential to synchronous calcium release and contraction in the cell.[15,16] PSC-CMs on the other hand are highly variable in shape as they are more circular with misaligned sarcomeres and do not have T-tubules.[17] Part of this may be due to in vitro culture of PSC-CMs on a flat rigid surface.[18,19]

Intercalated discs

In vivo CMs form connections with neighboring CMs to improve force and action potential conduction.[20] The CMs are electrically coupled through gap junctions made from Connexin 43, which allows ions to travel between cells.[21] The intercalated discs also have desmosomes to link intermediate fibers with other cells and fascia adherens to connect sarcomeres. In PSC-CMs, Connexin 43 is distributed around the cell membrane rather than in punctate dots at the ends of adult CMs.[22] This leads to a lack of anisotropy in conduction velocity.[23]

Electrophysiology

PSC-CMs spontaneously contract, while adult CMs do not usually contract without stimulation. The beating rate is generally 40 beats per minute and is attributed to expression of the funny channel *HCN4* which leaks sodium current.[24] This may also be caused by spontaneous calcium release that results in depolarization as sodium flows in through the calcium-sodium exchanger. The resting membrane potential

in PSC-CMs is often between -50 to -60 mV, which is higher than mature CMs at -90 mV.[14] All of these combine to form an abnormal action potential shape when compared to adult CMs. The action potential shape can be quantified by a number of parameters including dV/dtmax, which is a measure of sodium influx speed and is lower in PSC-CM, and a shorter action potential duration (APD50) indicative of a shorter plateau phase. These changes may be due in part to downregulation of major ion channel expression including the inward rectifying potassium channels *KCNH2* and *KCNJ12*.[6] Differences in upstroke velocity may be caused by lower levels of the voltage-gated sodium channels SCN5A.[22] Patch clamping of PSC-CMs shows barely detectable levels of the slow delayed-rectifier potassium current, contributing to the lack of a plateau phase in the action potential.

Calcium Handling

Calcium plays a central role in excitation contraction coupling. Excitation-contraction coupling is the process linking a depolarization from an action potential to sarcomeric shortening through opening of voltage-sensitive L-type calcium channels, located in the t-tubules, to allow calcium to flow into the cell.[25] This calcium influx leads to a calcium induced calcium release of the calcium in the sarcoplasmic reticulum through ryanodine receptors. The cytosolic calcium then binds troponin-C, a subunit of troponin, that leads to a conformational change in troponin moving the tropomyosin and allowing the myosin head to bind the actin pulling the sarcomere z-bands together.[22] The calcium is then pumped into the sarcoplasmic reticulum through *SERCA2A* and out of the cell allowing relaxation of the sarcomere. The intracellular calcium concentration can be measured by fluorescent video imaging of a calcium-sensitive dye to construct a trace of the calcium transient. PSC-CMs have both slower release and reuptake of calcium. In addition, PSC-CMs are often insensitive to drugs that alter SR release and uptake. This may be caused by dysregulation of calcium handling gene transcription

as calsequestrin and phospholamban are present at low levels.[26]

Contractility

Adult human cardiac myocytes produce 44 mN/mm^2 peak twitch force.[6] PSC-CMs contract with less than 1% of this force. Neonatal rat ventricular myocytes produce similar amounts of force. Engineered heart tissues (EHTs) have been shown to generate nearly 13 mN/mm^2 of this after long term culture with mechanical and electrical stimulation.[27] The length of a relaxed, adult sarcomere is 2.2µm while PSC-CM sarcomeres are 1.7 µm.[28] The contractile immaturity may be based on the expression of immature isoforms of titin, myosin light chain 2, myosin heavy chain, and troponin I. PSC-CMs also express non-myocyte genes including smooth muscle α-actin and vimentin.

Proliferation and multinucleation

Embryonic CMs divide as heart growth is driven by proliferation. In the perinatal window, they withdraw from the cell cycle and transition into hypertrophic growth. During this time, the majority of cells transition from mononucleated to multinucleated through DNA synthesis and nuclear division without cytokinesis.[29] Most human CM nuclei will become polyploid. Not much is known about what drives polyploidization, but it is possible that this and the loss of regenerative capacity may be related to thyroid hormone concentration.[30] Binucleation rate differs by species as 3 in 4 CMs are binucleated in rodents while only 1 in 4 CMs are binucleated in humans.[2] The heart is one of the least regenerative organs as CM proliferation in healthy and diseased hearts is very low. Maturation has been studied in multiple animals including sheep and swine. While the rates of development and maturation differ, the hallmarks are the same.[31]

Activating CM proliferation to induce cardiac regeneration could be a treatment

for ischemic heart disease. The proportion of mononuclear CMs is linked with the regenerative potential and is dependent on the background genetics, which varies greatly in different mouse strains.[32] Cell cycle withdrawal has been found to be regulated by many genes and pathways including microRNAs, hippo/YAP, ERBB2, PI3/Akt, cyclins, cyclin-dependent kinases, and inhibitors of cyclin dependent kinases. Metabolism has been linked to proliferation as changes in glucose and fatty acid concentrations in media alter $Ki67^+$ cells. Oxidative DNA damage may drive cell cycle exit in CMs as this coincides neonatally with increased oxygen levels. Exposing mice to hypoxic conditions has been shown to produce a regenerative response.[33] Overexpression of cell cycle regulators CDK1, CDK4, cyclin B1, and cyclin D1 in the mouse heart induced CM division.[34] PSC-CMs divide frequently during differentiation and are able to divide long after differentiation if cultured in vitro, but the rate of proliferation decreases from 30% to less than 5% of cells. PSC-CMs can continue to proliferate if they are cultured at low densities with Wnt modulation.[35]

Metabolic maturation

Immature CMs primarily use glucose as their source of energy, but transition to fatty acid postnatally due to an increase in energy demand and oxygen levels.[36] Glycolysis produces 2 ATP molecules per glucose, while fatty acid β-oxidation of palmitate can generate 129 ATP molecules.[37] The majority of the ATP is used for contractile function with the next largest sink being SERCA and other ion pumps. Mitochondrial density expands rapidly and they change morphology by becoming oval shaped and increasing in size.[38] The mitochondrial permeability transition pore is open in fetal myocytes. While an open state in adults drives apoptosis by leaking cytochrome c in adult mitochondria, it lowers the mitochondrial membrane potential in fetal CMs and lowers their ability to perform oxidative phosphorylation.[39] In addition, cristae become very dense in adult CMs compared to the low density of cristae. This density

is directly related to the capacity for respiration. PSC-CMs resemble fetal myocytes in their reliance on glycolysis and mitochondrial ultrastructure.[38]

Methods of improving maturation

Microenvironment

Many microenvironmental strategies have been applied to PSC-CMs to improve maturation. One has been to culture PSC-CMs on a deformable surface. This allows the culture surface to match the stiffness of the in vivo heart (10 kPa) as rigid cell culture plastic is very stiff (1 MPa).[29] Polyacrylamide, PDMS, or hydrogels that can be tuned to a specific Young's Modulus. This allows PSC-CMs to become more rectangular and mature.[40] A theme of many of these approaches is to create biomimetic solutions to recreate an in vivo environment. Specific extracellular matrix (ECM) molecules are also regulators of maturation as Laminin-511/521 potently enhances CM maturation aspects including increased maximal respiration and binucleated cells.[41]

Electrical and mechanical stimulation stimulation

In the heart wall, CMs are electrically stimulated and subjected to stretching. Culture systems have been set up to mimic these conditions in vitro. A 3D self organized tissue ring was designed to allow the action potential to propagate around the ring repeatedly with the goal of maturing myocytes.[42] Others have used a micropillar electrode array to mature cardiac spheroids.[43] it has been shown that introducing electrical stimulation during differentiation can increase the proportion of conduction system cells.[44] Electrically conductive extracellular materials added to engineered heart tissue patches improve maturation with better alignment of sarcomeres and the formation of an initial intercalated disc.[45]

Mechanical stimuli is translated to changes in cell morphology and gene expression

through mechanotransduction. Cyclic stretching leads to elongation and more CMs with a rod-like shape.[25] Mechanical stress results in improved contractile properties and an increase in expression of β-myosin heavy chain and cardiac troponin T.[12] It has been proposed that hypoplastic right ventricle congenital heart disease is due to a defect in maturation during development.[46]

Hormone treatment and biochemical cues

Treatment with hormones has been shown to improve maturation. Specifically triiodothyronine (T3), which binds the thyroid hormone receptor, and dexamethasone, which binds the glucocorticoid receptor, promote morphological maturation in addition to functional aspects. Using a combination of these, a team was able to see t-tubule formation in PSC-CMs when also cultured on a matrigel mattress.[47] One-week of treatment with T3 was able to increase CM size, sarcomere length, cyclin-dependent kinase inhibitor p21 expression, contractile force, and mitochondrial respiratory capacity.[48] Knockout of the thyroid hormone receptor leads to immature myocytes that are proliferative in response to injury.[30] Recent efforts have confirmed the role of dexamethasone in maturation and found that it acts by promoting mitophagy leading to lysosomal aggregation in mitochondria. By blocking mitophagy, they were able to negate the effects of dexamethasone on CM maturation.[49] Retinoic acid has also been found to promote maturation, specifically increasing mitochondrial DNA copy number, electrophysiological parameters, oxidative phosphorylation, and calcium handling.[50] Retinoic acid binds to the retinoic acid receptor (RAR) which heterodimerizes with PPAR family members. Pharmacological inhibition of centrosomes was able to prevent cell division pushing PSC-CMs towards a matured state.[51] Other soluble factors may promote CM as blocking excretion of these from the placenta resulted in less mature myocytes.[52] It is clear that nuclear receptors activated by hormones play a crucial role in maturation.

Co-culture

Others have looked into the co-culture of PSC-CMs with fibroblasts, endothelial cells (ECs), smooth muscle cells, or neurons since these cell types are present in the heart. CMs make up 80% of the volume, but roughly 30% of the cells by number.[53] The non-myocytes can secrete growth factors like VEGF and bFGF, which improve differentiation and function. They can also alter the ECM to deliver microenvironmental cues to CMs.[23] 3D culture systems often put together a combination of these factors by creating an engineered heart tissue between two deformable posts. Fibroblasts are added to provide structure and the systems allow for electrical pacing. Single cell RNA-seq analysis of fibroblasts in the developing mouse heart showed they have stage specific subtypes and influence CM maturation by modulating the microenvironment.[54]

Giacomelli and colleagues constructed 3D microtissues using CMs, fibroblasts and ECs. They found that PSC-CMs formed t-tubules, with improved contractility, respiration, and action potential parameters.[55] They proposed that this occurs through the coupling by Connexin 43 gap junctions and higher intracellular cyclic AMP levels. Co-culture with sympathetic neurons results in improved maturation of both cell types. The neurons are able to couple and modulate the beating rate as they do in vivo. The sympathetic neurons were differentiated from PSCs and could be optogenetically excited.[56]

Altering metabolism

Many of these pathways have been shown to be interconnected and tied to metabolic maturation.[57] Most culture media contains a high concentration of glucose. However, recent studies have shown that low glucose, fatty acid-rich media promotes maturation.[58] This is seen in vivo as postnatal CMs switch from glycolysis to fatty acid oxidation as their primary source of energy. These studies added oleic acid, carnitine, linoleic acid, and palmitate and saw a switch of energy source, mitochondrial

number, and structural maturation.[59,60] Conversely, the high levels of glucose in normal media was shown to inhibit CM maturation.[39] In vivo, the reduction in glucose uptake begins in late gestation and it was found that glucose promotes nucleotide biosynthesis via the pentose phosphate pathway.[61] The mitochondrial permeability transition pore can be closed using cyclosporine A to induce mitochondrial maturation.[62] PSC-CMs matured with a medium containing oxidative substrates was able to improve PSC-CM function in modeling long QT syndrome and dilated cardiomyopathy.[63]

In vivo transplantation

The only method that has yielded mature myocytes has been the in vivo transplantation.[64] Our group has shown that mouse PSC-CMs injected into the neonatal rat heart leads to mature myocytes 1-2 months later. However, if they are injected in the adult or later postnatal hearts, they do not fully mature. This could indicate that there is a critical window where microenvironmental or biochemical cues instruct CMs to mature. This was not confirmed by the other study of in vivo transplantation that saw mature myocytes form in adult hearts.[65] However, that study focused on morphological and immunostaining of myofilament proteins that switch isoforms rather than functional endpoints. Initial studies indicate that species matching is required as human PSC-CMs injected into the macaque heart matured, but human PSC-CMs injected into rat hearts remained immature. One drawback from this is that it is extremely low throughput yielding hundreds of mature CMs. This is due to the size of the rat heart and low engraftment of injected PSC-CMs. The largest conclusion is that it is possible for PSC-CMs to become fully mature. Injecting PSC-CMs into adult athymic rats and subsequent single cell RNA-sequencing showed upregulation of mature gene markers and pushed the cells toward ventricular phenotypes.[66]

Combination approaches

Since multiple biochemical factors have been shown to promote maturation, it was found that a combination of T3, dexamethasone and insulin-like growth factor-1 improved multiple aspects of maturation although not synergistically.[67] A similar study combined microgroove alignment with T3 and electrical pacing finding that some microenvironmental stimuli can prime CMs for other biochemical cues to enhance maturation.[68] One study seeded single PSC-CMs into a rectangular scaffold and results indicated that transcriptomic and functional calcium handling changes occurred.[69] Exposing PSC-CMs to pulsatile hemodynamic forces improves by maintaining oxygen levels and mimicking blood flow.[70]

PSC-CMs can be aggregated into engineered heart tissue (EHTs) and organoids to better model the myocardium. In a combination of electrical and mechanical stimuli from C-Pace IP from Ionoptix and a custom PDMS channel to create cyclic stretch, LaBarge *et al.* found that PSC-CM spheroid maturation was promoted after 7 days of stimulation compared to unstimulated spheroids.[71] Using cardiac organoids made from PSC-CMs in a 96-well format, Mills and colleagues screened growth factors, metabolic substrates, and ECM to optimize CM maturation.[72] While all of these have improved maturation, none have produced adult-like myocytes that can match the force production and lack of spontaneous beating.

Transcriptomic maturation

CM maturation encompasses differential expression of thousands of genes. There are multiple isoforms of contractile proteins with each being associated with skeletal or cardiac muscle and fetal or adult stages. Troponin I is a contraction regulatory protein that is responsible for sensing calcium and allowing myosin to bind actin in the excitation-contraction coupling. Embryonic cardiomyocytes express the slow

skeletal muscle isoform in the *TNNI1* gene, but switch to expression of the cardiac isoform *TNNI3* after birth.[25] This change is conserved in rodent and human hearts. This isoform switch has functional consequences as *TNNI3* leads to increased tension and has different calcium affinity. Myosin heavy chain, a motor protein, also has an isoform switch. In humans, the alpha isoform *MYH6* is expressed fetally and the beta isoform *MYH7* is expressed in adults. However, this switch is the opposite in rodents as they express *MYH6* in the adult heart which leads to faster activity and binding which is required as their heart rate can reach 800 beats per minute. In addition to temporal specific switches, there are spatial changes as myosin regulatory light chain 2 (*MLC2*) has isoforms associated with atrial and ventricular CMs. These myofilament protein expression changes and are partially captured in PSC-CM long term culture. Forced expression of the adult form of cardiac troponin I in PSC-CMs was able to promote CM maturation by altering relaxation kinetics.[73] While the cellular identity of cardiomyocytes does not change, there is a shift in the transcriptomic signature.

Gene regulatory network of maturation

The use of high throughput sequencing has begun to characterize the gene regulatory network (GRN) of maturing myocytes. This has been focused on identifying critical proteins required for CM maturation through knockout screens. A landmark study in the field used a meta-analysis of more than 200 microarray datasets to build a study of mouse heart development and maturation from early embryonic stages to adult hearts. This identified predicted upstream regulators and the temporal dynamics of key pathways.[74] Mechanical forces are known to regulate CM maturation so Fukuda *et al.* looked into the mechanism of how cells translate mechanical stimuli into transcriptional changes. They found that vinculin is essential for maturation and recruits slingshot protein phosphatase SSH1 and actin depolymerizing factor cofilin to regulate myofilament maturation.[75,76] mTOR-signaling pathway has been shown

to promote maturation by increasing expression of p53 to push CMs into a quiescent state.[77] Treated PSC-CMs showed better contractility with improved mitochondrial capacity.

Multiple factors have now been implicated in the regulation of CM maturation. The Estrogen-Related Receptor (ERR) has been identified as a nuclear receptor required for maturation.[78] Knocking out ERR in vivo was perinatally lethal with CMs showing arrested maturation. ERR was found to regulate key maturation genes by suppressing those associated with fibroblasts and directly activating cardiac contractile machinery genes. The maturation of the mitochondria, corresponding to an increase in size and cristae density, was found to be regulated by BUD23-dependent ribosome generation.[79] Knocking out BUD23 led to cardiomyopathy and death due to lower mitochondrial function. In a study of regeneration, it was found that Meis1 is a cofactor of Hoxb13. They are regulated by calcineurin, a calcium-activated phosphatase, and control genes involved in CM maturation, hypertrophy, and cell cycle progression.[80]

In vivo postnatal maturation was elegantly probed through the use of the CRISPR/Cas9-AAV based somatic mutagenesis (CASAAV) system to generate a mosaic knockout in a fraction of the cells to prevent effects on CMs associated with global heart dysfunction. CASAAV uses an AAV9 vector to introduce guideRNAs targeting the gene of interest for loss of function into a Cre-inducible Cas9-GFP for somatic mutagenesis.[81] Serum response factor (SRF), which had previously been shown to be required for maturation using a conditional knockout, was found to regulate T-tubule formation, cell size, and sarcomere ultrastructure.[82] Interestingly, knockout of SRF in the adult heart did not result in the same changes suggesting SRF is required for a stage specific maturation, but not maintenance of adult function. This study did not investigate whether SRF activation promoted maturation of PSC-CMs. This technique was also applied to build an in vivo CRISPR genetic screen in the mouse heart. A library of guideRNAs was to create a high throughput, low animal method for assessing the relevance of

genes to CM maturation. Among the top hits were RNF20 and RNF40. They found that these were epigenetic transcriptional regulators of key genes for CM maturation.

Single cell RNA sequencing of cardiomyocyte maturation

Time series analysis of single cell RNA-seq have provided insights into changes during maturation. This has been applied to PSC-CM differentiation where one study found HOPX to be a regulator of hypertrophy and is expressed in long term PSC-CM culture. They overexpressed HOPX in PSC-CMs and found that it increases cell size. While they identified a key regulator of PSC-CM maturation, it may be more important to study in vivo myocytes that actually become fully mature.[83] One of the first datasets generated of CM maturation was Delaughter *et al.*'s study of heart development. They used drop-seq on more than 1,200 cells from E9.5 to P21. However, the quality of reads and CM number after P3 sharply dropped off due to CM shearing in the microfluidics channels used to encapsulate cells in drop-seq.[84] Their study groups cells by spatiotemporal location and were able to use principal component loading to determine the maturation of PSC-CMs, which they showed were closest to E14.5 at 30 days of culture and E18.5 at one year of culture. Due to the limitations of sorting CMs, single nucleus RNA-seq has been used to study maturation. However, this lacks read depth and mitochondrial reads important to aspects of GRN reconstruction and cell signature determination.

Other methods have been developed to quantify the maturation state of PSC-CMs. Entropy, a measure of the distribution of reads among genes, can determine the maturation status as adult cells have reads more concentrated in a smaller number of highly expressed genes. Individual maturation markers including *Myom2* have been found that correlate highly with maturation and increase 8 fold from embryonic to adult stages.[74] Proteomics has been used to quantify the protein levels of specific maturation

markers such as MYOM1 and TMEM65.[85] Cell surface markers of maturation are particularly useful for sorting PSC-CMs using FACS. CD36, a fatty acid translocase, was identified as a marker of maturation that striated CMs by maturation status.[86] Machine learning techniques like random forest have been applied to characterize maturation state.

Chapter 2

Identifying upstream regulators of cardiomyocyte maturation

Background

Our strategy to improve PSC-CM maturation is to correct dysregulated gene expression by studying the expression patterns in the mouse heart. The goal is to characterize the gene regulatory network of CMs across multiple stages of development to see where PSC-CMs differ. Our group had previously generated a large meta-analysis data set that has been used to track gene expression from the early embryo to adult.[74] The study concluded that PSC-CM maturation is arrested at the late embryonic to early postnatal function. Therefore, we needed better temporal resolution and improved sequencing depth as they had used microarray which provides less reliable normalization. We intend to use gene regulatory network prediction algorithms to identify potential drivers of maturation.

Cardiac cell atlases

Other groups have generated large datasets looking into the maturation of CMs.[84,87,88] However, they usually focus on early development and formation of the heart or on the adult stage. Another problem is that CMs were sorted using conventional FACS or drop-seq, which is not suited to the large size of CMs. These datasets then have poor

cell survival as the sorting and isolation process leads to apoptosis and cell shearing.[84] We have recently shown that CMs can be successfully sorted and sequenced using large particle FACS.[89]

In this chapter, we sought to identify upstream regulators of CM maturation. To do this, I gathered public RNA-seq datasets spanning postnatal CM development. We used bioinformatic analyses to predict based on gene expression changes. To gain improved resolution, we used single cell RNA-seq to track the heterogeneous maturation of the mouse heart.

Materials and Methods

Collection of raw data

Datasets were selected using Gene Expression Omnibus (GEO) for cardiomyocyte or heart high throughput sequencing of timepoints in late embryonic, postnatal or adult stages in mice. Mouse embryonic stem cell-derived cardiomyocyte datasets were also collected. FASTQ or SRA files for each dataset were downloaded from the Sequence Read Archive or European Nucleotide Archive.

Mapping and Alignment

FASTQ file quality scores were assessed using FastQC.[90] Reads were trimmed using trimmomatic sliding window quality cutoffs to remove nucleotides with quality cutoff of 35. They were mapped to the mm10 genome using HISAT2.[91] Mapped reads were aligned to exons using RefGene using subRead featureCounts and output as a counts table.[92]

Differential expression, principal component, and pathway analysis

The counts table was imported into R for analysis using DESeq2.[93] Following size factor normalization, differential expression statistics were calculated. Principal component analysis was performed using a wrapped prcomp function on the rlogged, normalized counts. Ingenuity Pathway Analysis (IPA) was used to generate predicted upstream regulators using gene regulatory networks.[94] DAVID was used to assess KEGG enrichment and PantherGO with Revigo TreeView was used to visualize gene ontology terms.[95,96] Mitochondrial gene expression was visualized in a heatmap from with pheatmap.

Neonatal Cardiomyocyte isolation

For P0 cardiomyocyte isolation, the Miltenyi Biotec gentleMACS Dissociator was used with the neonatal mouse heart dissociation Kit. P0 mouse hearts were harvested and transferred into PBS on ice then pumped to wash out blood. Under a dissection microscope, blood vessels and connective tissue were removed. Enzyme mix 1 was incubated at 37 C for 5 minutes then 2362.5 µL were added to 127.5 µL of enzyme mix 2. The ventricles were placed in a gentleMACS C Tube and the supernatant was removed. 2.5 mL of the enzyme mix were added to the C Tube. The tube was tightened and then inverted and placed cap down in an incubator at 37 C for 15 minutes. The C Tube was placed on the sleeve of the gentleMACS Dissociation and the gentleMACS m_neoheart_01 program was run. The 15 minutes of incubation and program were repeated twice more. Afterwards, the C tube was detached and 7.5 mL of DMEM+10% FBS was added. The solution was then filtered through the pre-separation 70µmfilter and 3 mL of media were used to wash through any additional cells. The flow through was then centrifuged at 300 rcf for 15 minutes. The supernatant was aspirated then the cells were resuspended in the media.

Adult Cardiomyocyte Isolation

Mouse hearts aged P7 to P56 were isolated in this manner. A non-hanging langendorff perfusion was used to dissociate the hearts as previously described.[64] First, the mouse was anaesthetized with isofluorane. If they were unresponsive to a toe pinch, they were euthanized by cervical dislocation. The mice were not heparinized so the heart excision and cannulation was performed rapidly. The hearts were perfused with a digestion buffer for 6-9 minutes depending on the age of the mouse at 1.5 mL per minute to enzymatically degrade the extracellular matrix. The perfusion buffer contained 120 mM NaCl, 1 mM $MgCl_2$, 5 mM 2,3-butanedione monoxime (a non-selective myosin ATPase inhibitor), 5 mM Taurine, 5.5 mM glucose, 20 mM $NaHCO_3$, 5.4 mM KCl, and 1.2 mM NaH_2PO_4 which is then set to pH 7.4. The digestion buffer is 40 mL of the perfusion buffer with 2 mg Protease (Sigma P5147) and 35.8 mg Collagenase Type II (Worthington CLS-2). The ventricle was cut from the cannula and minced for 30 seconds using scissors in 10 mL of perfusion buffer. The mixture was pipetted vigorously up and down using a wide tipped plastic eye dropper to dissociate CMs. The mixture was filtered through a 100µmscreen to remove large chunks then centrifuged for 1 minute at 800 RPM in an Eppendorf 5702 centrifuge). It was resuspended in 10 mL of Tyrode's buffer with bovine serum albumin to stop the enzymes. CMs pelleted at the bottom by gravity over 10 minutes. The supernatant was removed and cells were resuspended in 10 mL of Tyrode's buffer in a small beaker.

Gene regulatory network analysis

Weighted gene co-expression network analysis was used to identify modules of co-expressed genes in CM maturation.[97]

Statistics

IPA generates a z-score for confidence of upstream regulator activation and a p-value for each factor. KEGG generated a q-value of for the enrichment of each term. Top terms were shown and ranked by q-value in figure 2-2.

Single cell sequencing

mcSCRB-seq was used to prepare libraries.[98] Cells were sorted directly into a 96 well U-bottom plate using the Union Biometrica COPAS-FP-500 LP-FACS. Each well contained 4 µL lysis buffer made of 411.4 µL ultrapure RNase-free water, 27.5 µL of 20 mg/mL Proteinase K, and 1.1 µL of 5x NEB HF Phusion buffer. Each well contained 1 µL of barcoded oligo-dT primer at 2 uM. Following sorting, they were sealed and placed directly on dry ice then stored at -80 C until library preparation. Plates were thawed at room temperature then spun down for 30 second at 1000 rcf. They were then placed in a thermocycler for 10 minutes at 50 C for Proteinase K digestion, then 80 C for 10 minutes for heat inactivation. Reverse transcription mix was prepared by adding 88 µL of ultrapure water, 165 µL PEG 8000, 220 µL 5x Maxima RT buffer, µL of 25 mM dNTPs, 22 µL TSO E5V6NEXT unblocked 100 uM, and 11 µL Maxima H Minus RT (200 units/uL). 5 µL was added to each well then sealed and centrifuged at 1000 rcf for 30 seconds. The 96 well plate was incubated in a thermocycler for 90 minutes at 42 C. Next, pooling beads were prepared by adding 15 g PEG 8000, 20 mL of 5M NaCl, 500 µL 1M ph 8.0 Tris-HCl, 100 µL 0.5 M EDTA, 50 µL IGEPAL 10% solution, 250 µL Sodium Azide 10% solution, and ultrapure water to bring solution to 50 mL. PEG was solubilized in solution by incubating at 40 C and vortexing. Sera-Mag Speed Beads were resuspended in the bead stock. All wells were pooled in a 2 mL tube then 960 µL of the Pooling Beads were added and incubated at room temperature for 5 minutes to allow cDNA binding to beads. Beads were magnetically pulled down and the supernatant was removed and discarded. They were washed

with 1 mL of 80% ethanol twice then air dried for 5 minutes. cDNA was eluted by adding 17 µL of ultrapure water. This was transferred to a new tub and added to 2 µL of exonuclease 10x buffer and 1 µL of exonuclease (20 units/uL). The library was placed in a thermocycler for 20 minutes at 37 C for exonuclease digestion then 10 minutes at 80 C for heat inactivation. The pre-amplification mix was prepared by combining 25 µL of 2x terra direct buffer, 1 µL of 10µmSINGV6 primer, 1 µL of Terra polymerase (1.25 units/uL), and 3 µL of ultrapure water which was added to the digested sample. The 50 µL sample was amplified in a thermocycler by 3 minutes at 98 C then 15 cycles of 15 seconds at 98 C, 30 seconds at 65 C, then minutes at 68 C, followed by 10 minutes at 72 C. Clean up beads were washed with a solution containing 11 g PEG 8000, 10 mL of 5M NaCl, 500 µL 1M ph 8.0 Tris-HCl, 100 µL 0.5 M EDTA, 50 µL IGEPAL 10% solution, 250 µL Sodium Azide 10% solution, and ultrapure water to bring solution to 50 mL. The solution was added to the beads then washed after adding additional Tris-HCl and EDTA. 40 µL of clean-up beads were added to the PCR result and set at room temperature for 5 minutes. Beads were pulled down on a magnetic stand and washed twice with 150 µL of 80% ethanol. cDNA was eluted with 15 µL of ultrapure water then the concentration was quantified using high sensitivity DNA Qubit. For tagmentation, 10 µL of tagment DNA buffer (2x was added to 5 µL of Amplicon tagment mix, 4 µL of ultrapure water, and 1 µL of diluted cDNA (0.8 ng/uL). This was then incubated at 55 C for 10 minutes in a thermocycler. The reaction was stopped by adding 5 µL of NT buffer, pipetted upland down then incubated at room temperature for 5 minutes. For 3' enrichment PCR, 15 µL of NPM PCR Mix, 0.5 µL of P5NEXTPT5 (5 uM), and 9 µL ultrapure water were added to the sample along with 0.5 µL i7 index primer. It was then cycled through 13 cycles of 10 seconds at 95 C for denaturation, 30 seconds at 55 C for annealing, and 1 minute at 72 C for elongation which was preceded by 3 minutes at 72 C and followed by 5 minutes at 72 C. The result was mixed with 50 µL clean-up beads for 5

minutes at room temperature. It was pulled down with a magnet and washed twice with 150 µL of 80% ethanol. cDNA was eluted with 20 µL of ultrapure water then run for 10 minutes on a 2% Agarose E-Gel EX. The gel frame was pried open and the library was excised by cutting from 300 to 900 bp with a scalpel. The Qiagen MinElute Kit was used to isolate the cDNA from the agarose gel. Briefly, 450 µL of Buffer QG was added to the gel in a 1.5 mL eppendorf tube and incubated at 42 C for 10 minutes. 150 µL of isopropanol was added to the sample and mixed, then transferred to a spin column and centrifuged at 16,000 rcf for 1 minute. The flow through was discarded and 700 µL of Buffer PE was added then centrifuged as done previously. The column was transferred to a new 1.5 mL eppendorf tube and 20 µL of ultrapure water was added to the column then centrifuged again. Samples were submitted to the Deep Sequencing and Microarray Core for quality control using the Aligent 2100 Bioanalyzer with a High Sensitivity DNA Analysis kit. Libraries were then pooled and sequenced on an Illumina NextSeq 500. Samples were demultiplexed using bcl2fastq and mapped using the zUMIs master script.[99]

This contains spike-ins and UMIs to allow accurate counts of strands. Paired end reads were sequenced with the Illumina NextSeq500 through the Deep Sequencing and Microarray Core. zUMIs was used to map and count reads through STAR and subRead featureCounts.[92,99,100] The Monocle2 R package was used to order cells in pseudotime then create a trajectory.[101]

Results

Development of a maturation transcriptome map

We built a meta-analysis dataset of publically available RNA-seq of the mouse heart. We were able to collect embryonic (E14.5), perinetal (P0, P1), neonatal (P4, P7), adolescent (P14), and adult timepoints. Clustering using PCA leads to clear grouping

by time point with a clear temporal trend. A time series trajectory forms as principal component 1 has most of the variance and is able to order the samples (Figure 2.1). At this point, we notice that there are a few large jumps, particularly from P7 to P14, which we describe as the critical window for maturation.

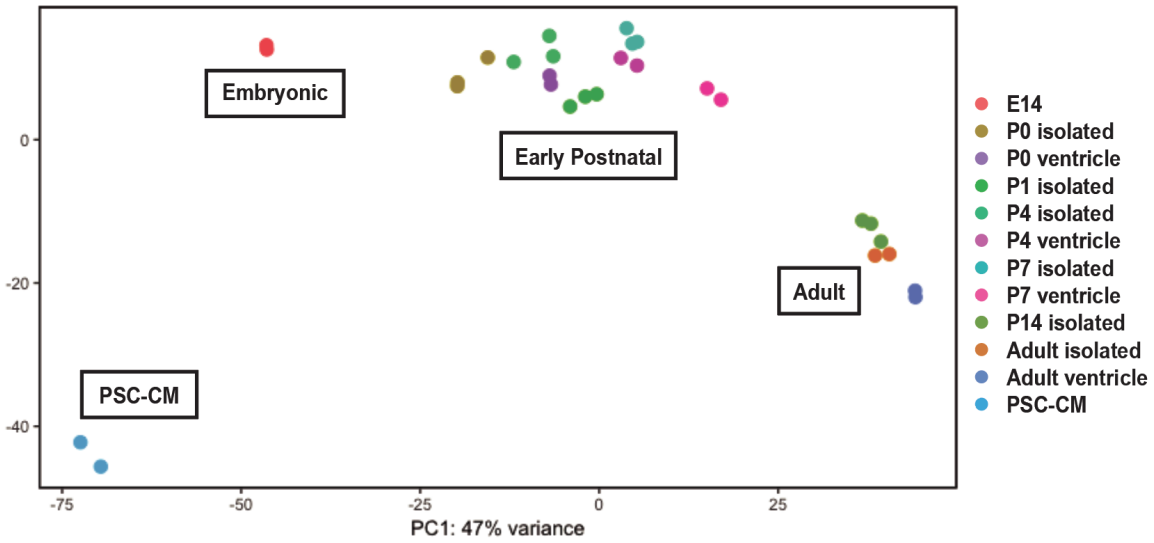

Figure 2-1. Principal component analysis of bulk RNA-seq meta-analysis of ventricular and isolated myocytes. PC1 captures 45% of the variance and shows a clear temporal trajectory

Isolated cardiomyocyte samples, which have been estimated by the authors to be more than 95% cardiomyocytes, and whole ventricle samples were used. While a third of the heart by volume contains nonmyocytes, predominantly fibroblasts and endothelial cells, isolated and ventricle samples cluster closely. Although this study contains samples from multiple institutions across several continents, large batch effects were not observed in the PCA cluster although individual gene reads despite normalization showed trends. In addition, the PSC-CM cells did not cluster closely with the late embryonic cells, which they resemble morphologically and functionally.

After building a meta-analysis dataset that captured temporal maturation, I wanted to see show the CM transcriptome changed as it matured. We know that contractile proteins increase in expression and isoform switches occur specifically in *Myh6/7* and

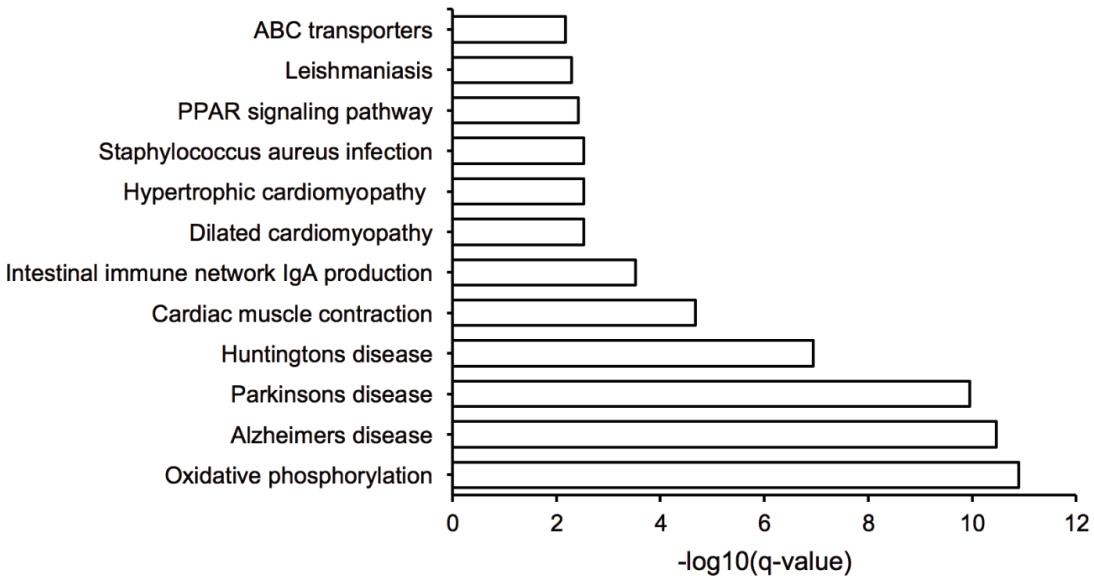

Figure 2-2. KEGG analysis of deferentially expressed genes with at least 2 fold change comparing early and late timepoints

TNNI1/3. However, the temporal change in all mRNA at this resolution and read depth has not been determined. Differential expression analysis was performed and yield with >2-fold change in expression and p-value <0.05. A KEGG analysis of the upregulated genes (Figure 2.2) shows that the pathways for oxidative phosphorylation, cardiac muscle contraction and PPAR signaling were enriched. Multiple top terms were related to neurodegenerative diseases, but these show up because they have been mechanistically linked to mitochondrial dysfunction. This finding supports functional changes noted in maturation as immature CMs use glycolysis as their energy source and adult CMs use fatty acid oxidation.

Generation of a gene regulatory network of maturation

With the goal of understanding which gene programs are activated during maturation, we used weighted gene co-expression network analysis (WGCNA) to identify co-expressed clusters across maturation. A heatmap showing coexpression between genes and their assigned modules (Figure 2.3) indicates that specific clusters form through

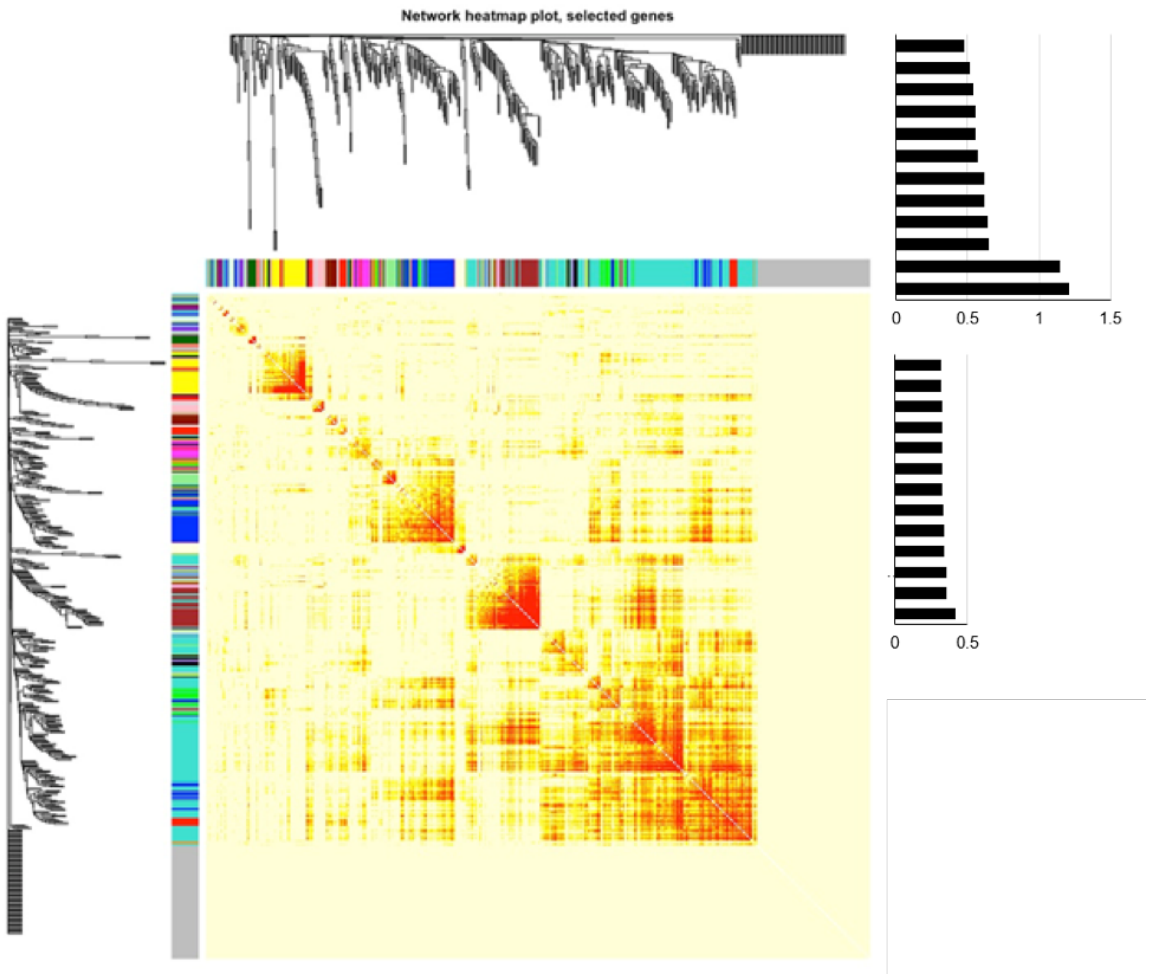

Figure 2-3. Weighted gene co-expression network heatmap for cardiac gene regulatory network. Genes were hierarchically clustered and assigned module color is presented.

development and turquoise is the largest.

To track module relevance to maturation, the correlation of each module with developmental time was computed (Figure 2.4). Gene ontology was used to summarize the genes in the two top clusters that are the most strongly associated with correlation positively (red) and negatively (turquoise). The GO terms were sorted by log of fold enrichment and presented showing the red module contained metabolic and oxidative phosphorylation genes. The turquoise module is a suppressed group of genes that are related to activation of the cell cycle and mitosis. Once we identified genes within the top correlation network module, we wanted to select the activated as potential

targets for modulation to promote PSC-CM maturation. We found that the red module contained 35 putative transcription factors including RXRG and PPARA, which form a nuclear receptor transcriptional complex together, along with E2F6, which is involved in suppressing cell cycle progression.

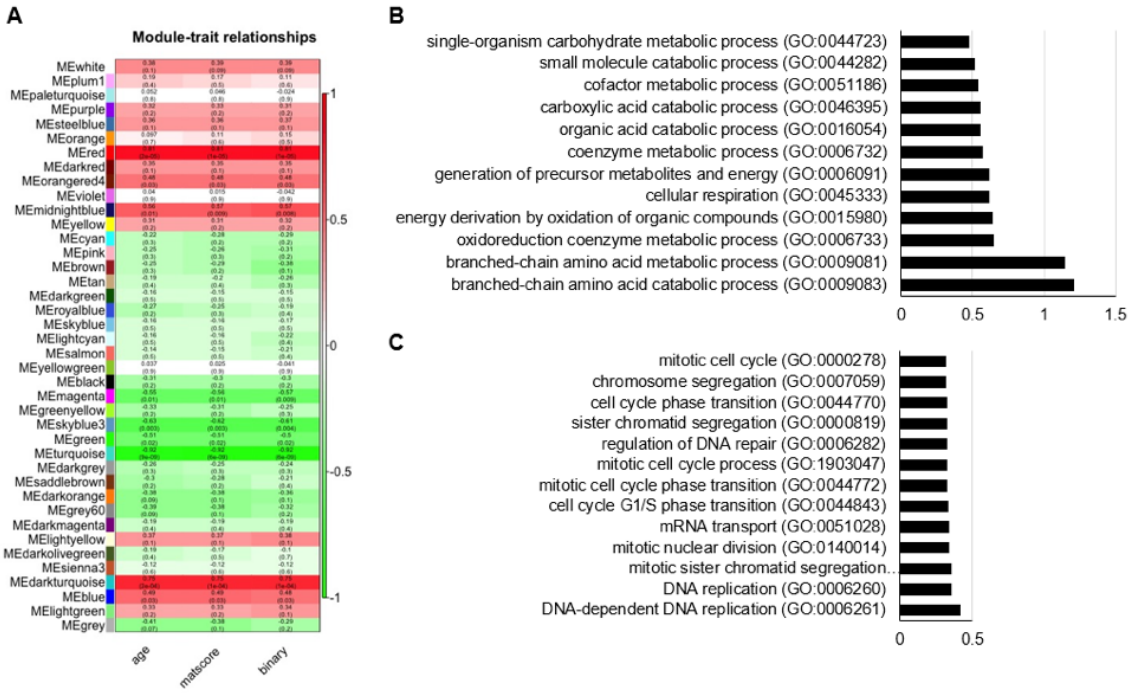

Figure 2-4. A. Correlation of gene module expression with CM maturation. B. Gene ontology top terms for red module which is positively correlated with maturation. Axis represents log of fold enrichment. C. Gene ontology top terms for turquoise module with is negatively correlated with maturation.

Prediction of upstream regulators of postnatal maturation

We next wanted to use the bulk RNA seq to predict top upstream regulators, primarily transcription factors, whose activation of genes matched the differentially expressed genes. IPA Generated a Z score for activation and the top genes with the log fold change (Figure 2.5).[94]

This identified a list of potential drivers of maturation. Nuclear receptors, specifically the PPAR family, showed up repeatedly on the top predicted upstream regulators

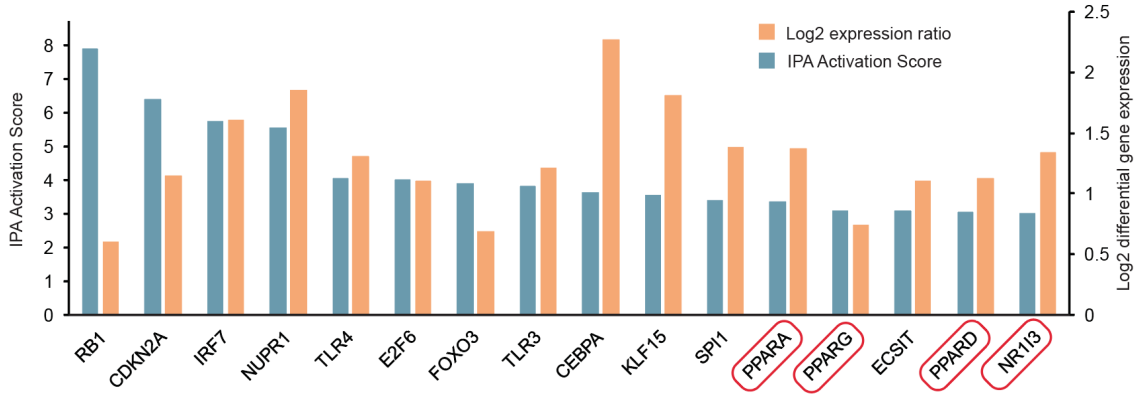

Figure 2-5. Prediction of upstream regulators using Ingenuity Pathway Analysis

that also increased in expression by at least 1.5 fold. From this, we concluded that PPAR is activated during postnatal maturation.

Single cell transcriptomics defines a maturation trajectory and maturation scores

We designed a comprehensive analysis of cardiomyocyte maturation at postnatal stages. We used myocytes collected at P0, P7, P14, P21, and P28. Previous studies have not been able to generate high quality sequencing data because, as we had recently shown, most cell sorters lead to cell shearing. Therefore, we used large particle fluorescence activated cell sorting (LP-FACS), which is able to maintain cardiomyocyte shape and viability. Here, I have performed single cell RNA-seq on CMs isolated at neonatal, postnatal and adult stages (Figure 2.6) every 7 days following birth. Suraj Kannan assisted with LP-FACS and prepared the single cell RNA-seq libraries. Dr. Brian Lin performed the Langendorff heart perfusions.

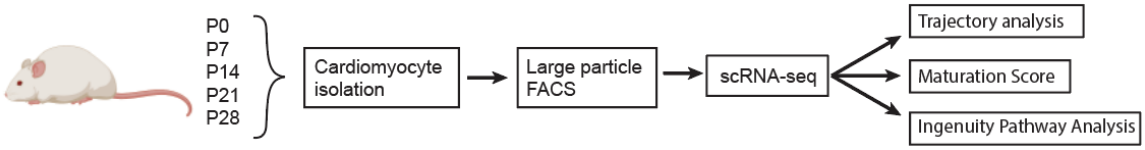

Figure 2-6. Single cell RNA-seq experimental design. Mouse hearts were collected using large particle fluorescence activated cell sorting. 96 CMs in each group were sequenced except for P0 where 192 CMs were sequenced.

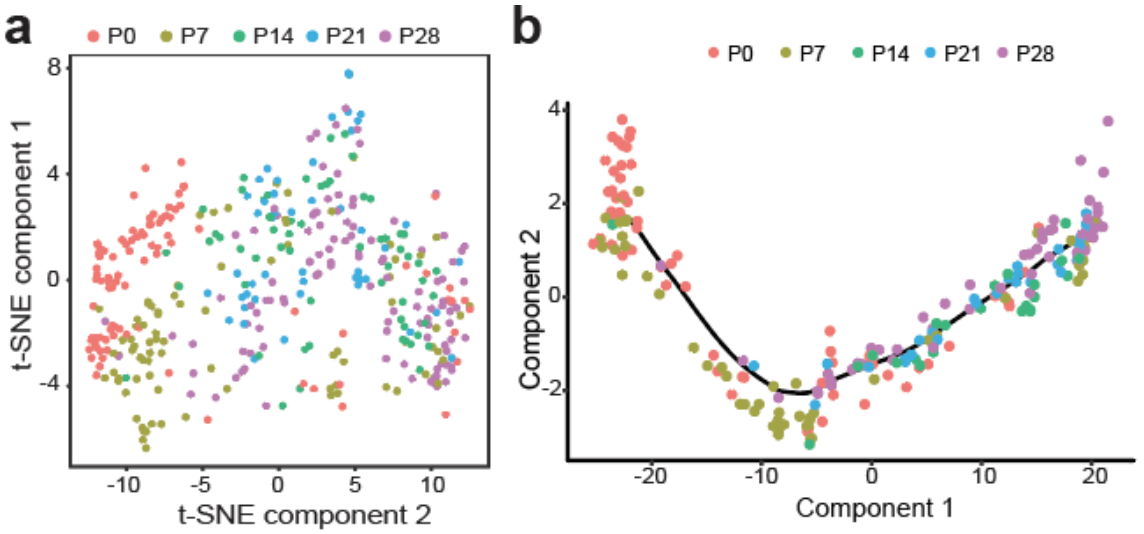

Figure 2-7. A. t-SNE clustering showing CMs are heterogeneous. B. Trajectory across pseudotime of CM maturation

Mouse myocytes were dissociated using MACS or Langendorff followed by sorting by cell size using LP-FACS. t-distributed stochastic neighbor embedding (t-SNE) clustering finds overlap between cells from different stages (Figure 2.7). This is supported by uniform manifold approximation and projection for dimension reduction (UMAP), which created clusters mostly based on timepoint with some intermixing (Figure 2.10). This could indicate that transcriptome signatures are similar for different stage CMs and that they mature at different rates. To track the trajectory of maturation, we ordered CMs in pseudotime using Monocle. The maturation score, which is normalized pseudotime, shows a jump from P7 to P14 (Figure 2.8). This is the same timepoint difference that we dubbed the critical window from initial bulk RNA-seq meta-analyses. Another key point was the heterogeneity as adult P28 CMs were not fully heterogeneous. The variability in P14 and P21 timepoints is likely caused by the number of cells sampled. This heterogeneity roughly matches the time of flight measurements from LP-FACS, which show size shifts.

Next, I plotted the expression trends of genes known to change through maturation (Figure 2.9). We see that structural genes key to contraction were upregulated

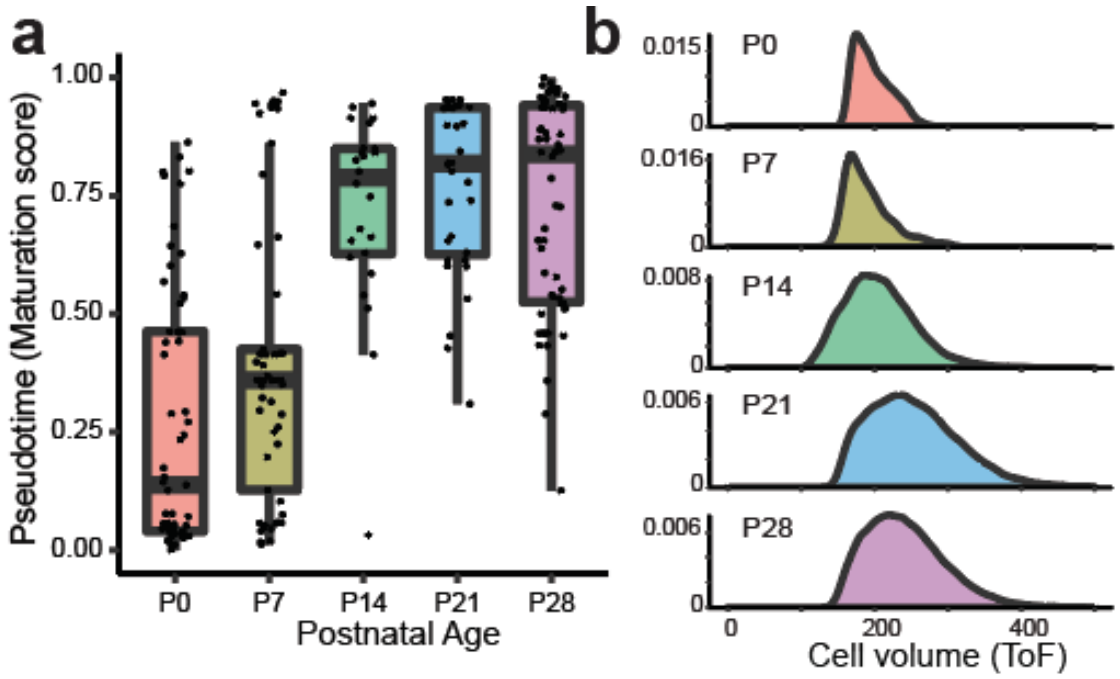

Figure 2-8. A. Distribution of CMs for each timepoint based on maturation score. Individual cells are overlaid. B. Time of Flight measurements for sequenced CMs.

including *Tnni3*, *Myh6*, and *Myom2*. Key calcium handling genes and ion channels were also upregulated. As expected, cell cycle regulators driving proliferation were downregulated.

The hypertrophy genes appear to be activated early on and taper off in expression. To categorize the large changes that occur, gene ontology analysis of differentially expressed genes was visualized (Figure 2.11), which indicated that the upregulated genes are predominantly related to oxidative phosphorylation, fatty acid oxidation, and muscle contraction.

We then wanted to determine whether mitochondrial genes, those in the mitochondrial genome, were also upregulated. Using a heatmap with hierarchical clustering, (Figure 2.12). This could indicate an increase in the mitochondrial density.

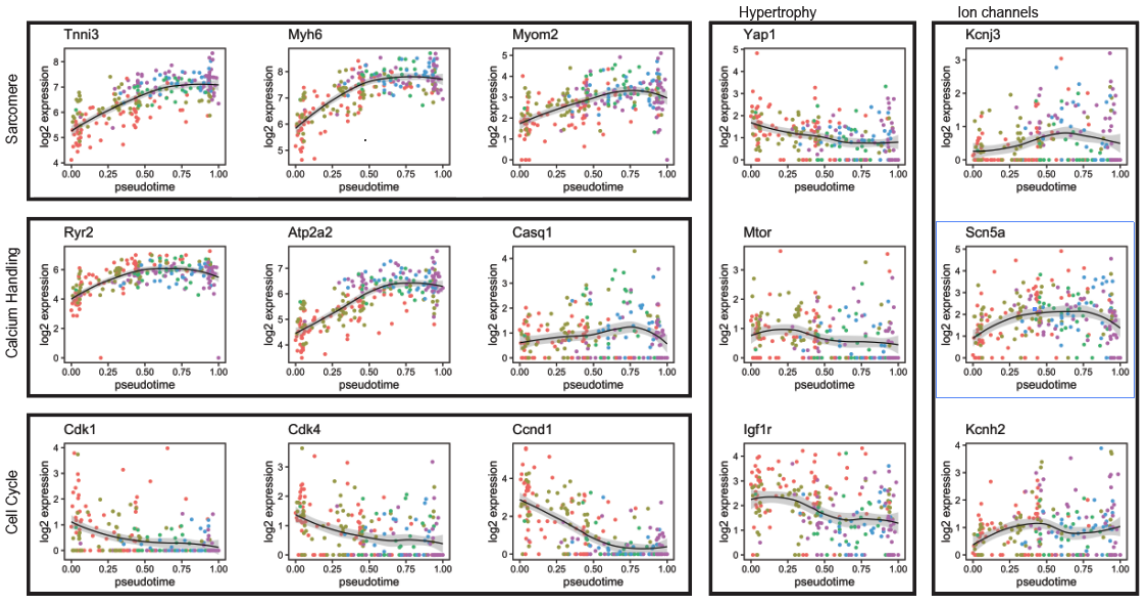

Figure 2-9. Gene expression over pseudotime for key cardiac genes. Genes were clustered by function.

Gene Network analysis of maturation using single cell RNA-seq

While the downstream gene changes associated with maturation have been documented, the regulatory mechanism has not been determined. With the goal of determining upstream regulators of postnatal CM maturation, I used IPA to predict drivers of maturation. We first noticed that nuclear receptors were commonly activated in this gene set (Figure 2.13). To narrow it down, we used a q-value cutoff of 10e-5 then ordered them by the top p-value. PGC1α and PGC1β were among the top predicted transcriptional regulators (Figure 2.14). This was supported by the upregulation of mitochondrial and fatty acid oxidation genes.

To track the expression over development and maturation, we used quantitative polymerase chain reaction (qPCR) and found that nuclear receptors increase in expression (Figure 2.15). We collected hearts from embryonic (E9.5, E14.5, E18.5), perinatal (P0), adolescent (P14), and adult (P28) mice. In addition, we used mouse PSC-CMs collected at 10, 20, and 30 days after the beginning of differentiation. qPCR

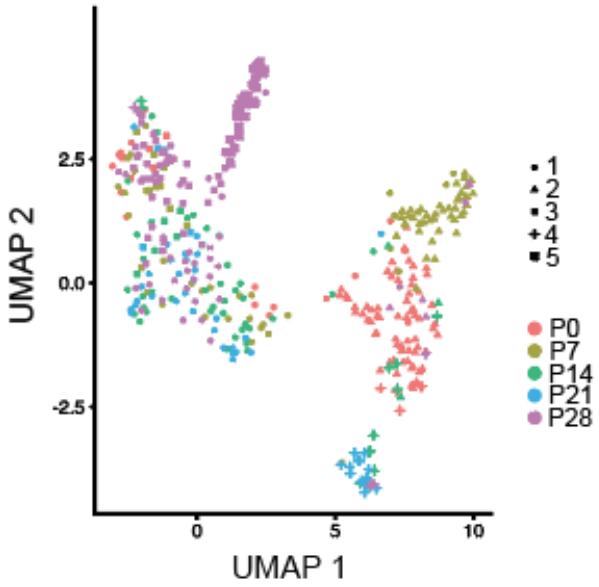

Figure 2-10. UMAP clustering shows cells segregate mostly be timepoint with some mixing between groups indicating heterogeneity in maturation status

of the mRNA levels of these nuclear receptors in PSC-CMs showed that most increase through differentiation except for *Pgc1α* and *Pgc1β*, which are misregulated. Looking at these regulators in our scRNA-seq results, we see a 2 fold increase in *Pgc1α* and *Ppara* expression over pseudotime (Figure 2.16). This could indicate that PGC1α and PGC1β are activated in postnatal maturation and may be the cause of maturation arrest that keeps PSC-CMs immature in vitro.

Discussion

I have shown CM maturation can be described by a temporal transcriptome atlas of postnatal development. The gene expression signature can be used to determine the pseudotime age, which corresponds with maturation state. This was completed in high depth bulk RNA-seq and in high resolution single cell RNA-seq. Both datasets showed an enrichment of metabolic, mitochondrial, and fatty acid oxidation genes in the upregulated gene sets. These indicate that these processes transition during postnatal maturation and support the known switch from glycolysis to oxidative

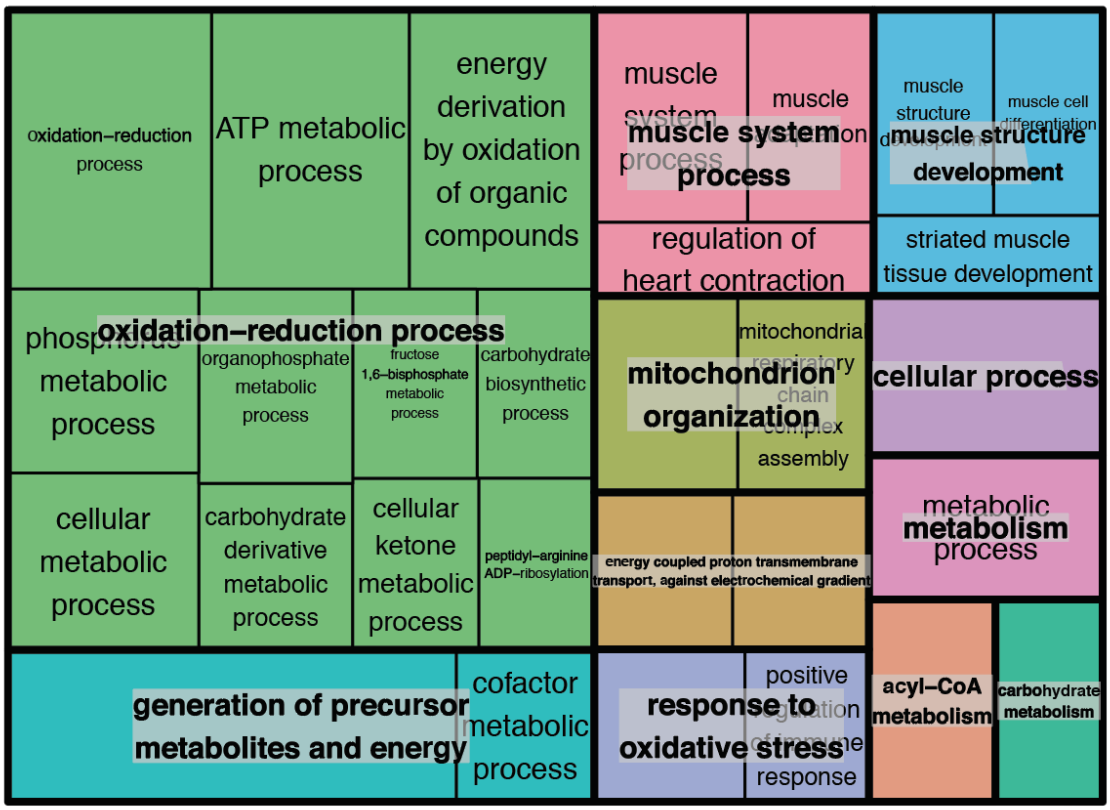

Figure 2-11. Visualization of top GO terms generated for unregulated genes in scRNA-seq. Mitochondrial, metabolism, and myofilament GO terms are present.

phosphorylation. KEGG pathway analysis showed the presence of genes related to neurological conditions including Alzheimers and Parkinsons (Figure 2-2). This is not due to neuronal contamination, but the links between mitochondrial function and these diseases. This study provides the best temporal resolution of postnatal maturation, which is key to PSC-CM maturation due to the maturation arrest at a stage similar to neonatal CMs. Interestingly, we showed that there is a critical window from P7 to P14. This jump in transcriptomic signature is accompanied by changes in function and morphology including cell cycle cessation and hypertrophic growth. External stimuli could cause this jump as cells respond to the increase in oxygen and reactive oxygen species pushing a switch to fatty acid oxidation and causing oxidative DNA damage slowing proliferation.[33]

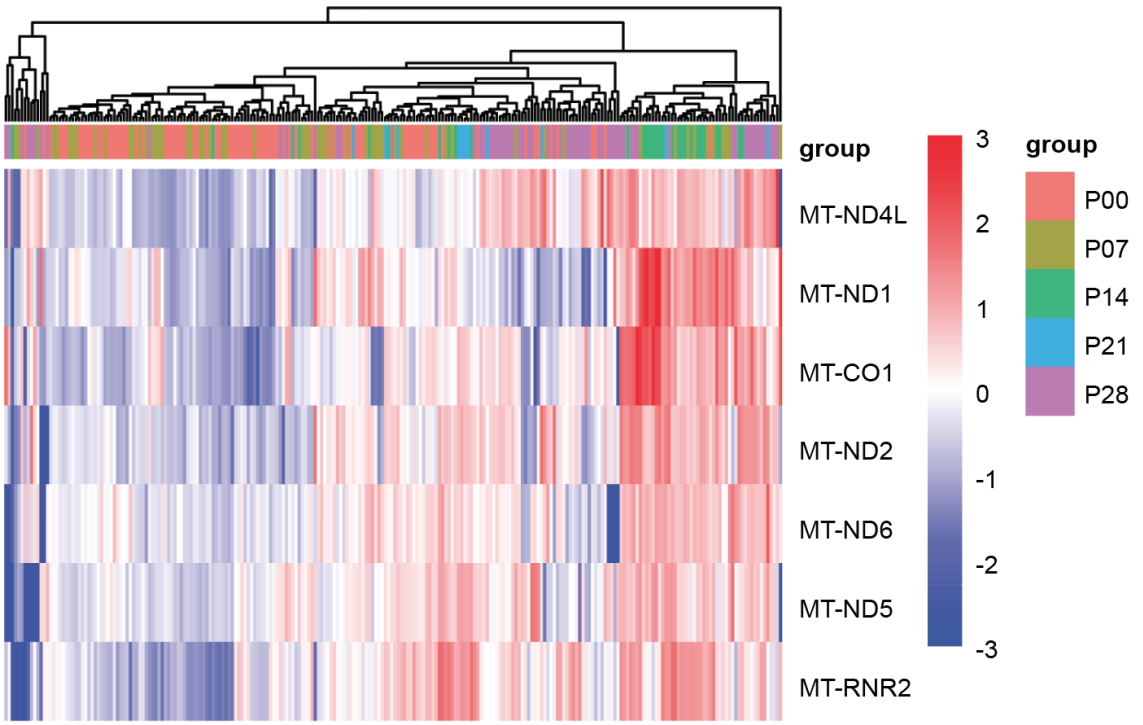

Figure 2-12. Heatmap showing expression of mitochondrial genes with hierarchical clustering showing P28 and P14 having the highest mitochondria levels. All 7 expressed mt-genes are upregulated.

In our GRN analysis and quantification of transcript levels, nuclear receptors appear to be consistently activated, particularly the PPAR family including PPARα, PPARδ, and PPARγ. Nuclear receptors affect gene regulation by binding an agonist then enter the nucleus to bind DNA and regulate gene expression. Other nuclear receptors have been shown to promote maturation including thyroid hormone receptor and glucocorticoid receptor.[1] PGC1α was also a top hit and is a co-activator of PPARs. This is supported by knowledge of an energy metabolism switch early postnatally that occurs 2-3 days after birth. NFkBIA was the top predicted upstream regulator, but we decided not to select it for further investigation because its expression levels are relatively flat through maturation. In addition, PGC1/PPAR have been better characterized in the heart.

While bulk RNA-seq provides deep reads allowing us to track expression of low

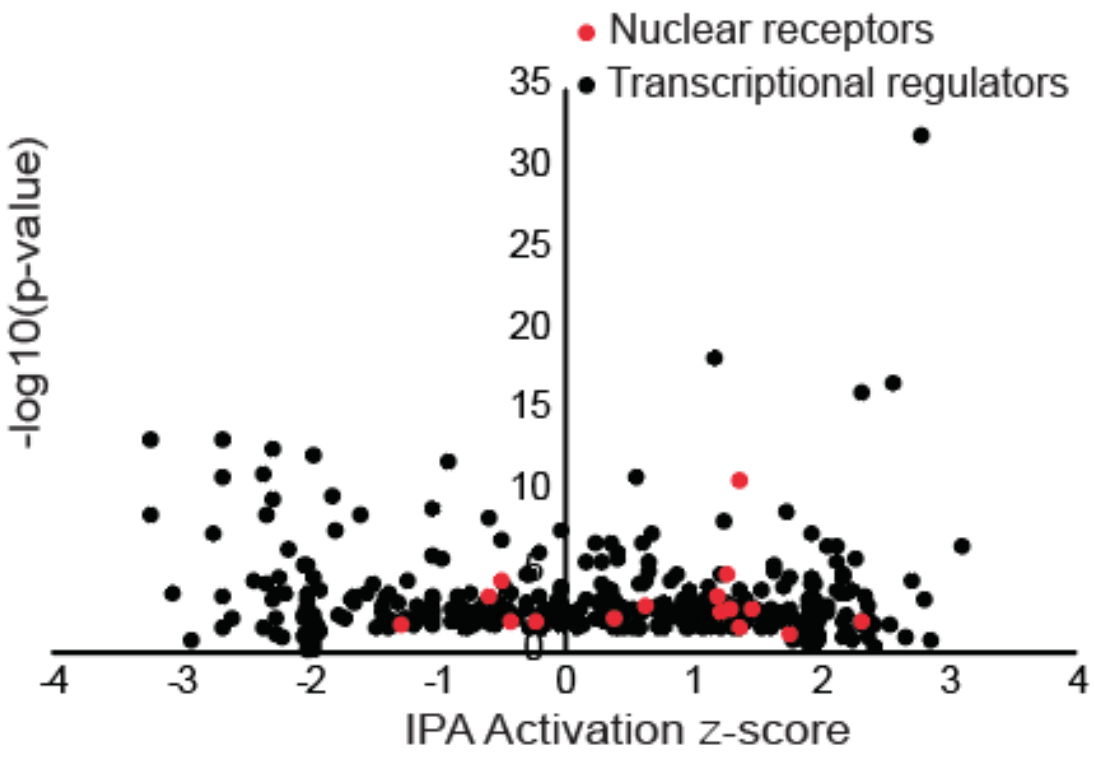

Figure 2-13. Nuclear receptors are activated in IPA of CM maturation. Red dots highlight nuclear receptors, which mostly have positive activation z-scores.

count mRNA molecules, it has multiple drawbacks. Primarily, the combination of multiple cell types. However, in PCA clustering, our isolated CMs, which the authors of the study that collected this dataset estimated that they were at least 95% CMs, were very close to the whole ventricle isolation. Therefore, there was a need for single cell RNA-seq of postnatal maturation as this would provide insights into a cardiomyocyte specific trajectory without fibroblast and endothelial cell contamination. Our single cell results also depict the broad heterogeneity present in cardiomyocytes. It appears that the rate of maturation differs. Future studies could see if the less mature cells are located spatially in one region or if they are distributed throughout the heart. Spatial RNA-seq, which became readily available following the completion of this work, can be applied to create a map of maturation in the heart.

This used two types of gene regulatory network generation in IPA and WGCNA.

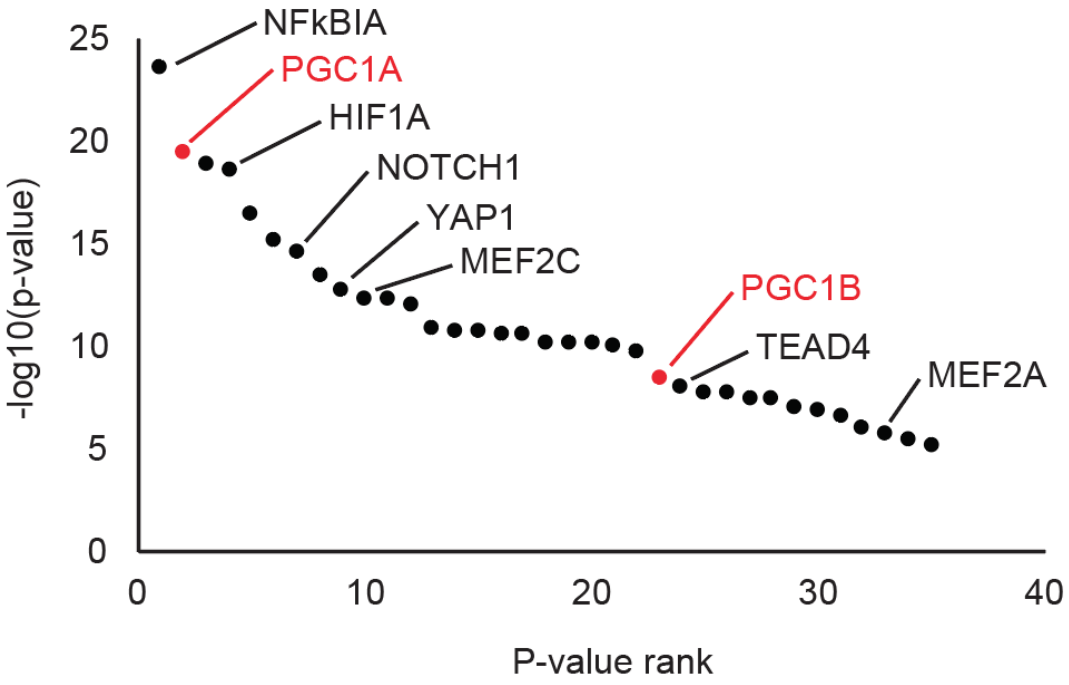

Figure 2-14. PGC1α and PGC1β are among the top predicted upstream regulators of CM maturation from IPA

There were similar results in the predicted upstream regulators list and the transcriptional regulators that were present in the WGCNA modules that were positively correlated with maturation. We used both because IPA uses known connections between genes, while WGCNA infers all connections from the data provided. WGCNA could determine co-regulated genes specific to CM maturation as genes can play different roles in various cells.

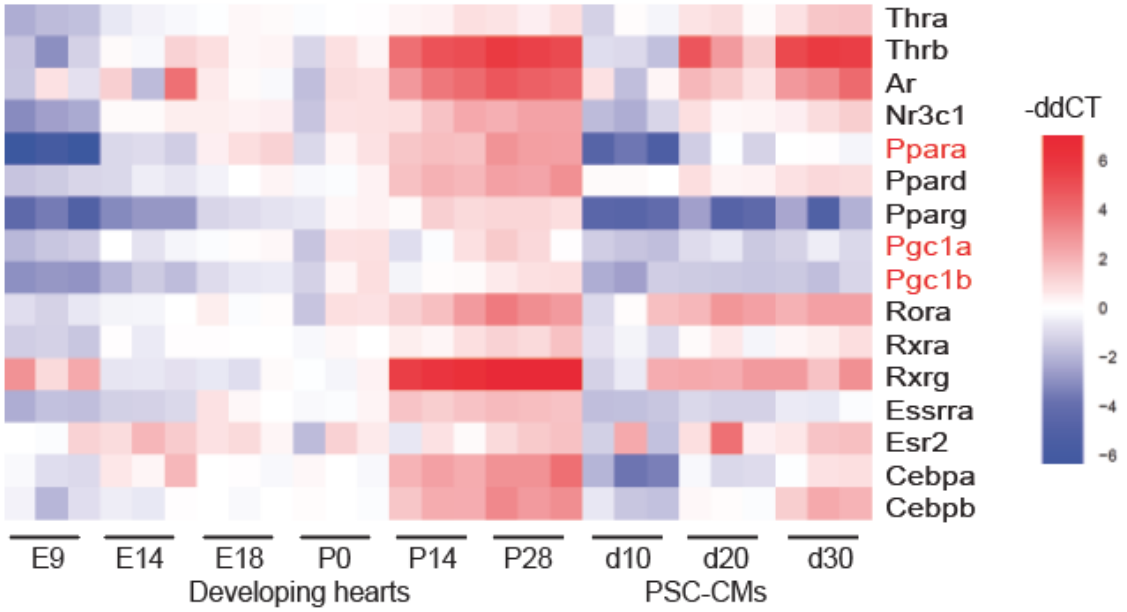

Figure 2-15. Heatmap showing nuclear receptor expression in both mouse hearts and PSC-CMs. Increasing trends in expression occur in all nuclear receptors in the developing hearts. Most increase in PSC-CMs except for PGC1 and PPAR showing dysregulation.

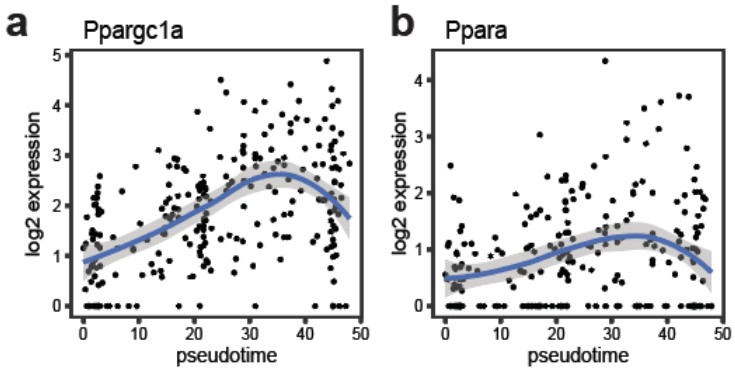

Figure 2-16. Expression of PGC1α and PPARα in single cells over pseudotime indicates upregulation

Chapter 3

PGC1α in the heart

Background

PGC1

PGC1α is a transcriptional coactivator of many transcription factors that regulates mitochondrial biogenesis.[102] It was identified by a 2-hybrid screen in brown fat to find binding partners of PPARγ since PPARγ is a target of drugs used to treat diabetes mellitus. In muscle, PGC1 has been shown to interact with NRF-1 and TRB-1 to regulate mitochondrial protein expression.[103] PGC1α also binds ERRs, PPARα and PPARδ to regulate glycolysis and fatty acid oxidation genes, specifically oxidation enzymes and fatty acid transporters. ERR was recently shown to directly bind and regulate cardiac contraction genes.[78] ERR has also been shown to form a crosstalk loop with PGC1 as there is an evolutionarily conserved binding site for ERR in the PGC1 promoter.[104] PGC1 has a short half-life of 20 minutes due to PGC1α degradation by the proteasome after ubiquitination.

PGC1α upregulates expression of the majority of the respiratory chain and ATP complexes in addition to all of the enzymes in the citric acid cycle.[105] Cardiac specific overexpression of PGC1α leads to CMs packed with mitochondria and heart failure due to disruption of myofibrils, but these changes were reversed when PGC1α was repressed.[104] Induction of cardiac PGC1α overexpression in adults did not lead to

mitochondrial proliferation showing that it only drives mitochondrial biogenesis during maturation.[104] ERRα overexpression in rat neonatal CMs upregulates both glycolysis and fatty acid oxidation. More than 98% of mitochondrial genes are in the nucleus, but PGC1 also regulates the genes in the mitochondrial genome by inducing TFAM, which drives mitochondrial genome transcription and replication, through NRF-1.[105]

PPAR

PPAR transcription factors bind DNA by heterodimerizing with retinoic acid-activated receptors (RXRs).[104] These upregulate metabolic and peroxisomal genes and have been targeted for pharmacologically treating diabetes. PPARα is expressed in the heart, brown adipose tissue, liver, and kidneys, which all use fatty acid as their energy source. Cardiac overexpression of PPAR results in higher fatty acid oxidation and lower glycolysis, but leads to lipotoxicity since fatty acid uptake was higher than usage.[105] PPARα knockout results in the opposite metabolic behavior with higher glycolytic activity and lower fatty acid β-oxidation. PPARδ overexpression leads to higher fatty acid oxidation and higher glucose utilization and does not result in heart dysfunction.[105]

Regulators of PGC1α

PGC1 is regulated by phosphorylation of conserved sites. p38 phosphorylation can prolong its halflife. AMPK directly phosphorylates PGC1α to increase its activity. However, Akt kinase can block PGC1α activition.[105] Other post-translational modifications such as acetylation and methylation are regulated by Sirt1 and Bcl3, respectively.[104] PGC1 activity is based on input from levels of ADP to ATP ratio, stress, and the redox state. It can also sense calcium as it is regulated by calcineurin.[105]

PGC1α in maturation

PGC1α null mice have no large changes in phenotype unless they are exposed to exercise, fasting, or cold.[106] This is thought to occur because PGC1β rescues function due to an overlap in targets to compensate for the loss of PGC1α. Lai *et al.* generated a double knockout of PGC1α and PGC1β.[107] They found that cardiac specific PGC1α and PGC1β deletion is neonatally lethal. Characterization of the hearts showed that there was a maturation defect as myocytes were smaller with less mitochondria. Gene expression comparison measured by RT-PCR showed that they had a fetal signature as *Myh6*, *Serca2a*, and *Pdk4* were down-regulated.[107]

Birket and colleagues set out to develop a model of heart disease by dysregulating reactive oxygen species (ROS) levels in PSC-CMs. This study found that PGC1α was required for mitochondrial capacity and electrophysiological function in PSC-CMs by using PGC1α shRNA to knockdown PGC1α expression during cardiac differentiation. They focused on the role of ROS levels in maturation and concluded that PGC1α knockdown was beneficial to some aspects of maturation, which was recapitulated by altering ROS levels.[108]

Recently, PGC1α has been shown to activate maturation in PSC-CMs, supporting our initial findings. They used ZLN005, an activator of PGC1α, on PSC-CMs after differentiation and found that it improved multiple aspects of maturation.[109] Multiple aspects of maturation were improved including calcium handling, sarcomere length, and Connexin 43 gap junction development. As expected, metabolic maturation was improved over control.[109] PGC1α has been shown to be important in PSC-CMs and in embryonic development, but its role in postnatal maturation has not been investigated.

Mosaic knockouts

The first mosaic knockout system used to dissect gene function in the heart was the CRISPR/Cas9 AAV-based somatic mutagenesis platform (CASAAV).[110] A recombinant AAV expresses Cre in cardiomyocytes because it is under a cTnT promoter then multiple single guide RNAs create indel mutations in the gene of interest.[81] The AAV is delivered to mice that have a loxP-stop-loxP-Cas9-P2A-GFP so that Cas9 is Cre-activated with a fluorescent marker. This will create a loss of function mutation in vivo. This was created to make it possible to generate a knockout without germline engineering. An added benefit is that the AAV dose can be lowered to only create mutagenesis in a fraction of the cells, which is important in the heart because cellular defects can result in secondary effects. This allows us to study the gene quickly in a cell autonomous manner. One limitation of this study is that the mutagenesis may not lead to protein dysfunction. In a knock down of SRF, they found that mRNA levels were approximately halved.

CASAAV has been used to study junctophilin-2 (JPH2) where a high dose resulted in lethal heart failure, but a low dose did not affect heart function. Since loss of function was lethal, it had not been previously studied in postnatal hearts. The study also looked for other genes that would affect T-tubule development, which was visualized by fluorescent staining. This group has gone on to generate knockouts of key cardiac genes *Ryr2, Nkx2-5, Mef2c, Gata4, Tbx5,* and *Tead1* including to see if they influence cardiac maturation. They found that SRF plays a critical role in postnatal maturation in a cell autonomous manner.[82] A cardiac conditional knockout led to lethal dilated cardiomyopathy, showing CASAAV's ability to assess the relevance of genes that could not have been studied previously. Vandusen and colleagues then combined CASAAV with a library approach to knock out all genes in a screen for cardiac maturation. They found epigenetic regulators RNF20/40 to be required for postnatal maturation. Others have used CASAAV to rescue CMs with a hypertrophic

phenotype and tested regulators of heart failure.[111]

Since PGC1 had been identified as an upstream regulator of CM maturation, we wanted to determine if it was required for CM maturation. We used a conditional mosaic knockout to determine the cell autonomous role of PGC1. Cell size, contractility, and transcriptomic maturation were investigated to assess maturation state.

Materials and Methods

Fuzzy clustering and pathway analysis

Monocle2 was used to cluster and order cells for preparing trajectories.[101] Pseudotime was normalized for the maturation score. Fuzzy clustering was done with mFuzz R package and visualized with ggplot2 and coloring package.[112] For Gene Ontology, PantherGO provided statistics and top enriched GO terms.[95] Visualization of top selected GO terms was made with a custom R script using ggplot2. Codes used can be found in appendix ii.

Animal Handling and Genotyping

PGC1α/β flox mice were received from the Jackson Laboratory and then bred to produce knockout lines. All protocols involving animals followed US NIH guidelines and were approved by the animal care and use committee of the Johns Hopkins Medical Institutions through the JH Research Animal Resources facility. Genotyping was performed by cutting tails at 3 weeks after birth. Mouse were ear tagged for tracking. DNA was isolated using the Phire Animal Tissue Direct PCR Kit (ThermoFisher Scientific). The mouse tail tissue was added to 19.5 µL of Dilution buffer and 0.5 µL of DNA Release additive. Samples were incubated at room temperature for 10 minutes then 98 C for 5 minutes. A 10 µL polymerase chain reaction (PCR) was prepared by adding 0.25 µL of 10 uM primers, 0.5 µL of samples, 5 µL of GoTaq Green Master

Mix (Promega), and 4.5 µL of ultrapure water. They were then thermocycled for 35 cycles for 5 second at 98 C and annealed for 30 seconds at 59 C then extended for 30 seconds at 72 C. Primers used can be found in appendix i and were designed by the line generators and obtained from the Jackson Laboratory.

Adeno-associated virus

AAV9-cTnT-iCre was obtained from Vector Biolabs. It was diluted in cold PBS and stored on ice until injection. Each P0 pup was injected subcutaneously. Mice were anesthetized prior to injection. Mice were monitored following injection and then returned to the cage with the mother.

Library Preparation and Sequencing

Single cell RNA sequencing was performed as previously described in the Chapter 2 methods.

Dissociation of myocytes

A langendorff setup was used to perfuse hearts with Type II Collagenase and Protease digestion buffer over 9 minutes as previously described in Chapter 2. Cells were centrifuged at low speeds then resuspended in Tyrodes Solution containing bovine serum albumin. In 10 minute increments with a change of 0.25 mM calcium, CMs were stepped up to 1 mM calcium in a tyrode's solution.

Immunofluorescent Staining

Hearts were fixed overnight in 4% paraformaldehyde at 4 C. They were then transferred to a 30% sucrose solution overnight at 4C. Hearts were embedded in OCT and flash frozen using dry ice and methyl butane then stored at -80 C until sectioning. A cryotome was used to prepare 8-12 um thick slices that were mounted onto glass slides.

Dissociated CMs were cultured on glass coverslip in DMEM media containing FBS and blebbistatin to prevent contraction for 45 minutes then fixed with 4% PFA for 10 minutes at room temperature. Once fixed, they were stored in phosphate buffer solution (PBS) overnight at 4 C. Heart slices were rehydrated in PBS then blocked and permeabilized in PBS containing fetal bovine serum, bovine serum album, and 0.1% triton X-100 for 1 hour. They were treated with the mouse anti α-actinin primary antibody diluted 1:200 overnight at 4 C on a rocker. Slides were washed in PBS 3 times for 5 minutes. The goat anti mouse alexa fluor 488 secondary antibody diluted 1:500 was applied for 1 hour at room temperature. Following 3 PBS washes for 5 minutes, samples were counterstained with wheat germ agglutinin (WGA) and DAPI to visualize the nuclei and plasma membranes. They were briefly dried and covered with prolong diamond and mounted on a glass slide. They were imaged using confocal microscopy with a 63x oil objective on a Leica SP8. Image quantification was blinded and performed with ImageJ FIJI.

Calcium Handling and Contractility

Cells were sorted into a 24 well plate with laminin-coated glass slides. They were then loaded with Fura2AM Calcium dye (Fura2 LeakRes from Abcam) for 10 minutes. They were then tracked with IonOptix imaging system (Myocam) then analyzed with IonWizard software. CMs were paced at 1 Hz under an inverted microscope (Nikon, TE2000). The sarcomere shortening and calcium transient measurements were completed at 37 C in a Tyrode's solution with 1mM calcium and 0.01% DMSO. The results were analyzed using CytoSolver (CytoCypher, BV) through their cloud-based software.

Statistics

ANOVA with post hoc Bonferroni tests were used to determine significance in comparison of 3 or more groups. Statistics were completed using R or excel analysis toolpak. Student's t-test was used for a comparison of 2 groups.

Results

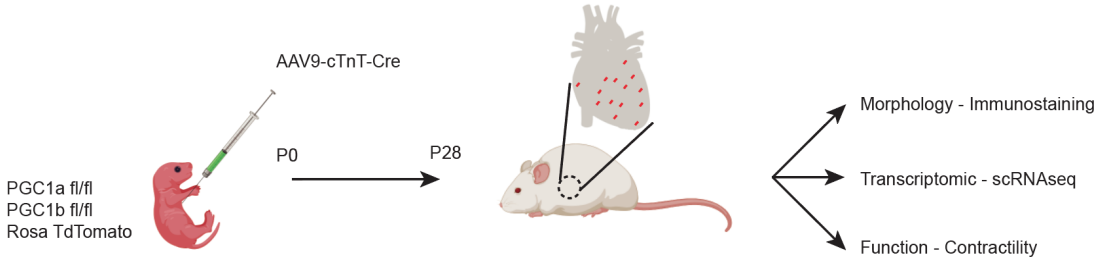

Figure 3-1. Schematic showing PGC1 floxed mice with a Rosa locus TdTomato reporter were injected with AAV9 on the day of birth at low doses to form a mosaic. Cardiomyocytes will be isolated on P28 for morphological measurements, transcriptomic measurements, and function assays

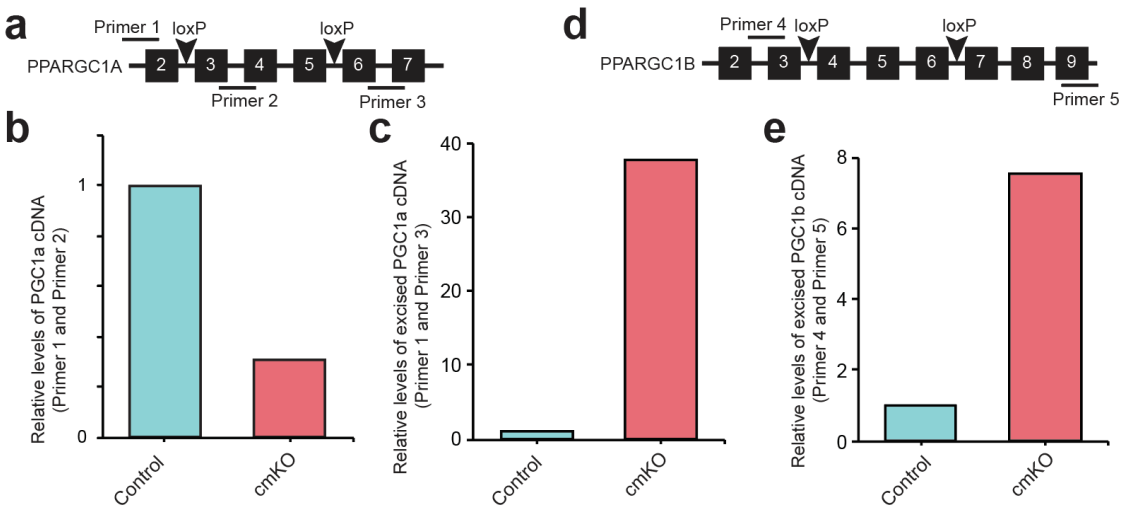

Figure 3-2. Confirming the PGC1 knockout. a. Primer design for determining efficiency of excision at PGC1a locus. b. Relative levels of PGC1a cDNA in control and RFP positive CMs. c. Relative levels of excised cDNA. d. Primer design for assessing PGC1b levels. e. Relative levels of excised PGC1b (n=2 mice in each group)

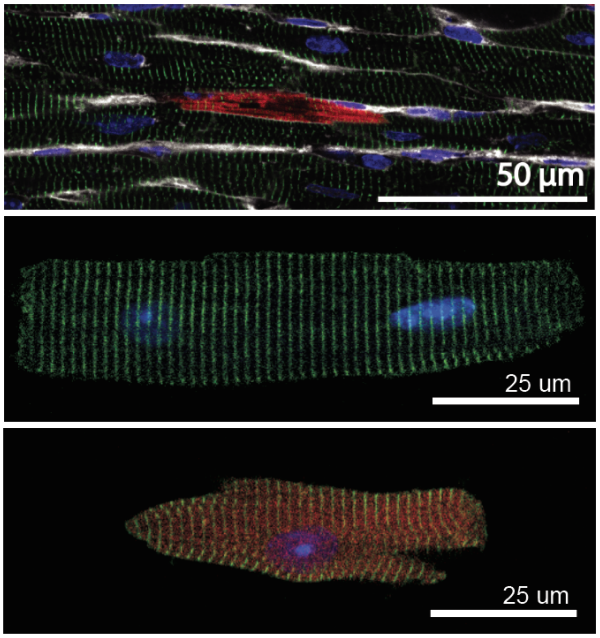

Figure 3-3. Confocal images of fluorescently immunolabeled a-actinin (green), TdTomato (red), and nuclei (blue) in sections and dissociated CMs.

Generation of PGC1α/β conditional mosaic knockout

We hypothesized that PGC1 is a key driver of maturation based on the results of the time series analysis of transcriptomic maturation. Global knockout or cardiac conditional knockout of PGC1α and PGC1β results in lethality within 24 hours of birth.[107] Knockout of PGC1α or PGC1β leads to a mild phenotype as they compensate in loss of function of the other. To test our hypothesis, we made conditional mosaic knockout (cmKO) mice to study the postnatal role of PGC1 in maturation. To do this, *Pgc1a* flox/flox *Pgc1β* flox/flox mice with a Rosa locus lopx-stop-loxp tdTomato reporter were injected on P0 with AAV9-cTnT-iCre (Figure 3.1). Danielle Rigau assisted in animal work to create the *Pgc1* floxed mice. This leads to expression of Cre recombinase only in cardiac myocytes. The AAV9 dose was titrated to 2e10 GC per mouse to result in 5-10% RFP positive cells in the heart so that the cell autonomous effects could be investigated. LP-FACS was then used to sort single cells by fluorescence and size for use in assays of morphology, transcriptomics, and function.

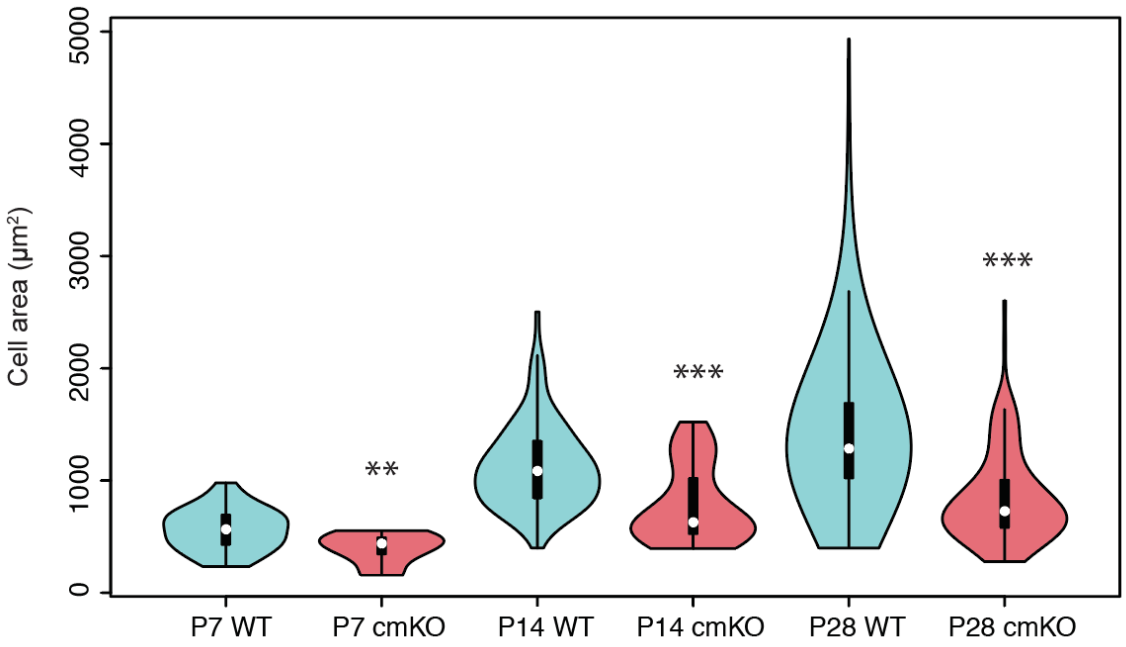

Figure 3-4. Violin plots showing the distribution of CM areas at P7 (WT n=44, cmKO n=11), P14 (WT n=90, cmKO n=49), and P28 (WT n=522, cmKO n=132). ANOVA with post hoc Bonferroni tests were used. P-value *<0.05 **<0.01 ***<0.001.

The virus was injected on P0 with functional tests run on P28 CMs. Morphological and transcriptomic analyses were run every 7 days from P0 to P28.

To confirm that the sorted RFP+ myocytes lack intact *PGC1α* and *PGC1β*, custom qPCR primers were designed (Figure 3.2) to quantify levels of normal and excised *PGC1α/β*. We found that the excised mRNA is much higher in our RFP+ cells and normal *PGC1α* mRNA is knocked down. Previous studies found comparable knockout efficiency using a CRISPR/Cas9 knockout system.

Hypertrophy resulting in an increased size is a hallmark of CM maturation. CMs were dissociated and imaged with fluorescence microscopy (Figure 3.3). We measured the cell size of our PGC1 cmKO RFP+ myocytes and found that size was significantly reduced at P7, P14, and P28 (Figure 3.4). The hypertophy is not just delayed, but arrested as later adult stages still showed significantly smaller myocytes. To rule out affect of the AAV9-cTnT-Cre virus on maturation, we injected it at P0 into Rosa

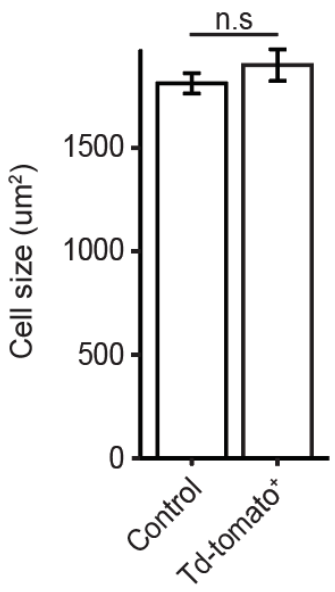

Figure 3-5. Injection of AAV9-cTnT-Cre into P0 mice with only a Td-Tomato reporter show no significant change in cell size at P28. n.s=p-value>0.05. Control n=87, Td-tomato n=26

tdTomato mice and found no significant change in cell size (Figure 3.5). Matthew Miyamoto took images of the PGC1 cmKO CMs. which were quantified by Sandeep Kambhampati.

Next, we looked into the effect of PGC1 cmKO on CM contractility. Video microscopy was used to track sarcomere shortening and contraction parameters. We see that fractional shortening and contraction velocity are significantly lower (Figure 3.6). This indicates that force produced by CMs is lower in PGC1 cmKO cells. Dr. Brian Lin collected data on Calcium handling and sacromere shortening and was blinded to experimental groups. For this analysis, 1-3 CMs were used from each isolated heart from 11 P28 mice for each condition. Other parameters of contraction were not significantly different including tau, return velocity, time to 90% of Baseline, and Peak Height (Figure 3.7). Calcium handling was also affected as the peak height and departure velocity were lower for the PGC1 cmKO (Figure 3.6). Other parameters quantifying the calcium transient showed differences, but were not significant including

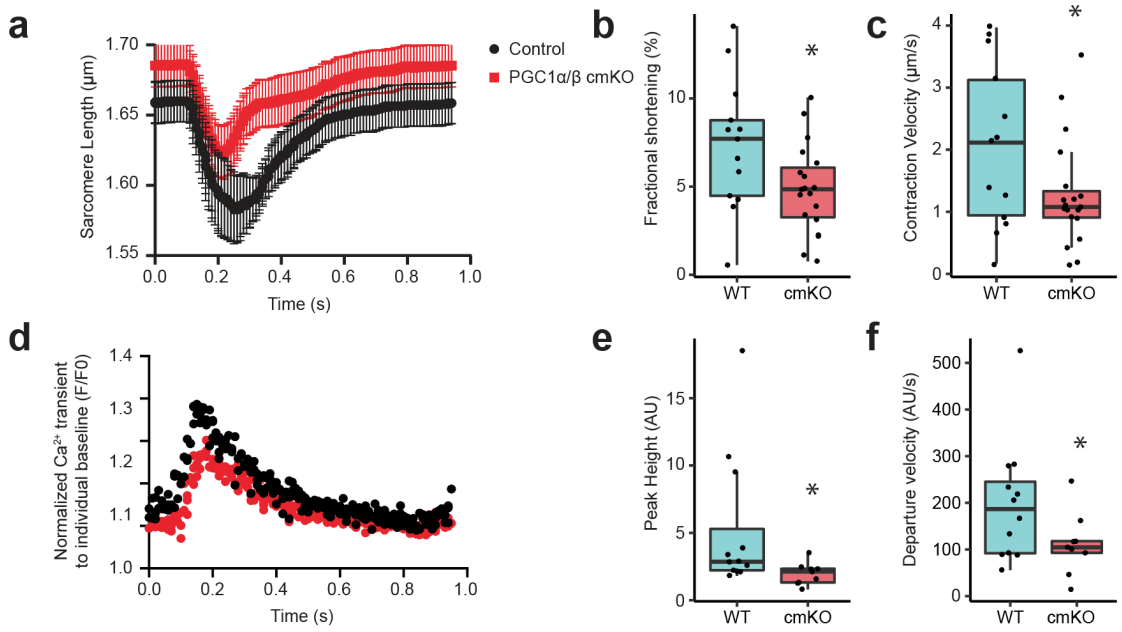

Figure 3-6. Contractility and Calcium Handling of P28 PGC1 cmKO CMs. a. combined shortening traces of control and PGC1 cmKO CMs. b. Fractional shortening c. Contraction velocity. d. combined calcium transient traces. e. Peak Height. f. Departure velocity. Student's t-test was used. *=p-value<0.05 WT n= 9, cmKO n= 13

tau, baseline calcium, and return velocity (Figure 3.7). However, time to 90% of Baseline was much slower for PGC1 cmKO. These results indicate that PGC1 is required to develop mature contraction and calcium cycling functionality.

PGC1 regulates genes in hypertrophy, calcium handling, and mitochondrial activity.

Since PGC1 was shown to play a key role in functional and morphological maturation, we investigated its role in transcriptional regulation. In the same manner as the functional study, RFP+ PGC1 cmKO cells from P7-P28 were collected for single cell RNA-sequencing. Cells were then ordered into a trajectory using Monocle (Figure 3.9). The pseudotime was converted into a normalized maturation score and clearly shows that there is a significant difference at all time points. Therefore, PGC1α/βcmKO results in a less mature state (Figure 3.9). While this brings up the question of whether maturation is stopped or slowed, cell size does not continue to increase as P56 PGC1

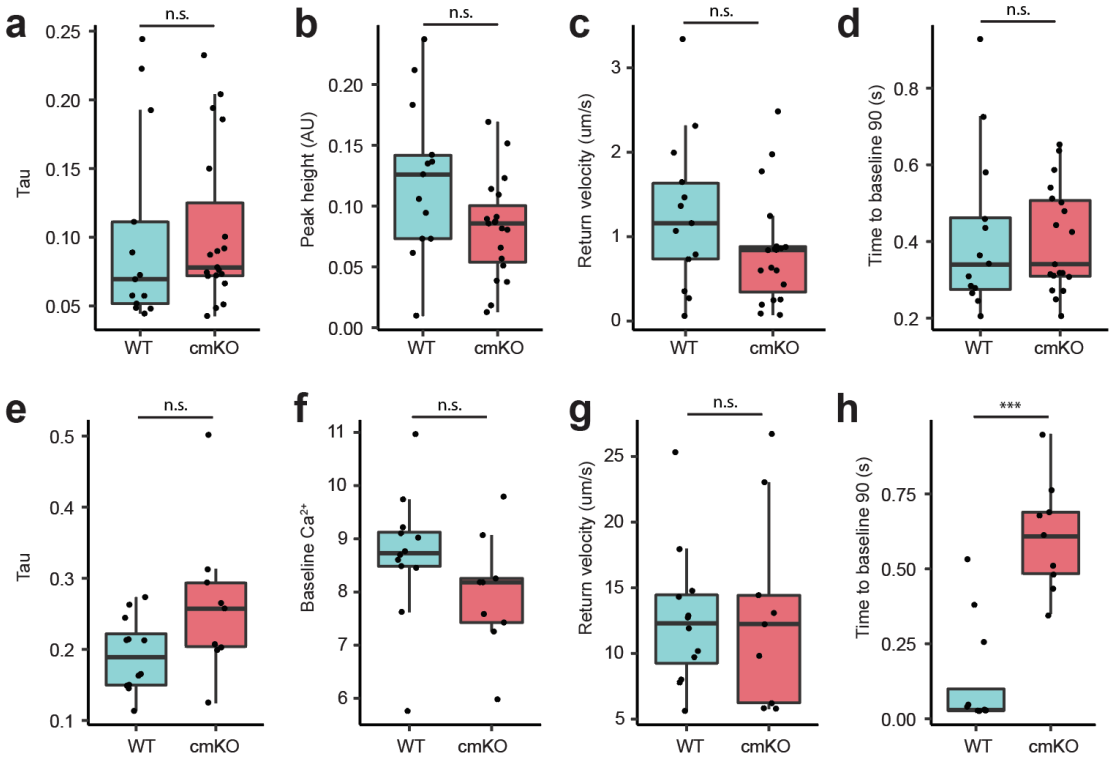

Figure 3-7. P28 PGC1 cmKO CM shortening (a-d) and calcium transient parameters (e-h). a. Tau b. Peak height c. return velocity d. time to baseline 90 e. Tau f. baseline calcium g. return velocity h. time to baseline 90. Student's t-test or Mann-Whitney-Wilcoxon test were used. ***=p-value<0.001, n.s.=p-value>0.05 WT n= 9, cmKO n= 13

cmKO myocytes do not catch up to the control CMs.

To determine how cardiomyocyte maturation signaling is perturbed by the loss of PGC1, we used fuzzy clustering to group genes by their expression pattern over time. The top upregulated and downregulated clusters were selected from each group (Figure 3.10). When comparing PGC1 cmKO with WT CMs, we see that less than 7.6% of upregulated genes and 16.2% of downregulated genes overlap. This shows that the gene regulatory network of the PGC1 cmKO CMs is disrupted. We used GO term enrichment to characterize the expression changes over time. We see that fatty acid oxidation and cardiac contraction terms were enriched in the downregulated gene while metabolic processes were upregulated (Figure 3.11). This finding confirms the role of PGC1 in mitochondrial biogenesis and unveils a possibly new role in regulation

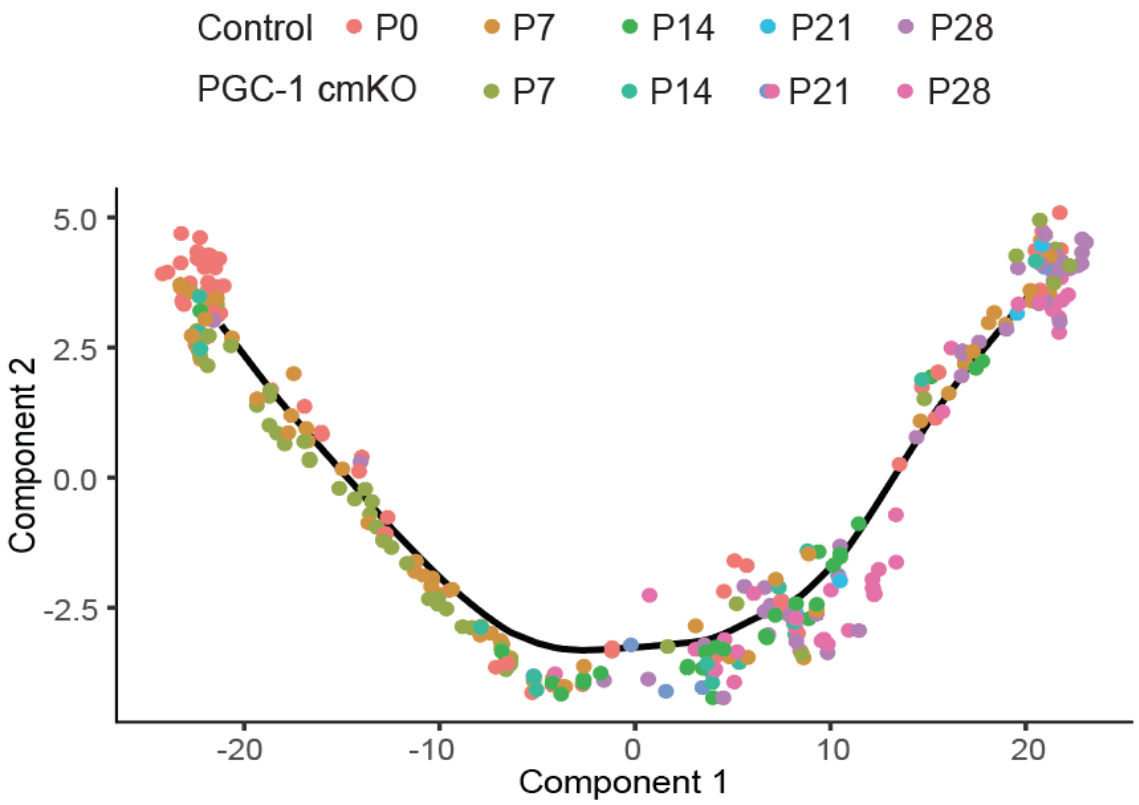

Figure 3-8. Trajectory containing both control and PGC1 null CMs from P0, P7, P14, P21, and P28.

of other aspects of CM maturation.

Discussion

Here, we present the first cmKO using the Cre-lox system to knock out function of PGC1. This is more thorough than CRISPR-Cas9, which may have unintended off target genomic disruption. In addition, the indel mutagenesis may not lead to a knockout of the protein, but a change in function. PGC1 conditional knockouts had previously been generated and led to neonatal death due to heart dysfunction. However, PGC1's postnatal role had not been investigated. Using the cmKO system, we were able to generate a knockout of both PGC1α and PGC1β after birth. A strength of this experimental setup is that it control CMs come from the same mouse

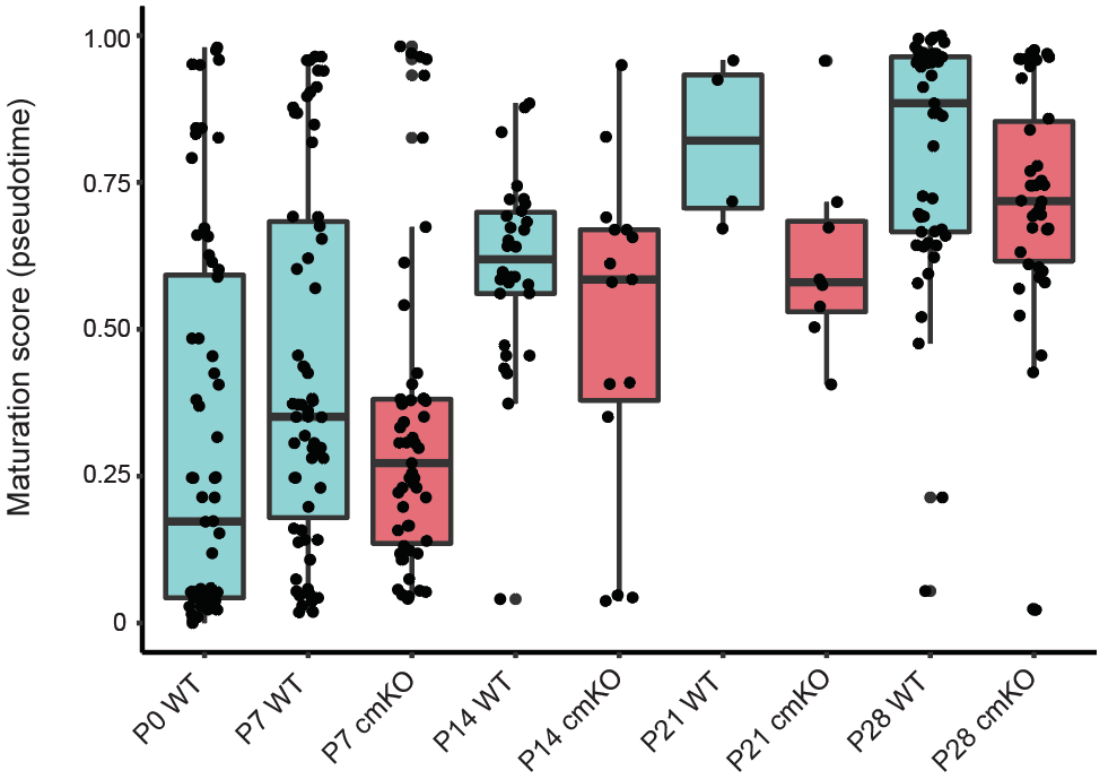

Figure 3-9. Maturation score by timepoint and condition showing cmKO cells are transcriptomically immature

heart. This is important as it may ameliorate batch effects caused by dissociation, sorting, and sequencing. Since PSC-CMs arrest at a late embryonic to neonatal stage, we were most interested in the P0 to adult development. The mosaic knockout allows us to determine its role during the critical window previously identified. We decided to deliver the AAV9-cTnT-Cre at P0 as there may have been challenges in dosing, consistency, and efficiency when attempting to deliver the virus through the pregnant mouse.

Our measurements of PGC1 cmKO indicated that PGC1 is required for hypertrophy. This was initially surprising since PGC1 is a co-activator of transcriptional activators of mitochondrial genes. Although we were not able to quantify the volume change, we did see that area was significantly reduced. We confirmed that this was not due to off target effects from the AAV9 vehicle. It also resulted in functional changes

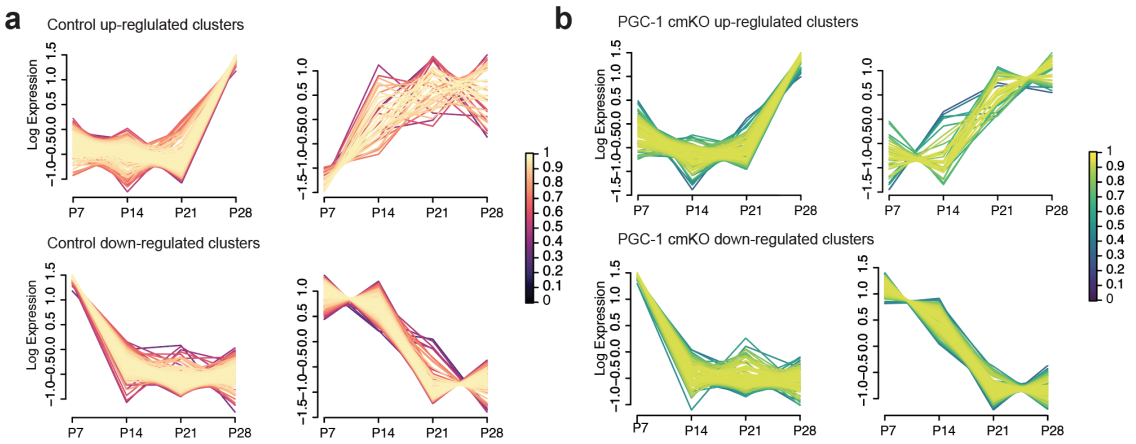

Figure 3-10. Fuzzy clustering of gene expression patterns in control and cmKO. Upregulated clusters and down regulated clusters were selected for each group.

to calcium handling and contractility. Knockout of PGC1 leads to disruption of the gene regulatory network of maturation. This indicates that it is key to development. When comparing the differentially expressed genes, we see that it includes metabolic and fatty acid oxidation genes, as expected, but also includes contraction genes. This indicates that PGC1 may directly or indirectly regulate non-metabolic aspects of CM maturation.

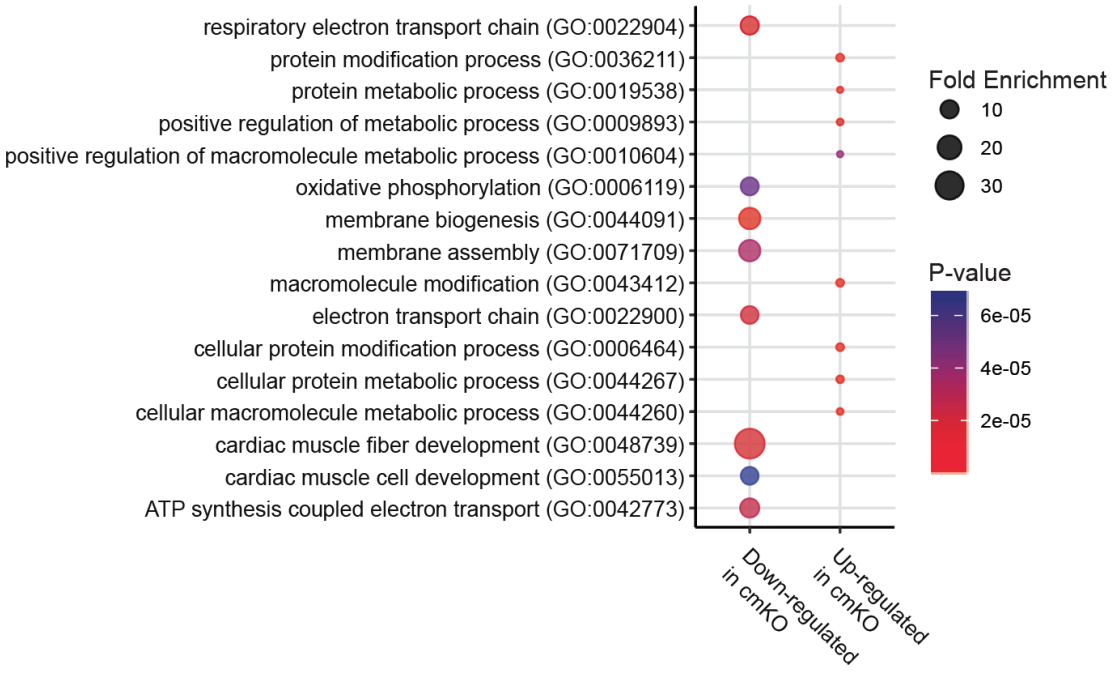

Figure 3-11. GO terms for differentially expressed genes from a comparison of control and PGC1a cmKO separated into up and down regulation

Chapter 4

PGC1a promotes maturation in PSC-CMs

Background

Cardiomyocyte maturation is a leading obstacle holding them back from entering the clinic or for widespread use in pharmacological testing and disease modeling. Many strategies have been used to improve including electrical stimulation, stretching, culture on a surface, co-culture with fibroblasts. However none of these alone or in combination have yielded mature myocytes. Therefore, we aim to use our new insight into the gene regulatory network of CM maturation and test the idea that PGC1 activation can promote maturation. We propose that PGC1α is a driver of maturation and will test this in immature PSC-CMs. Small molecules have previously been used to improve maturation as T3 and Dexamethasone lead to PSC-CM hypertrophy, increased contractility, and other aspects.[47,48] A combination of these with culture on a matrigel mattress was able to form t-tubules in PSC-CMs. However, when cultured on matrigel coated tissue culture plastic, a network of t-tubules does not form so our expectation is not that this will produce fully mature myocytes. Future studies could investigate combining this with 3D tissue culture, but that is outside of the focus of this study.

PGC1 had been identified as a predicted upstream regulator and was confirmed

as required for CM maturation. Our next goal was to see if it had the ability to improve PSC-CM maturation. We used genetic and small molecule techniques to activate PGC1. We quantified the effect of PGC1 agonist treatment on cell size, force production, and metabolic capacity.

Materials and Methods

Stem cell culture and differentiation

Human (H9) and mouse embryonic stem cells (E14) were differentiated into cardiomyocytes. All Johns Hopkins Medical Institutions and US NIH guidelines for culture and disposal of stem cells were followed. Mouse ESCs were maintained in a flask coated with 0.1% gelatin for 5 minutes. Stem cell maintenance media (GMEM + 10% FBS with 1 uM PD98059, 3 uM CHIR99021, Glutamax 1:100 (Thermo Fisher Scientific), non-essential amino acids 1:100, and sodium pyruvate 1:100). PSCs were differentiated into cardiomyocytes by forming emrbyoid bodies over 48 hours by plating 80,000 cells/ mL into an uncoated 25 cm plate in differentiation medium (75% IMDM, 25% Ham's F12 (Cellgro), B27 without vitamin A, N2, BSA, glutamax, penicillin/streptomycin, L-ascorbic acid, and α-monothioglycerol. After the 48 hour embryoid body formation, the media was changed to differentiation media containing Bmp4 and Activin A. Precisely 48 hours later, cells were dissociated and plated onto a gelatin-coated surface in differentiation medium with XAV939 added (Sigma). PSC-CMs generally start being 7-8 days after emrbyoid body formation and were then selected by using a 4mM lactate DMEM media without glucose or 1 µM puromyocin. PSC-CMs were replated onto new gelatin coated 24 or 96 well plates for treatment with PGC1α or PPAR agonists.

Electron Microscopy

2% FA in 0.075 cacodulate with 5 mM MgCl2 was used to fix D30 PSC-CMs overnight at 4C. Samples were then rinsed with a 3% sucrose buffer 3 times for 15 minutes then treated with 1.5% KFeCN6 and 2% osmium at 4C for 2 hours. They were then rinsed with 3% sucrose and 0.1 M maleate buffer at pH 6.2 for 10 minutes three times. They were then placed in 2% UA in sucrose/maleate buffer for 1 hour in the dark. They were dehydrated using an ethanol ladder starting at 30% and going to 100% ethanol for 5 minutes in each bath. Samples were then treated with propylene oxide followed by an EPON resin with the catalyst overnight while rocking. Next, samples were treated with EPON resin and catalyst for 2 hours then put in an oven for 48 hours at 60 C. A Diatome diamond knight was used to cut sections and then collected on a 2x1 mm formvar-coated slot grid. They were stained with uranyl acetate then lead citrate. To image the slices, a Hitachi H-7600 TEM operating at 80 kV was used. Then an AMT XR-50 CCD was used to digitize the images.

Mitochondrial functional assay

A Seahorse XFe96 Analyzer was used to measure respiration rates. Before measurement, CMs were plated in a 96 well XF96 Cell Culture Microplate (ALigen Technologies) at 1.5e4 cells per well. They were cultured for 72 hours. Prior to the assay, medium was changed to RPMI without phenol red and sodium pyruvate was added. Cells were cultured in an incubator without supplemented carbon dioxide for 1 hour. Using the Mito Stress Test protocol and Seahorse Extracellular Flux Assay Kit, OCR was measured with inhibitor final concentration of 2.5 uM for Animycin A, Oligomycin, and Rotenone and 1 uM for FCCP.

Immunostaining and Confocal Imaging

PSC-CMs cultured on gelatin coated coverslips were rinsed with PBS then fixed in 4% paraformaldehyde for 10 minutes. They were rinsed with PBS for 5 minutes 3 times then stored in excess PBS at 4 C until staining. Samples were rinsed 1 time with PBS for 5 minutes then 0.2% Triton X-100 was added for 10 minutes. They were rinsed 3 times then 1% Bovine Serum Albumin and 1% Fetal Bovine Serum was added for 1 hour. Primary antibody was added to 1% Bovine Serum Albumin and 1% Fetal Bovine Serum at dilution of 1:200 then stored on a rocker overnight at 4 C. Samples were removed and rinsed 3 times with PBS for 5 minutes. The fluorescently conjugated secondary antibody was diluted 1:500 in PBS then placed on the rocker for 1 hour at room temperature. This and all future steps were conducted without light by placing the dish in a drawer or under aluminum foil to prevent photobleaching. Samples were rinsed 3 times for 5 minutes in PBS. Samples were counterstained with DAPI diluted 1:2000 and WGA diluted 1:100 in PBS. They were rinsed 3 times in PBS for 5 minutes each and placed on a glass slide with a droplet of ProLong Diamond. Coverslips were sealed using clear nail polish. A Leica SP8 was used to image samples using photon-counting mode with a 63x oil immersion objective.

Contractility experiments

Human PSC-CMs were analyzed using an high throughput automated calcium handling system in collaboration with the Colas laboratory at Sanford Burnham Prebys Medical Discovery Institute. Video imaging was analyzed for calcium transients.

Statistics

ANOVA with post hoc Bonferroni tests were used to determine significance in comparison of 3 or more groups. Statistics were completed using R or excel analysis toolpak. Student's t-test was used for a comparison of 2 groups.

Results

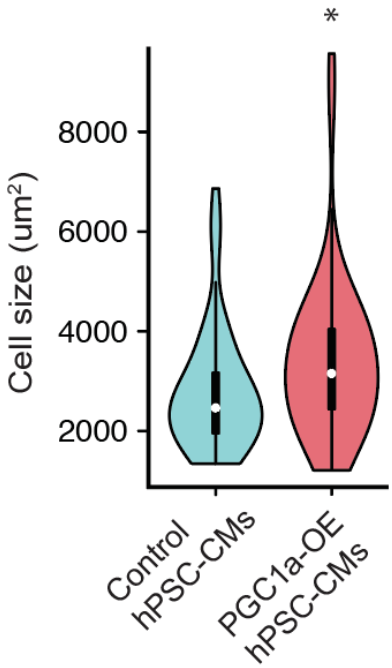

Figure 4-1. PGC1α overexpression increases PSC-CM size. Student's t-test was used. *=p-value<0.05. Control n=55, PGC1α-OE n=46

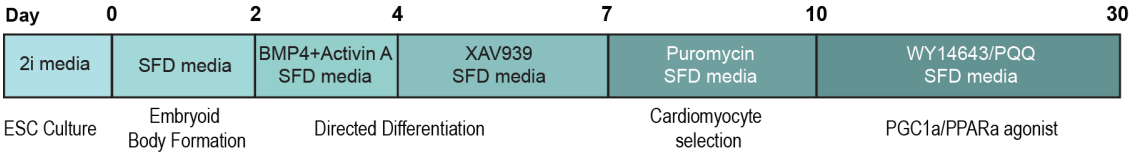

Figure 4-2. PSC-CM differentiation timeline. PSCs are cultured in 2i media. Embryoid bodies form over the first two days. Media is changed and supplemented with BMP4 and Activin A. Cells are dissociated and replated onto gelatin coated tissue culture plates. After beating occurs, puromycin or lactate selection is performed. Agonists or DMSO control are added to cell starting on d10.

PGC1/PPAR agonists increase size

Since PGC1 is misregulated in PSC-CMs with lower expression levels and it is required for aspects of CM maturation, we looked into the ability of activation of PGC1α in PSC-CMs to promote maturation. We overexpressed GFP-PGC1α in PSC-CMs and

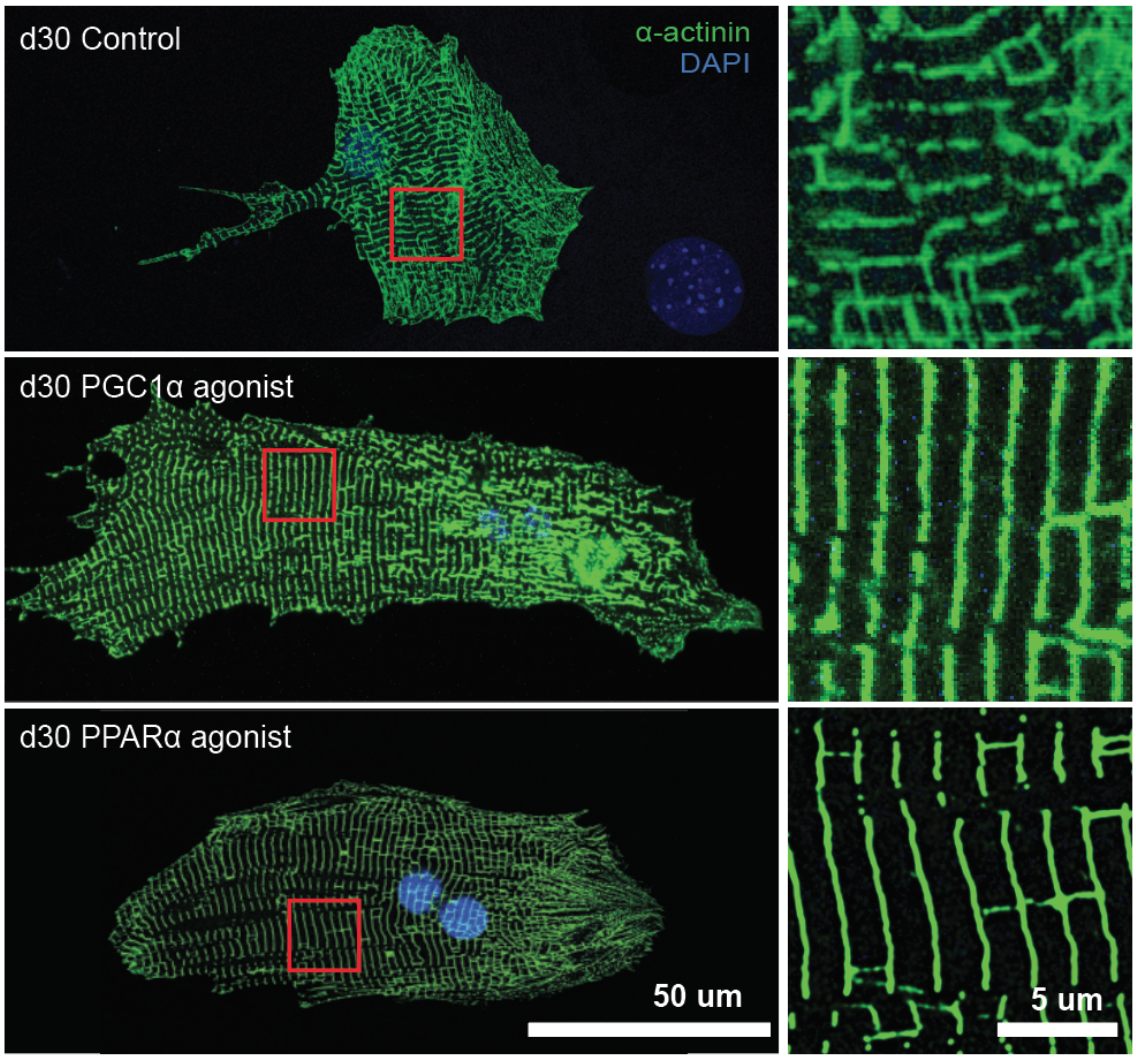

Figure 4-3. Staining of sarcomeres show better organization and elongation of agonist-treated PSC-CMs. Insets show better alignment of parallel myofilaments.

found a significant increase in the area (Figure 4.1). Therefore, PGC1α is involved in growth and hypertrophy of developing CMs. Since overexpression under a CMV promoter can lead to non-physiologically relevant levels, we used pyrroloquinoline quinone (PQQ) to activate PGC1α expression. Dr. Emmanouil Tampakakis performed the hPSC-CM differentiation and treatment.

Hypertrophic growth was observed in the PQQ-treated d30 myocytes (Figure 4.2). We found that WY14643, a PPARα agonist, was also effective in increasing cell size and sarcomere organization in blind measurements at d30 following 20 days of agonist

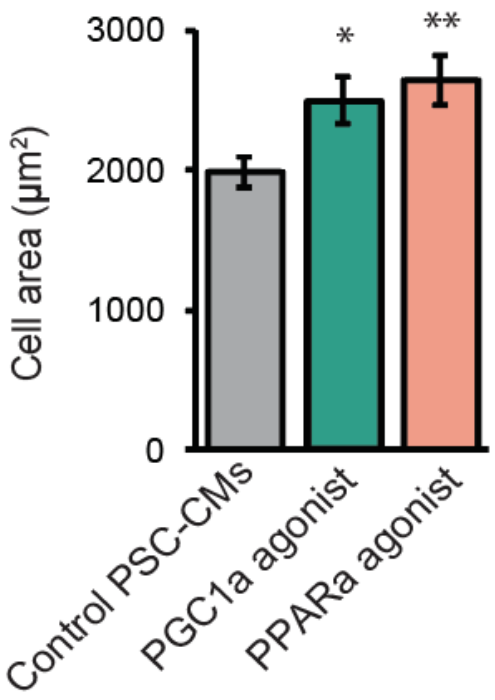

Figure 4-4. Cell area of PSC-CMs treated with PGC1/PPAR agonists. ANOVA followed by post hoc Bonferroni tests were used. *=p-value<0.05, **=p-value<0.01. Control n=192, PGC1α agonist n=162, PPARαn=119

treatment (Figure 4.3, 4.4). PSC-CMs were treated with the agonists from d10 to d30. Cell size was assessed by immunofluorescent staining of α-actinin and WGA, a cell surface marker, then imaged using confocal microscopy. Matthew Miyamoto differentiated and maintained most mPSC-CMs used in these experiments.

PGC1/PPAR activation improves mitochondrial function and contractility

One of the most important aspects of CM function is the contractility. To see if treatment with PGC1 and PPARα agonists resulted in increased force production, we used Fourier transform traction force microscopy (Figure 4.5). PSC-CMs treated with PQQ, WY14643, or a combination were compared to a DMSO control by replating them onto polyacrylamide gel with a Young's Modulus of 8 kPa and culturing 3 days before imaging on d30. The polyacrylamide gel stiffness was selected because it is close

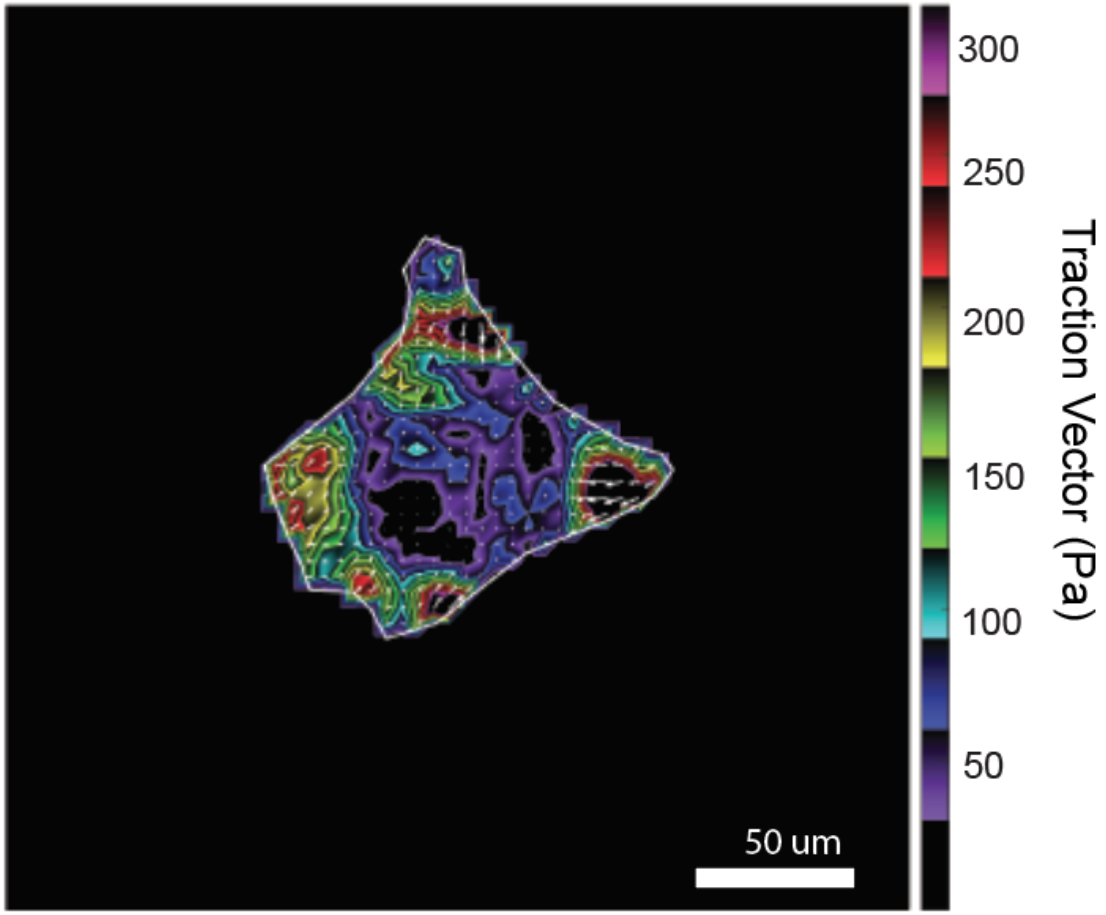

Figure 4-5. Heatmap showing force produced by PSC-CM and measured by Fourier transform traction microscopy

to that of the heart. High speed imaging was used to calculate the force produced as they deformed a gel containing fluorescent beads. Here, we see that PGC1α and PPARα increase force and that the combination results in less heterogeneity (Figure 4.6). These results indicate that PGC1/PPAR may be a driver of PSC-CM maturation. This work was completed in collaboration with Sam Paek and Dr. Steven An.

We were also interested in looking at the mitochondrial development since PGC1α is the master regulator of mitochondrial biogenesis. Transmission electron microscopy was used to quantify mitochondrial density of d30 PSC-CMs where we found that it more than tripled with treatment of PGC1α and PPARα agonists (Figure 4.7).

To characterize this mitochondrial function, we used a Seahorse analyze that

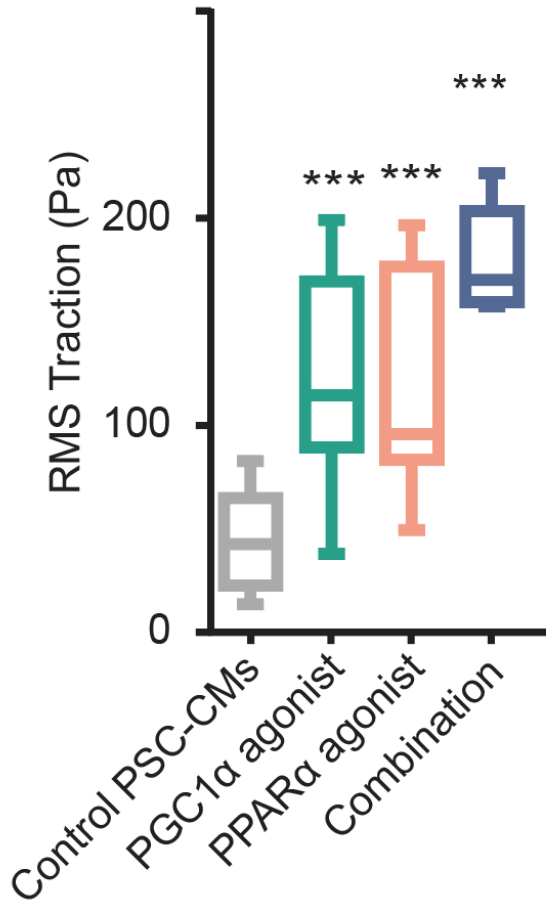

Figure 4-6. Force produced by agonist PSC-CMs show an increase in contraction force measured. ANOVA followed by post hoc Bonferroni tests were used. ***=p-value<0.001. Control n=5, PGC1α agonist n=6, PPARα agonist n=6, Combination n= 6

measures oxygen consumption rate. This provided the basal and maximal respiration of d30 mouse PSC-CMs treated with PGC1α or PPARα agonists or a combination of both. Maximal OCR normalized was significantly higher than the control cells (Figure 4.8). This indicates that they have more metabolic mitochondrial capacity consistent with higher mitochondrial density and large cell size. Since this works in mouse PSC-CMs, we wanted to confirm that this phenomenon was conserved in human PSC-CMs. We performed immunostaining for α-actinin and saw a larger cell size (Figure 4.9). Therefore, PGC1α 's role in maturation may be similar in rodents and humans.

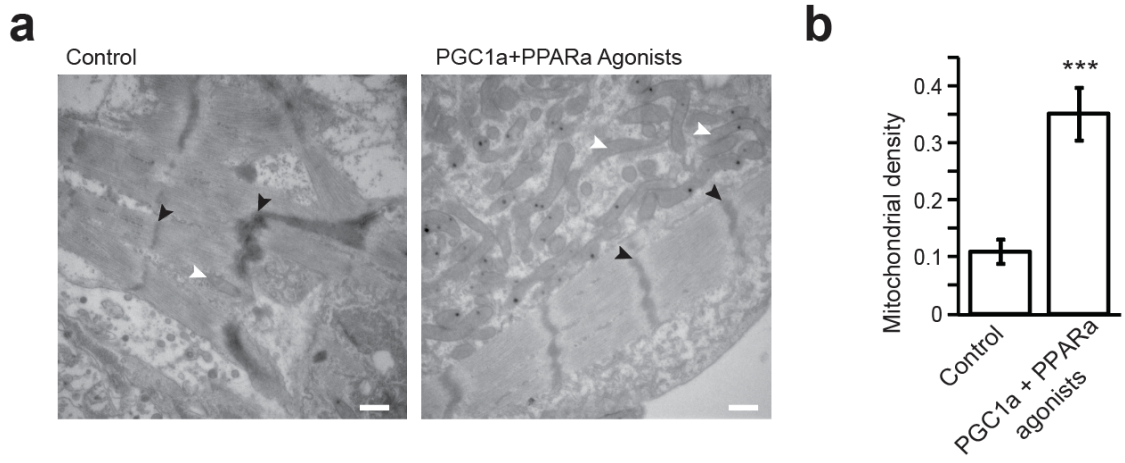

Figure 4-7. a. Electrion microscopy images of sarcomeres (black arrows) and mitoochondria (white arrows). b. Mitochondrial density from image analysis. Student's t-test was used. ***=p-value<0.001. Control n=9, PGC1/PPAR agonists n=14

Discussion

This shows that PGC1α activation promotes PSC-CM maturation. PGC1α has been characterized as a driver of mitochondrial biogenesis and is perinatal lethal. Since the heart forms normally, but cannot keep up with the need for cardiac output due to poor CM function, the defect is likely a cell autonomous one. As hypothesized, mitochondrial density was increased 3-fold. While mitochondrial maturation and ultrastructure was not investigated, oxidative phosphorylation capacity was measured through respiratory rate, which was significantly higher in those treated with PGC1α and PPARα. PGC1α activation resulted in increased cell size. This may be in part due to the increased energy produced as mitochondrial content provides a surplus of ATP. In addition, the higher mitochondrial content could take up more volume leading to larger cells. However, in a CASAAV knockout of mitofusin1 and mitofusin2, CM volume may be independent of mitochondrial function.[82] It is possible that PGC1α regulates expression of genes associated with hypertrophy.

PGC1α activates mitochondrial biogenesis and, importantly, increases contractile force. Our analysis of contractility through traction force microscopy showed that

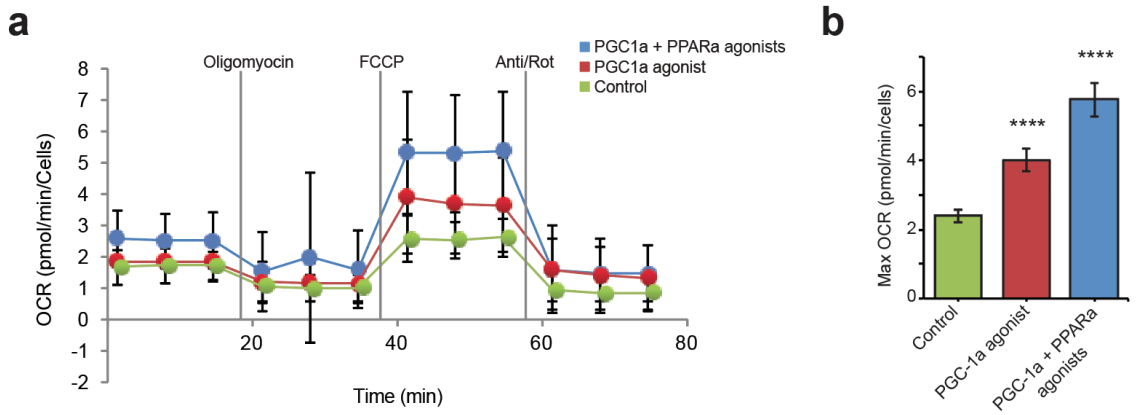

Figure 4-8. a. Oxygen consumption rate during Seahorse XFe96 stress test. b. Maximum OCR rate for treated PSC-CMs. ANOVA followed by post hoc Bonferroni tests were used. ****=p-value<0.0001. Control n= 17, PGC1α agonist n=18, PPARα agonist n=18

individual cells more than double in force production. This finding shows that PGC1α improves non-metabolic aspects of maturation. Combined with our data showing that calcium handling is altered in the PGC1 cmKO CMs, PGC1 could be a driver of multiple aspects of maturation. It is possible that they are intertwined and increasing one aspect of maturation leads to an increase in others, but this has not been demonstrated. Therefore, PGC1 could transcriptionally regulate other aspects of maturation through a mitochondrial independent mechanism.

Since PGC1α co-activates PPARα and PPARα activation also improves maturation, it could be that PGC1α predominantly acts through the activation of PPARα in promoting non-metabolic maturation. It is known that PPARα leads to upregulation of fatty acid oxidation genes and peroxisomal genes, but it is not known how. PPARα is a nuclear receptor that binds fatty acids. Multiple reports have shown that supplementing media with fatty acids promotes maturation in PSC-CMs. This could provide insight into the signaling mechanism responsible for fatty acids driving maturation. However, it is not well understood how fatty acid activation alters sarcomere organization, binucleation, and electrophysiological properties of PSC-CMs.

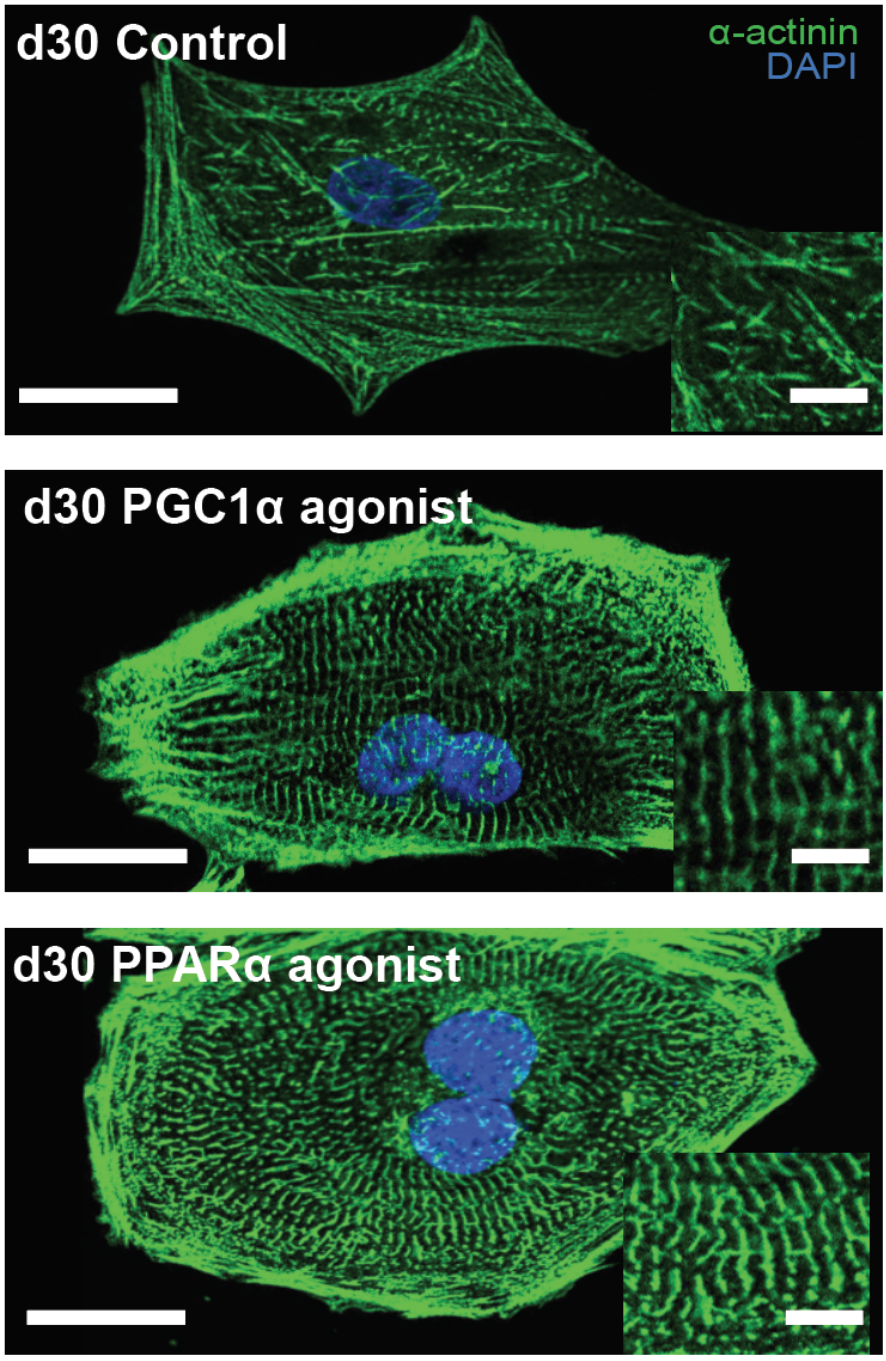

Figure 4-9. Agonists increase size of human PSC-CMs and form more organized sarcomeres

Chapter 5

Mechanism of action

Background

YAP in cardiomyocytes and in growth

Yes-associated protein (YAP) is a transcriptional co-activator that is important for growth and proliferation. It is inactivated through phosphorylation by the Hippo kinase cascade, which regulates organ size. YAP binds with TEAD1-4 to bind DNA and drive cell cycle progression. YAP/TAZ are able to act as mechanosensors that regulate single cell volume through maintaining intracellular cytoplasmic pressure.[113] Perez-Gonzalez *et al.* showed that this is independent of mTor, another regulator of cell size.

Altering Hippo/YAP signaling has been a therapeutic target to regenerate cardiac tissue through activating the CM cell cycle.[114] YAP has been shown to directly regulate a subunit of phopshoinositol-3-kinase in cardiomyocytes.[115] This shows that YAP can activate the PI3K-Akt pathway to promote cell division through blocking GSK-3β and increasing β-catenin levels.[116] YAP has also been shown to regulate proliferation in PSC-CMs based on the density of cell culture.[117] FAT4 regulates YAP1 control of heart growth as a part of the non-canonical Hippo pathway.[118]

Hippo/YAP controls the size of the organ by regulating cell proliferation and death. The adult heart growth occurs by hypertrophy rather than proliferation and this process

is influenced by YAP activation. It has been proposed that it is dose dependent where low levels drive hypertrophy and higher levels promote proliferation.[119] YAP's control of hypertrophy was investigated through a cardiac specific heterozygous knockout in TAC mice which lead to lower levels of hypertrophy and higher levels of fibrosis and apoptosis.[120] Inhibition of YAP in diabetic mice with TAC prevents the development of heart failure.[121] Hippo/YAP have been implicated as a mediator of physiological cardiac hypertrophy following exercise in adult rats.[122] In addition to regulation of proliferation and growth, YAP/TAZ may regulate metabolism and mitochondrial function, particularly in the metabolic remodeling in heart failure.[123]

Splicing in cardiac development

RNA splicing is the removal of introns from pre-mRNA and joining together of exons to form the mature mRNA.[124] Alternative splicing is the removal of exons in different combinations resulting in many mature mRNAs from a pre-mRNA. The majority of genes have been shown to undergo alternative splicing. This highly conserved, post-transcriptional process is performed by the spliceosome, which is a complex made of small nuclear RNAs (snRNAs) and proteins that recognize splice sites to position and catalyze the cutting. Splicing occurs in the nucleus by the major spliceosome and in the cytoplasm by the minor spliceosome, which recognizes different introns and is associated with alternative isoforms.[124] An array of different types of splicing can occur including skipping exons, removing mutually exclusive exons, retaining introns, and editing exons.

Splicing has been shown to play a key role in heart development and disease. Kalsotra and colleagues used splicing arrays to find 63 alternative splicing events in heart development linked to the CELF protein that is later downregulated 10 fold by adult timepoints. RNA-binding motif protein 24 (Rbm24) has been shown to regulate cardiac splicing events. Rbm24 knockout is embryonic lethal and null mice have struc-

tural heart defects with CMs exhibiting no sarcomerogenesis.[125] Postnatal maturation also includes alternative splicing changes as SFRS1 splices calmodulin-dependent protein kinase, cardiac troponin T, and LIM-domain binding3. A conditional knockout of SFRS1 resulted in death 6-8 weeks after birth as hearts dilated cardiomyopathy. Alternative splicing has been found to cause some myotonic dystrophies so therapeutics have emerged as a way to skip exons. SRSF2 is another protein where cardiac-specific null mice develop dilated cardiomyopathy, but do not die as a result.[125] SRSF2 is thought to splice the ryanodine receptor 2 postnatally. Aberrant splicing in cardiomyocytes has been shown to be both the cause of disease and the consequence of other mutations. Spliceosome component mutations can lead to muscular atrophy. Mutations in the splice sites can also lead to disease as heart disease can be caused by a cardiac troponin T 2 or myosin binding protein-C splice site mutation. In addition, a stressed heart can switch to alternative splicing of cardiac genes into the fetal isoforms including myomesin and titin. Next-generation sequencing has unleashed the potential to study alternative splicing.[126]

SF3B1 and SF3B2

The SF3B complex is part of the spliceosome and combines with U2 small nuclear ribonucleoprotein particle (snRNP). SF3B recognizes branch point sequences, which mark the 3' end of an intron and are used for to remove introns. It also has a role independent of U2 snRNP in exporting RNA by recruiting the transcription-export complex.[124] Splicing factor SF3B2 (also known as SAP145 and SF3b145) is highly conserved and has not been studied in the heart. SF3B2 has been shown to create a splice variant of the androgen receptor.[127] This was demonstrated in prostate cancer cells, but other targets of SF3B2 are unknown. Photoactivatable ribonucleoside-enhanced crosslinking immunoprecipitation (PAR-CLIP) was used to show that SF3B2 binds exons that are included and introns that are excluded from the androgen receptor

variant mRNA. SF3B2 can be altered through dimethylation of arginine residues by protein arginine methyltransferase 9 (PRMT9) to create alternative splicing.[128] SF3B2 has been implicated in regulation of cell cycle progression as the viral protein R (VPR) of human immunodeficiency virus type 1 induces cell cycle arrest.[129] This occurs by VPR binding SF3B2 to prevent formation of the SF3B complex and depletion of either SF3B2 or SF3B4 results in cell cycle arrest.

SF3B1, another member of the 7 component SF3B complex, has been linked to hypoxia-inducible factor 1a (HIF1a) and an alteration of fructose metabolism in heart disease.[130] HIF1a drives the transcriptional response to low oxygen levels that occur in heart failure. SF3B1 was identified as a target of HIF1a by its hypoxia response element in its promoter region. Mirtschink and colleagues showed that SF3B1 alternatively splices ketohexokinase (KHK), a fructose-metabolizing enzyme, from KHK-A to the high fructose affinity KHK-C. Fructose metabolism initiated by hypoxia leading to hypertrophy and diastolic dysfunction. Knockdown of SF3B1 via shRNAs in a transverse aortic constriction (TAC) treated mouse heart prevented the pathologic cardiac hypertrophy by preventing the switch to the KhK-C isoform.[130] It appears that SF3B family members may regulate key aspects of maturation including proliferation and metabolism.

In this chapter, we wanted to identify the mechanism of how PGC1 promotes non-metabolic aspects of maturation. Based on gene expression in maturation, we examined the role of YAP1 in PGC1's regulation of hypertrophy. We used a high throughput screen of putative PGC1 targets by measuring the effect of siRNAs on calcium transients to determine how PGC1 regulates calcium handling.

Materials and Methods

Chromatin Immunoprecipitation

Hearts from P7 mice were isolated, rinsed in PBS and minced following the protocol from van den Boogaard *et al.* They were fixed in 1% paraformaldehyde crosslinking buffer for 15 minutes then transferred to a crosslinking buffer with 125 mM glycine for 5 minutes.[131] Samples were washed twice with ice cold PBS then frozen and stored at -80 C. They were thawed and placed in 1 mL PBS on ice then homogenized at 20,000 rpm for 30 seconds until no chunks were visible. Samples were centrifuged at 2300 x g for 5 minutes at 4 C. The supernatant was discarded then resuspended in 1 mL of lysis buffer with protease cocktail for 1 hour at 4 C then ground with dounce homogenizer 20 times. DNA was fragmented using sonication for 20 cycles of 30 seconds on and 30 seconds off at 50% power. Shearing efficiency and distribution of read size was optimized through visualization on a 2% agarose gel. Each sample containing 3 P7 ventricles were diluted to 3 mL.

Contraction and Calcium Single Cell Analysis

The contraction kinetics of cardiomyocytes were measured by tracking the disturbance in the patterns of calcium oscillation. This was observed with Ca^2+-sensitive fluorescent dyes that were used to measure the effect on cardiomyocyte beat rate and pattern. The effect of siRNAs and small molecules on CM beating rate and contraction were measured by tracking calcium oscillation with a custom module in MetaXpress. The traces are the contraction pattern for a single representative cell. The contraction intensities were normalized to control for each siRNA-treated sample. We used two separate experiments to generate CM contraction data.

Statistics

ANOVA with post hoc Bonferroni tests were used to determine significance in comparison of 3 or more groups. Statistics were completed using GraphPad Prism software (2019) or excel analysis toolpak. Student's t-test was used for a comparison of 2 groups. Unpaired nonparametrix Kolmogorov-Smirnov test was used in the screen.

Results

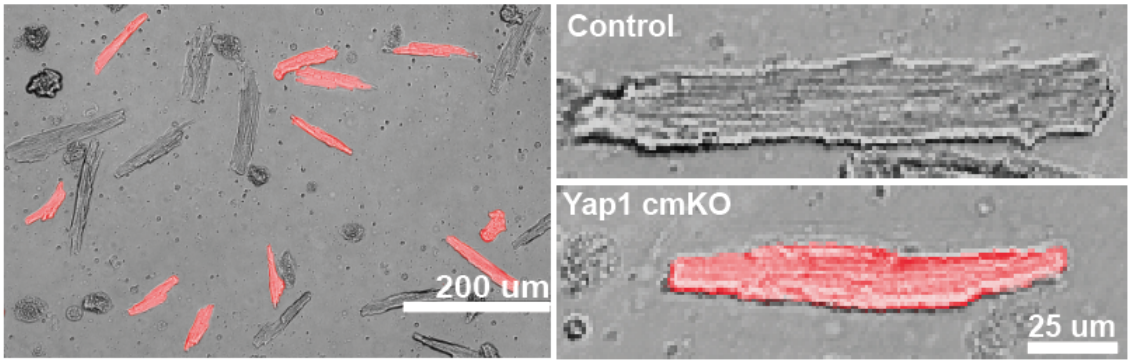

Figure 5-1. Brightfield and fluorescent imaging of dissociated YAP1 cmKO CMs

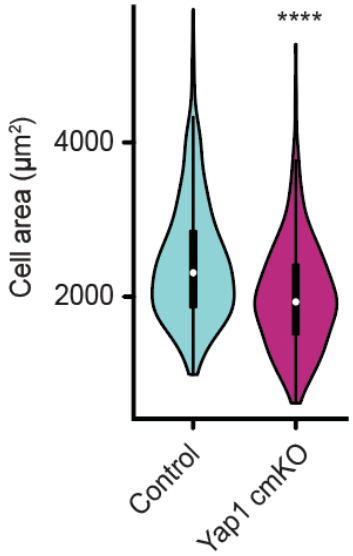

Figure 5-2. Image analysis of YAP1 cmKO shows cell area decreases compared to control CMs. Student's t test was used. P-value *<0.05

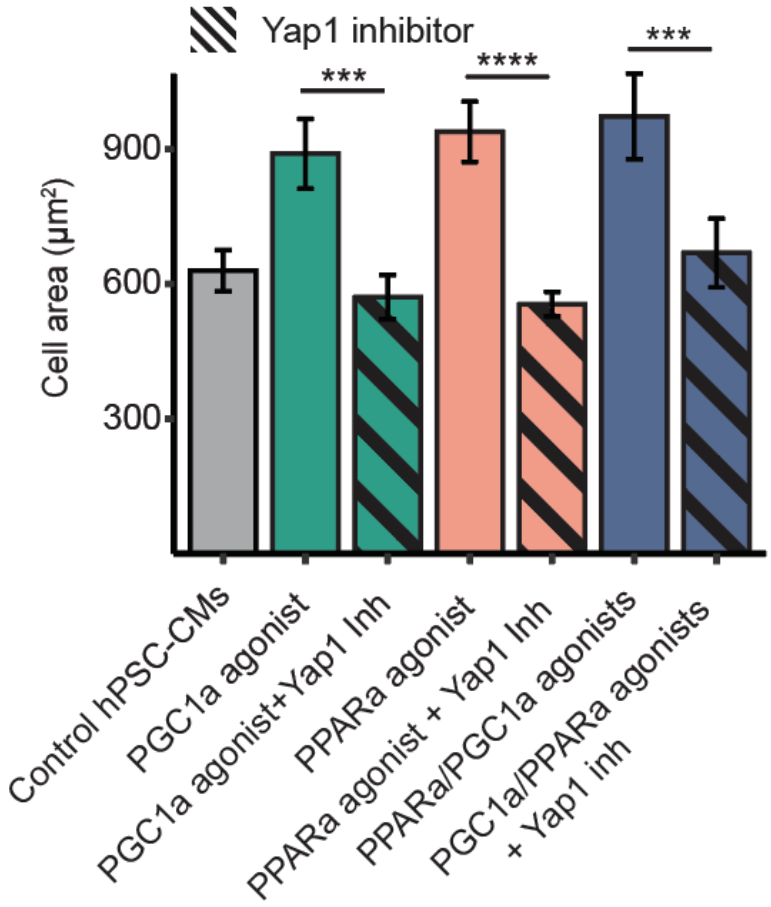

Figure 5-3. Cell area measurements for PGC1/PPAR agonist related PSC-CM. Addition of YAP1 inhibitor blunts the increase in cell size. Error bars represent SEM. P-value *<0.05 **<0.01 ***<0.001. Control n= 35, PQQ n=36, PQQ+YAP Inh n=43, WY n=59, WY+YAP n=40, PQQ+WY n=31, PQQ+WY+YAP Inh n=22

YAP1 is required for CM hypertrophy

To determine how PGC1/PPAR activation led to hypertrophy, we looked at the expression trends of known regulators of cell size. Examining *mTOR*, *YAP1*, and *IGF1*, we found that *YAP1* was downregulated in PGC1 cmKO cells at P7. To see if YAP1 affected cell size, we generated a YAP1 cmKO mouse and dissociated cardiomyocytes. AAV9-cTnT-Cre was injected at P0 into YAP1 flox/flox and cells were analyzed on P33. We saw a significant reduction in cell size in the postnatal YAP1 cmKO at P33 (Figure 5.2). Sandeep Kambhampati was responsible for analyzing the

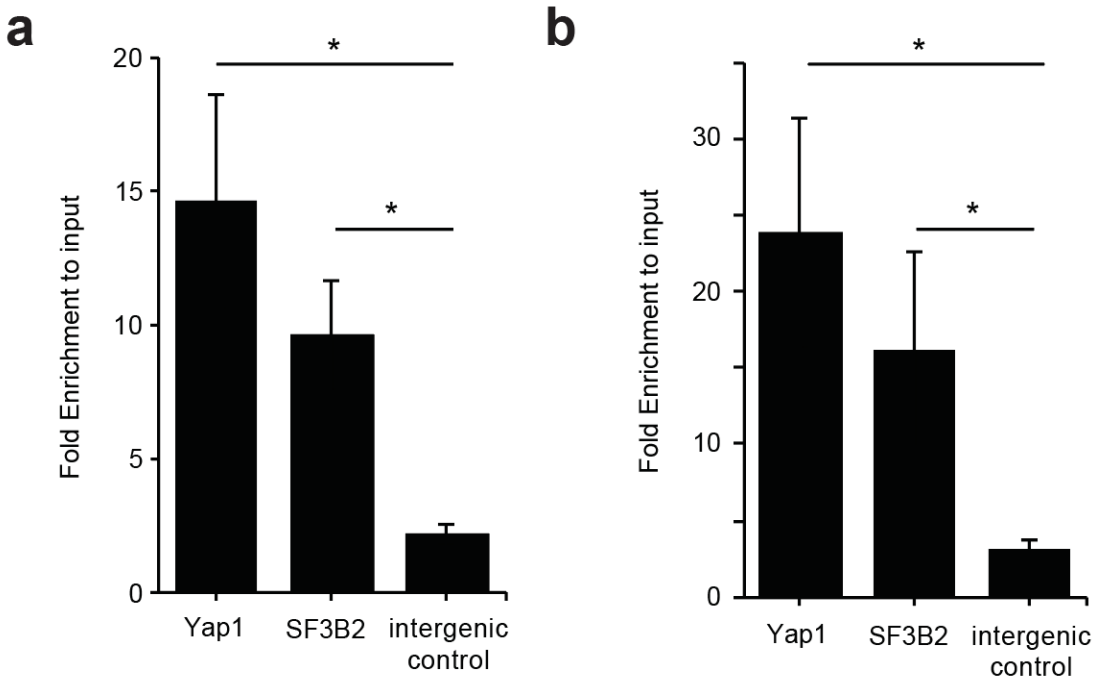

Figure 5-4. ChIP-qPCR shows enrichemnt of (a) PGC1α and (b) PPARα at the promoters of YAP1 and SF3B2. ANOVA followed by post hoc Bonferroni tests were used. *=p-value<0.05. n=6

images for cell size.

We next wanted to test whether YAP1 mediates the improvement in hypertrophy from PGC1/PPAR activation. To test this, we treated d15 hPSC-CMs with PGC1α agonists and YAP1 inhibitor (R)-PFI-2 for 72 hours and found that YAP1 blocked the increase in cell size (Figure 5.3). This indicates that YAP1 is needed for PGC1/PPAR activation to promote hypertrophy. This showed that YAP1 plays a postnatal role in hypertrophy associated with CM maturation. Another study had shown that PGC1α binds upstream of YAP1. We used chromatin immunoprecipitation combined with custom designed qPCR primers targeting the upstream region of YAP1 and found it to be enriched (Figure 5.4). We validated this finding by looking at the enrichment of known targets of PGC1/PPAR (Figure 5.5). This confirmed that control sequences were not enriched while the promoter regions of known binding sites were enriched.

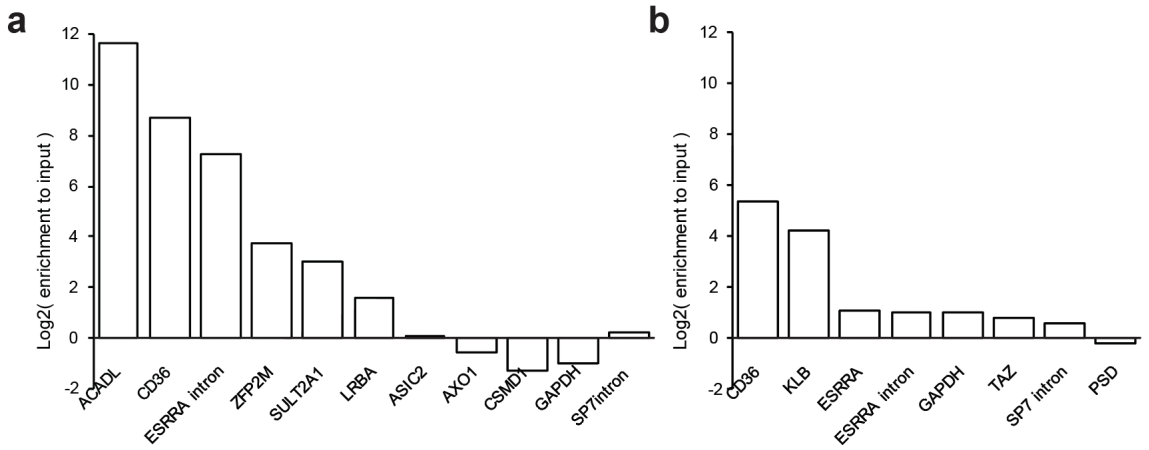

Figure 5-5. Antibodies were validated for (a) PPARα and (b) PGC1α known promoter binding sites.

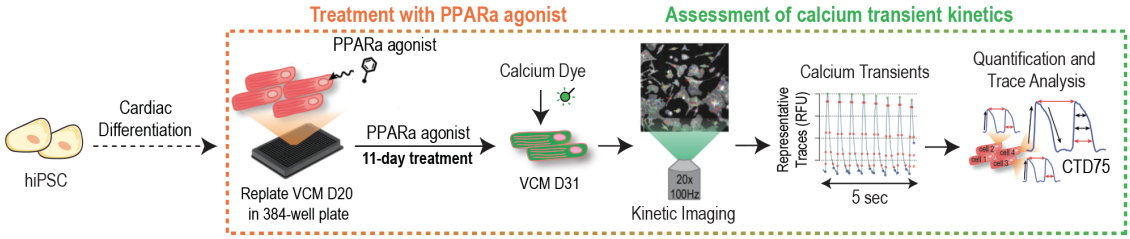

Figure 5-6. Experimental design to measure calcium transient kinetics in PPARα agonist treated PSC-CMs

Functional siRNA screen identifies SF3B2

Our measurements of calcium transients in vivo cmKO showed decreased function. We sought to determine how PGC1/PPAR regulate calcium handling. We used single cell high-throughput calcium handling function measurements to see how WY14643 altered calcium transients after 11 days of treatment following differentiation (Figure 5.6). We found that agonist treated PSC-CMs have shorter calcium transient duration (about 30ms shorter KS-D = 0.3114). The peak rise time was shortened from by about 10 ms showing faster intake of calcium and shorter calcium transient duration (Figure 5.7). This indicates that PGC1 and PPAR improve maturation through improving PSC-CMs ability to perform calcium uptake and release associated with a sarcoplasmic reticulum. These experiments were done in collaboration with Dr. Anais Kervadec

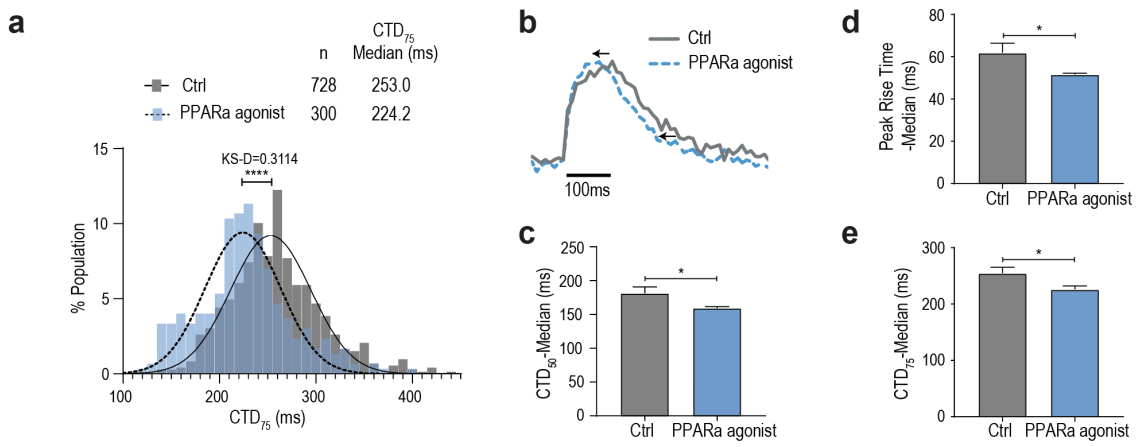

Figure 5-7. a. Distribution of calcium transient duration (CTD) 75. b. Sample calcium transient trace. c. median peak rise d. CTD50 shows a decrease in PPARα agonist treated PSC-CMs d. CTD75 shows the same. Error bars represent standard deviation. Student's t-test was used. * p-value < 0.05. n= 3

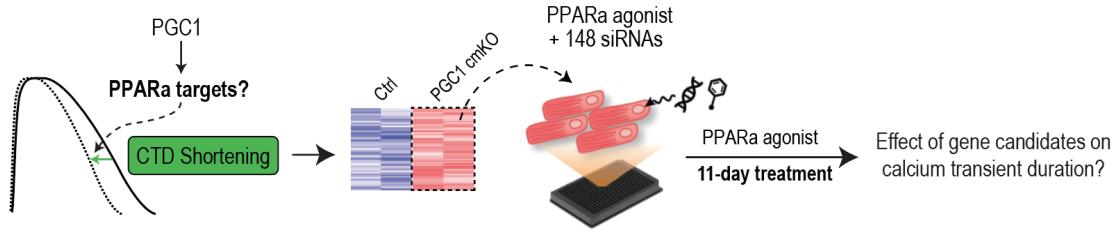

Figure 5-8. Schematic for functional siRNA screen to determine PGC1/PPAR targets regulating calcium handling. Student's t-test was used. *=p-value<0.05. n=4

and Dr. Alexandre Colas.

To determine how a PPAR ligand improves calcium handling, we used a high throughput screen of PSC-CM maturation. We had shown that 11-day teratment of WY14643 improved maturation so we selected genes that were downregulated in the single cell RNA-seq PGC1α cmKO dataset. We postulated that these genes are activated by PGC1/PPAR *in vivo* in maturation since they were lower in expression when PGC1 was knocked out. Therefore, we generated siRNAs targeting these 148 genes to see which would block the improvement in calcium handling. This would indicate which gene(s) PGC1/PPARα activate in order to regulate to calcium handling. PSC-CMs were differentiated and simultaneously treated with PPARα agonist

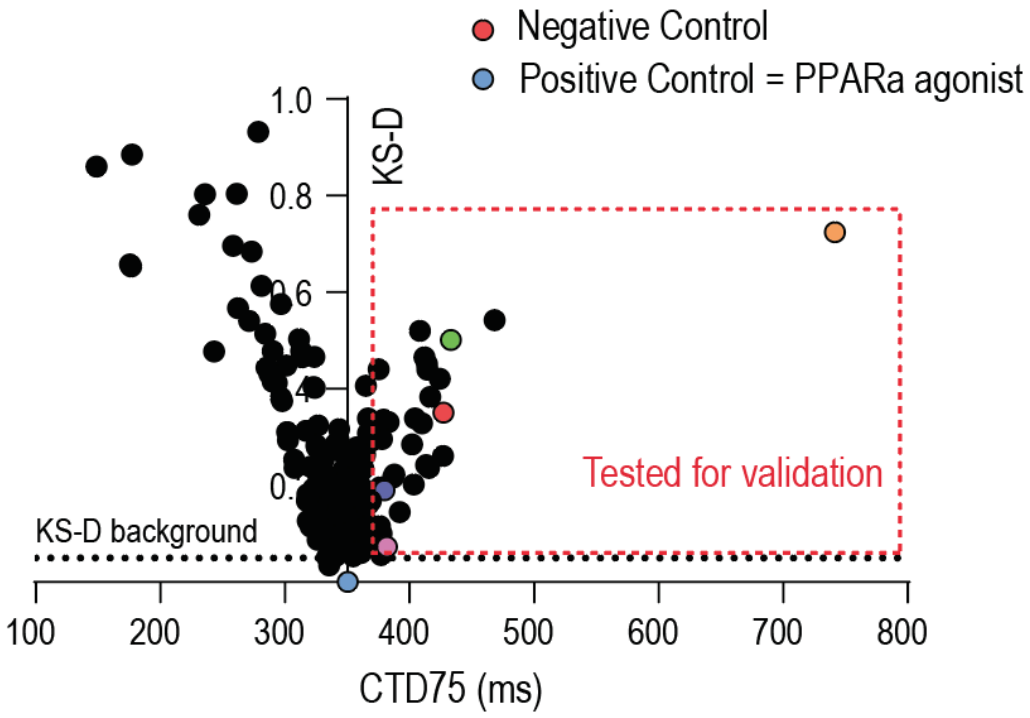

Figure 5-9. siRNA screen functional readout of CTD-75 and Kolmogorov-Smirnov Distance (KS-D). The positive control was PSC-CMs treated with a PPARα. Untreated PSC-CMs were the negative control. n=1

WY14643 and the siRNAs for 11 days (Figure 5.8). Calcium transients were automatically measured in a 386-well plate set and we selected all points that reduced CTD75 time to that of our negative control (Figure 5.9). These were then validated by repeating the experiment at n=4. The top 4 genes in terms of confidence were *SF3B2*, *SAP18*, *STRIP1*, and *TIMM50* (Figure 5.11). Representative calcium traces showing dysregulation in both the initial screen and the validation are shown (Figure 5.12,5.14). Using qPCR, we confirmed that the siRNAs, which were ordered from Dharmacon horizon as a smartPOOL of different siRNAs, were able to knock down mRNA levels (Figure 5.10). SF3B2 resulted in the largest change in CTD75 as it greatly elongated PSC-CM calcium transient duration (Figure 5.13). SF3B2 and SAP18 are splicing factors but have not been characterized in the heart. It is possible that these genes splice key calcium handling genes including ion channels and sarcoplasmic reticulum

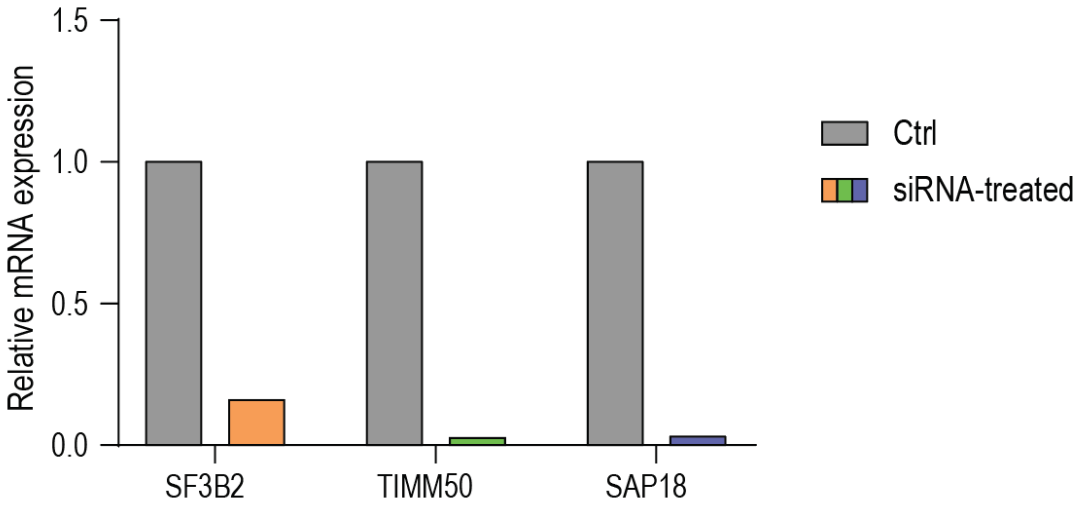

Figure 5-10. siRNAs are able to knockdown expression of targets efficiently. n=2

proteins.

Discussion

These results identify a novel link between PGC1 and YAP1 in CM maturation. YAP1 may have dual roles and it has been proposed that this is a dose-based response in that low levels of YAP activation result in hypertrophy and high levels lead to mitosis.[123] Hippo/YAP have been linked to ERBB2 as drivers of CM re-entry into the cell cycle and regeneration following ischemic injury. Our expression pattern of YAP supports this idea because it is expressed at high levels in CMs with low maturation scores. We also showed that the effect of PGC1/PPAR agonist on cell size and hypertrophy is mediated by YAP as treatment with inhibitors prevents a significant increase in cell size.

This study identified SF3B2 and SAP18 as novel targets of PGC1/PPARα (Figure 5.15). All four factors increased CTD75, indicating that calcium reuptake and spontaneous beat rate were slower. Cardiac gene splicing has been investigated with progress made in Titin splicing and isoform switching. However, splicing factors

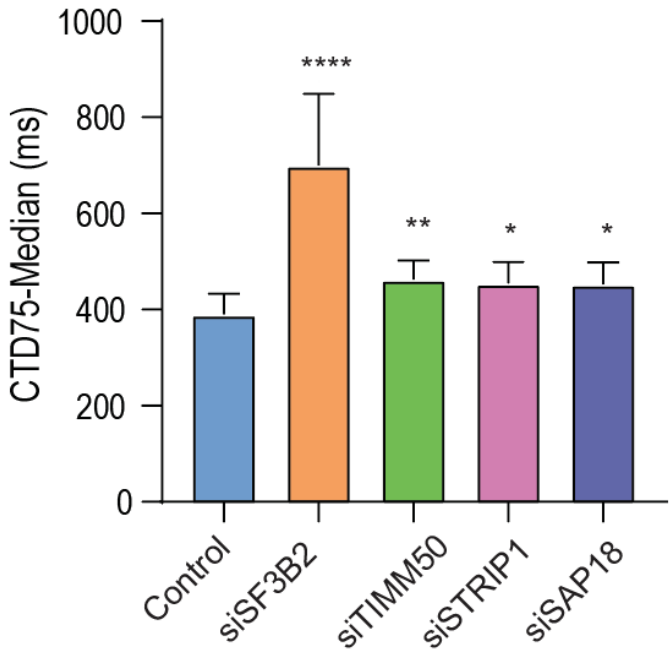

Figure 5-11. Median CTD75 shows validated screen hits significantly slow calcium transient dynamics. Error bars represent standard deviation. ANOVA with post hoc Bonferroni tests were used. P-value *$<$0.05 **$<$0.01 ***$<$0.001. n=4

as a critical regulator of maturation have not been studied. These splicing factors may be required for splicing of calcium exchangers or other genes associated with the sarcoplasmic reticulum. This suggests that PGC1/PPAR regulates maturation through direct regulation of genes involved in calcium handling rather than a mitochondrial-dependent mechanism where calcium transient shapes are improved by higher levels of ATP in the cell. Additional work would be needed to confirm this hypothesis.

The screen and subsequent validation also discovered TIMM50 and STRIP1. TIMM50 is a mitochondrial inner membrane translocase. Further investigation is required, but it may show that PGC1 also acts through a mitochondrial-dependent mechanism of promoting PSC-CM maturation. Striatin-interacting protein 1 (STRIP1) is expressed at high levels in the embryo and is known to regulate cytoskeletal organization. Overall, we have seen PGC1/PPAR improve PSC-CM maturation through regulation of the expression of SF3B2 and YAP1 to improve calcium handling

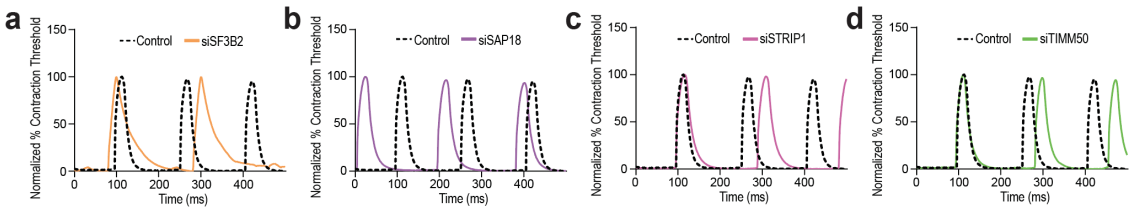

Figure 5-12. Contraction dynamics of control and siRNA treated PSC-CMs from the validation experiments. These are representative traces.

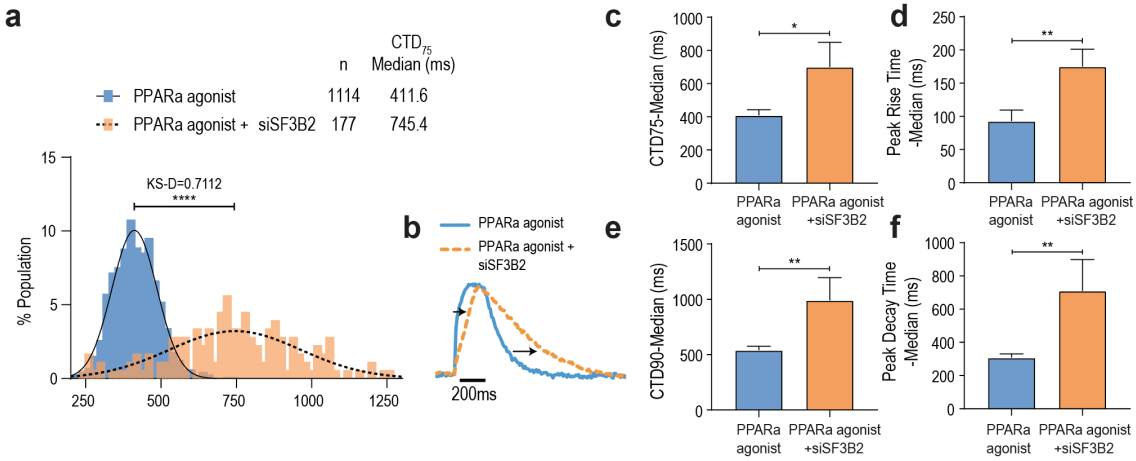

Figure 5-13. Calcium transient quantification of siSF3B2 treated hiPSC-CMs. a. distribution of individual cells CTD75. b. representative traces of calcium transient. c. Median CTD75. d. Peak Rise time median. e. CTD90 median. f. Peak Decay Time median. Error bars represent standard deviation. Student's t-test was used. P-value *<0.05 **<0.01. Control n=4, siSF3B2 n=3

and CM hypertrophy.

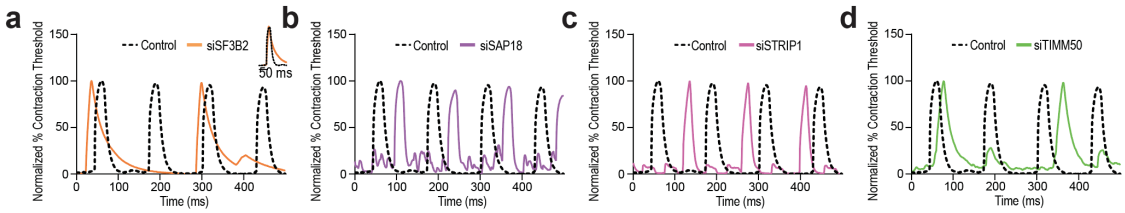

Figure 5-14. Contraction dynamics of control and siRNA treated PSC-CMs from the initial screen. These are representative traces.

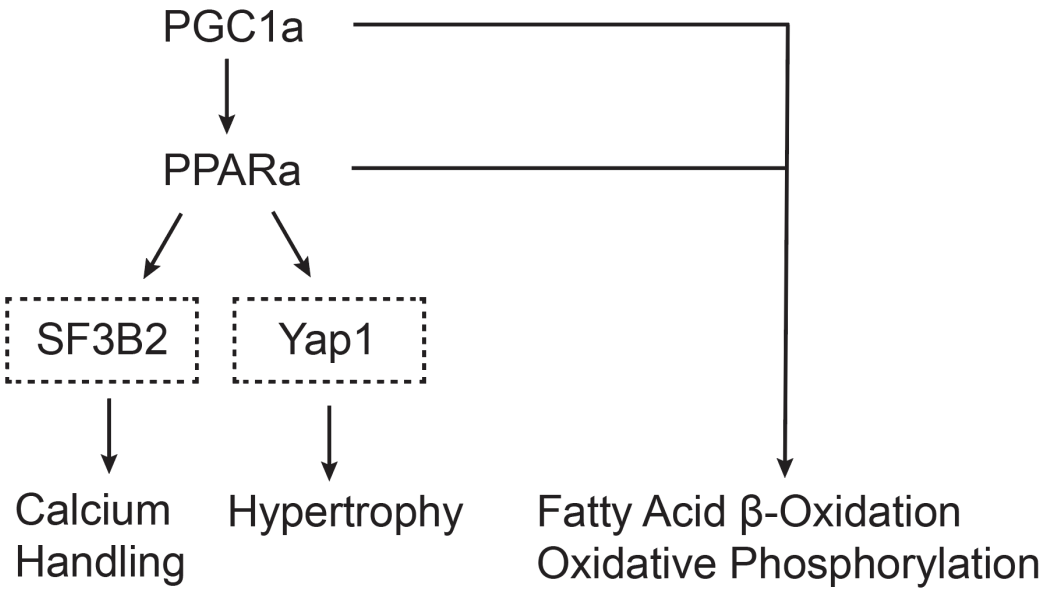

Figure 5-15. Working hypothesis for the role of PGC1/PPAR in CM maturation.

Chapter 6

Multiorgan maturation

Background

miRs in maturation

microRNAs are small 22 nucleotide RNA molecules that bind to mRNAs and lead to their degradation.[132] MicroRNAs are present in all cell types and some have been shown to be evolutionarily conserved. A single strand of RNA is transcribed and then forms a loop called primary miRNA which is cleaved by Drosha or Pasha to form the pre-miRNA. This loop is exported from the nucleus and cut by Dicer to form a mature miRNA.[133] These combine with an RNA-induced silencing complex (RISC) to regulate genes post transcriptionally by silencing them.[132] They do not have to be an exact match so each miRNA can have hundreds of targets.

MicroRNAs play critical roles in the differentiation and maturation of skeletal myocytes, erythrocytes, osteroclasts, neurons, retinal cells, cardiomyocytes, and adipocytes.[133–137] In a cardiac specific knockout of Dicer in the heart, mice develop dilated cardiomyopathy with postnatal lethality showing microRNAs are critical for heart function.[138] Treating fibroblasts with miR-1, miR-133, miR-208, and miR-499 were able to facilitate cardiac reprogramming.[139] Following microRNA-sequencing of day 20 PSC-CMs and 1 year old PSC-CMs, Let-7 was found to be highly upregulated.[140] Overexpression of let-7 in PSC-CMs promotes maturation by downregulation of the

PI3/AKT/Insulin pathway and increasing fatty acid oxidation.[140] One drawback of this is that 1 year cultured PSC-CMs are still immature compared to in vivo CMs. This motivated our decision to use microRNA-seq to study in vivo maturation. Overexpressing miR-125b, miR-199a, miR-221, and miR-222, which target ERBB4 signaling, was able to improve maturation that remained for 60 days after the transfection.[141] An integrated analysis of microRNA expression predicted miR-200c to be a blockade of PSC-CM maturation. Overexpression of miR-200c lowered levels of *Gata4*, *Tbx5*, and *Srf*. In addition, CACNA1C, a subunit of the L-type calcium channel was validated as a direct target.[142] These indicate that microRNAs play a crucial role in regulating gene expression and have been shown to repress and promote CM maturation.[143–145]

Global organ maturation

The transcriptome can be used to describe a unique signature for an organ and track the changes in gene expression over development. Organs change as they develop and the gene regulatory network governing their morphogenesis and maturation has not been described. With the goal of using RNA-seq to build profiles for use in pharmacological testing, 11 organs across 4 timespoints (2, 6, 21, and 104 weeks after birth) were collected in the rat in both male and female mice. They were able to identify splicing variants and sex-specific isoform expression.[146]

In an investigation of human embryonic development, Xue *et al.* built a database of gene expression from week 4 to week 9. However, they did not perform any analysis and proposed that this dataset be used for studies of development and disease.[147] In a subsequent comparison of embryogenesis in human and mouse, Xue and colleagues studied organogenesis similarities by looking for distinct temporal patterns of gene regulation.[148] Gene expression patterns were clustered by increases or decreases from each stage, but they did not characterize the biological relevance of these patterns or the genes in each cluster. They found that key genes in the Hedgehog, Notch, TGF-β,

and Wnt pathways were similarly regulated. These multiorgan datasets can be used to identify markers of maturation that are consistent between humans and mice.[8]

Cardoso-Moreira *et al.* used bulk RNA-seq to track differences in the rate of development across seven organs in multiple species including humans, rodents, rabbits, chickens, and macaques.[149] They found that the number of genes expressed decreases and have similar stages of transcriptomic development. In a separate study of this dataset, the dynamic expression of long noncoding RNAs (lncRNAs) was characterized. They found that there some lncRNAs are expressed across multiple lineages early on, but more organ-specific lncRNAs were predominantly expressed later on.[150] The Tabula Muris Consortium sought to build a transcriptomic single cell atlas. Previously they sequenced more than 100,000 cells from 20 different tissues in adult mice.[88] Most recently, they published a dataset of 350,000 cells from both male and female mice from 1 month to 30 months for analysis of aging. While this is a magnificent resource, neither focus on the key developmental window where cardimyocytes mature.[87] Most of these have been created as a resource rather than providing insight into the mechanism of maturation.

We are interested in identifying similarities in maturation across organs in both microRNA and mRNA expression. Using a microRNA-seq dataset of maturation in the brain, heart, and liver, we identify key microRNAs that are consistently upregulated in multiple organs. Using co-expression trends, we predict top regulators of global maturation from a meta-analysis of microarray datasets.

Materials and Methods

Data gathering

Affymetrix Mouse 430 2.0 microarray dataset were compiled from the National Center for Biotechnology Information (NCBI) Gene Expression Omnibus (GEO). Bioconduc-

tor in R was used to curate datasets from liver, heart, kidney, and brain. Datasets were selected to cover the major developmental stages from embryonic to adult. Datasets included 479 brain, 147 liver, 142 kidney, and 212 heart samples. All samples were wild-type non-treated conditions and were grouped into early embryonic, mid embryonic, late embryonic, neonatal, adolescent, and adult. Frozen robust multi-array average (fRMA) was used to normalize datasets.[151] Probe-sets with the largest dynamic range were selected to convert a probesets to gene official symbol.

Differential expression analysis

Differentially expressed genes were identified using limma in each specific organ.[152] Limma was used because it commonly used in microarray differential expression analysis whereas DESeq2 is designed for RNA-seq. We used a cutoff of p-value less than 0.01 and log fold change greater than 2.

Clustering

Principal component analysis (PCA) was used on the full probeset of expression data with the prcomp function in R. Gene expression data was collected by using probes with the largest interquartile range of expression. The mFuzz R package was used for fuzzy clustering.[112] We selected the number of clusters by iteratively increasing the clusters until the correlation between two clusters was greater than 0.85. The core genes with a membership greater than 0.5 were selected for further analysis.

Gene Regulatory Network Prediction

Weighted Gene CO-Expression Network Analysis (WGCNA) was used to group genes into modules by similarities in their expression patterns across samples.[97] The correlation network is a collection of pairwise correlations between genes that range from -1 to 1. Hub genes are centrally located in the group. Correlation networks were

made for each organ with a signed network using biweight midcorrelation, a maximum block size of 21000 and a soft thresholding power of 12. The developmental stages were set as an external trait so that each module could be correlated with time over maturation. The correlation with development and the p-value were used to select the most relevant modules. Genes were selected by taking the top 3000 based on module membership values or the top 300 genes based on intramodular connectivity scores. The consensus maturation network was made by using data from all organs. Ingenuity pathway analysis (IPA) was used to generate a list of predicted upstream regulators of maturation.

microRNA sequencing and analysis

Organs were harvested from E18.5, P0, P7, P14, and P28 mice. Tissues were cleaned in PBS the frozen at -80 C. RNA was isolated by adding 600 uL of TRIzol (Thermo Fisher Scientific). Tissue samples were homogenized then using Direct-Zol RNA isolation kit (Zymo Research). The Illumina TruSeq Small RNA Library Preparation kit with indexes 1-24 were used to prepare libraries for sequencing on a NextSeq 500 lane. FASTQ files were aligned with bowtie2 then aligned with featurecounts to the mouse genome.[92] The sRNAtoolbox was used to select hairpin and mature miRNA sequences present.[153] Differential expression analysis was completed with DESeq2 then visualized with ggplot2.[93]

Results

Cross organ maturation comparison

Since maturation has been shown to occur in multiple organs, we sought to investigate the similarities in development of the heart, liver, kidney, and brain. We compiled a meta-analysis of microarray data spanning early embryonic to adult timepoints from 980 samples. The expression was normalized using fRMA then visualized using

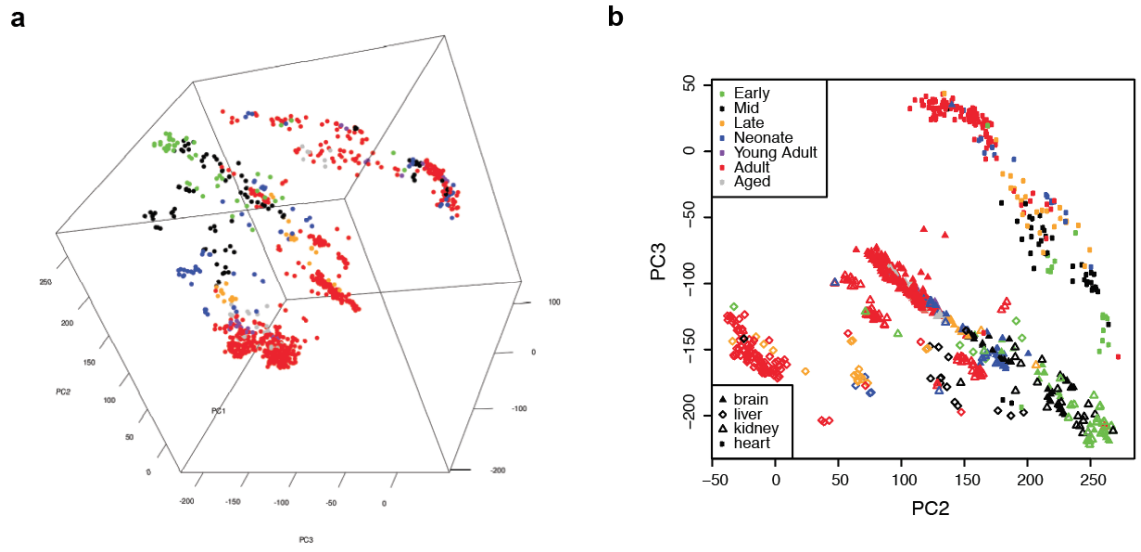

Figure 6-1. a. 3D PCA plot of multiorgan gene expression. b. PC2 and PC3 showing organ maturation with clustering at early stages.

principal component analysis (Figure 6.1). We see that the temporal pattern is captured by PC2 and PC3. PC1 primarily separates samples based on organ specific aspects of maturation. This shows that many of the early timepoints cluster closely together then diverge. However, they progress in the same direction. This indicates that there may be transcriptomic similarities. Our goal became to determine what common pathways are activated or repressed across multi-organ maturation. Individual PCA clustering of organ data (Figure 6.2) resulted in a clear clustering by timepoint and trajectory present in PC1. This indicates that there is a directional change in gene expression in all organs after formation that continues to occur postnatally.

To determine which genes were changing over the developmental trajectory, we used fuzzy clustering of expression. This normalizes each expression trend to a shape then groups genes based on that trend. This work was done in collaboration with Sandeep Kambhampati. Timepoints like E18.5 were binned by developmental stage such as late embryonic. We ran fuzzy clustering over the binned timepoints to generate clusters by increasing the number until cluster correlation was 0.85. The clusters with downregulation of genes were visually selected. There were two clusters per organ

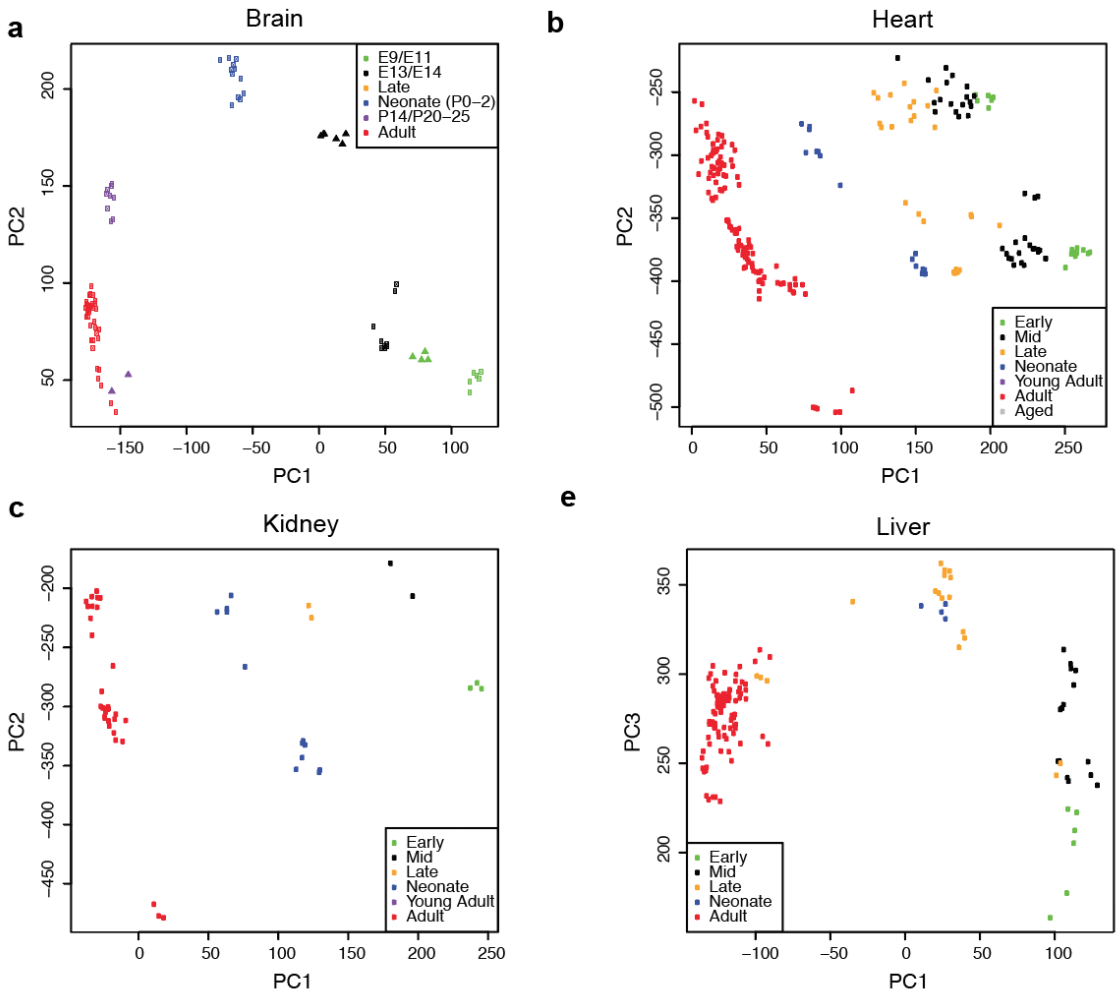

Figure 6-2. PCA plots showing time series trajectory for maturation of each organ.

where the core cluster genes continued to decrease in expression for each group (Figure 6.3). The genes in the decreasing expression clusters were selected for each organ and input into GO analysis to determine enriched GO terms through gene set enrichment analysis with a cut-off p-value of 0.05. From the 4 lists of GO terms, selected terms that were present in at least two of the lists were presented with their p-value and normalized enrichment score (NES) (Figure 6.4). The kidney and the heart have the most overlap in GO terms with the brain also showing enrichment for terms related to cell cycle. It appears that downregulation of cell cycle and mitotic genes are the most common terms present. This is expected as growth slows because the organ

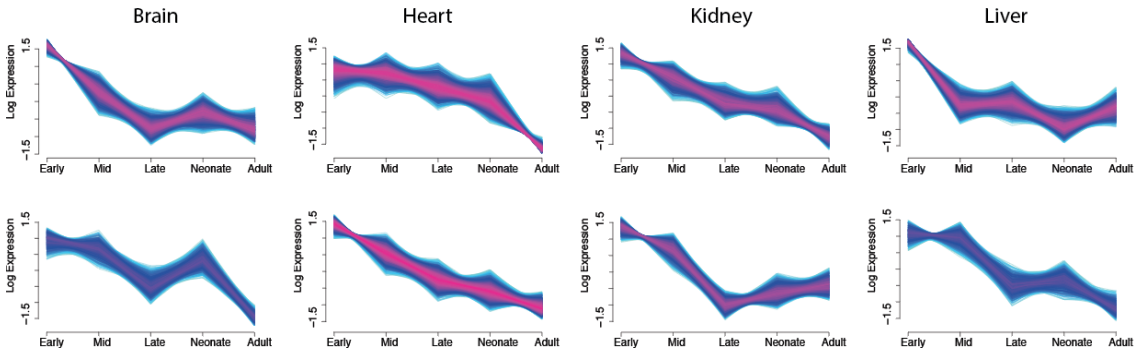

Figure 6-3. Downregulated gene clusters from fuzzy clustering for each organ.

reaches a steady state size. Cell cycle exit is a hallmark of maturation in multiple organs. The liver does not show enrichment for these terms. This could be caused by the regenerative nature of hepatocytes and epithelial cells of the bile duct. However, the liver overlap GO terms showed DNA conformational change, which could indicate that there is an alteration of chromatin structure in maturation, but continues in the cell cycle.

We then selected the upregulated gene expression patterns from the fuzzy clustering for each organ (Figure 6.5). GO analysis was run then a comparison of shared GO terms was compiled (Figure 6.6). There is a clear overlap in metabolic and mitochondrial-related GO terms such as fatty acid β oxidation and electron transport chain between the heart, liver, and kidney. The brain shows similar upregulation of genes involved in NFkB signaling along with calcium transport. The presence indicates an increased energy demand of the organs in adulthood compared to the embryonic and neonatal stages. The brain and kidney showed a strong enrichment of circadian rhythm genes.

We next sought to characterize the gene regulatory networks of the developing organs. First, the microarray dataset was used to generate a weighted co-expression matrix (Figure 6.7). Hierarchical clustering was then used to group co-expressed genes into modules. The eigenvalue of each module was calculated in relation to the developmental stage. This identified modules whose expression pattern was correlated

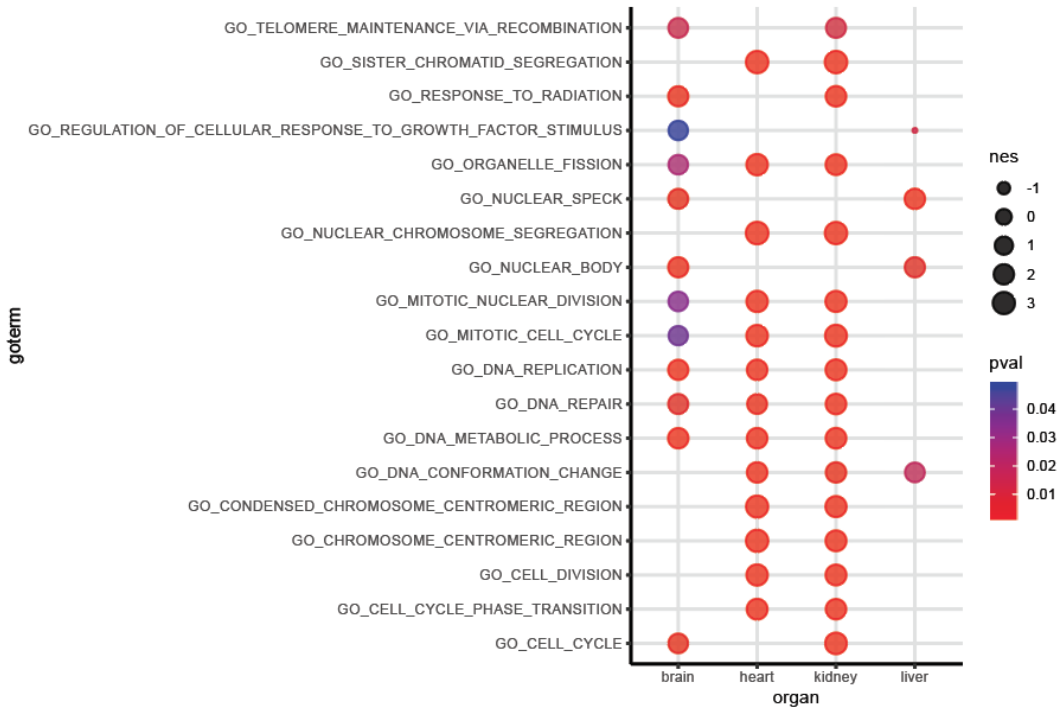

Figure 6-4. Top GO terms present in at least 2 individual organ GO term sets from fuzzy clustering downregulated clusters.

with time. We selected the top gene network modules positively and negatively associated with maturation for each organ. Genes that were present in multiple modules were selected and listed as hub genes.

After determining that cell cycle genes are commonly downregulated and the metabolic genes are upregulated, we wanted to identify upstream regulators. To predict the upstream regulators of maturation processes, IPA was used to evaluate the differentiatially expressed genes between stages and assess the activation state of regulators. The negatively enriched regulators which become more negative over time include cell cycle activators such as cyclin CCND1 and E2F family members such as E2F2, E2F3, TFDP1, and E2F1 (Figure 6.8). Other upstream regulators included MYC, IGF2BP1, and FOXM1. The same process was used to select the positive z-scored upstream regulators (Figure 6.9). As expected, multiple transcriptional regulators were related to mitochondrial and metabolic functions including PGC1α,

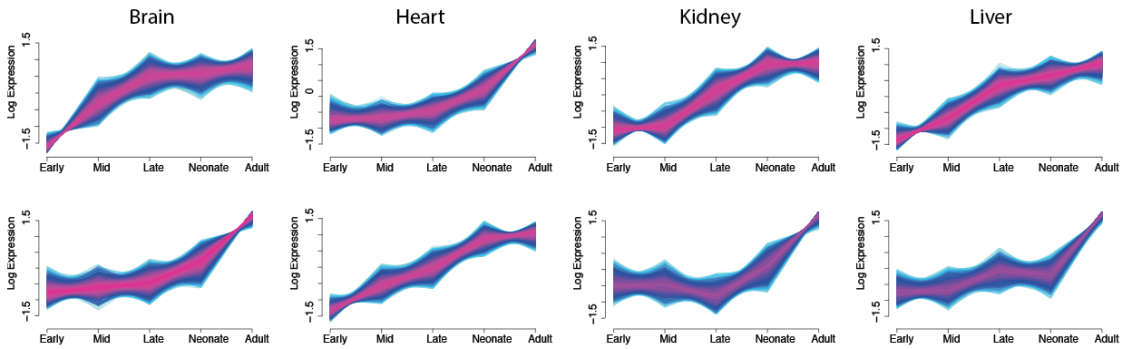

Figure 6-5. Upregulated gene clusters from fuzzy clustering for each organ.

PGC1β, PPARγ, and PPARα. This analysis also yielded cell cycle repressors including E2F6, TP53, and CDKN2A. Epigenetic regulators HDAC1 and HDAC2 are predicted to be positively activated during maturation across the heart, liver, brain, and kidney. Future studies could knock out these genes to see if maturation defects occur across multiple tissues.

microRNA across multiple organs in maturation

microRNAs have been shown to be very important in differentiation and maturation across multiple tissues. A cocktail of microRNAs is sufficient to induce cardiac cell fate reprogramming in fibroblasts. MicroRNA expression trends across multiple organs has not been investigated and may play a common role in post transcriptional gene regulation. To track miRNA expression, we used small RNA sequencing selected from the brain, liver, and heart at 5 timepoints from E13.5 to P28 in the mouse (Figure 6.10). We were able to map to both mature microRNA and primary microRNA (Figure 6.11). PCA clustering of each organ showed a temporal trend present in PC1. This indicates that microRNA patterns change with time showing that not only a few are differentially regulated. This may include gradual changes in microRNA or stage specific microRNA expression. We then plotted the PCA of all organs combined and found that they cluster by organ type rather than timepoint (Figure 6.12). This is a strong indication that the majority of microRNA expression is organ specific. Using a

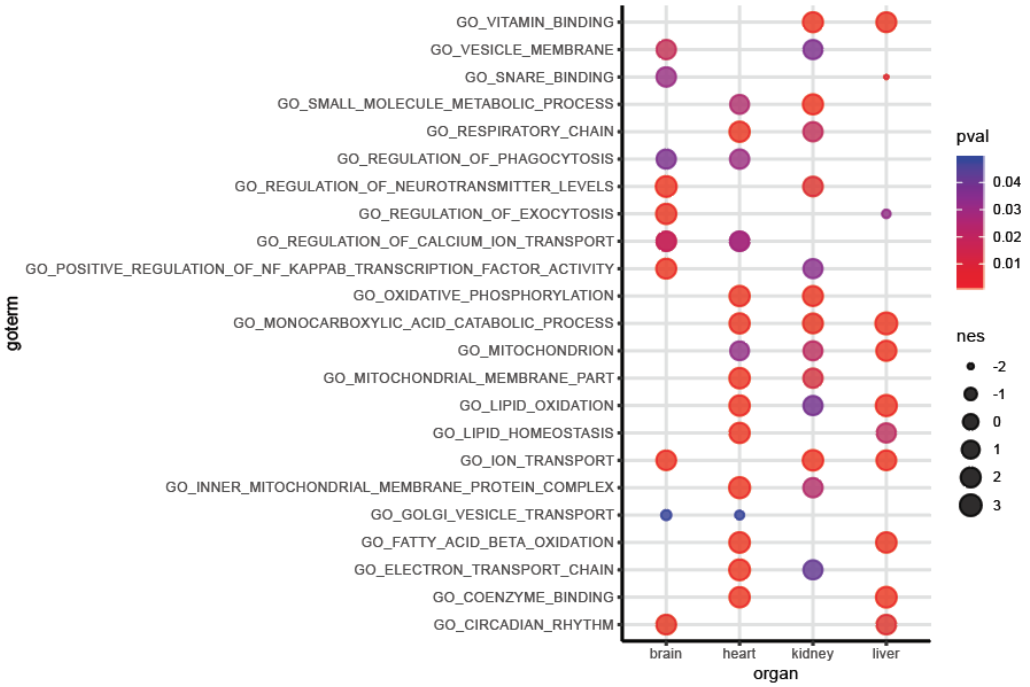

Figure 6-6. Top GO terms present in at least 2 individual organ GO term sets from fuzzy clustering upregulated clusters.

heatmap of normalized expression with hierarchical clustering of points, we see that the brain separates out while the liver and heart points are interspersed. Therefore the heart and liver may be more similar than the other pairings (Figure 6.13).

To identify the conserved microRNAs that are independent of organ type, differential expression was used to select microRNAs with a 2 fold change either up or down. The heart had 64 upregulated and 118 downregulated as brain had 112 up and 156 down and the liver had 64 up with 86 down. 11 microRNAs were conserved across the upregulated datasets and 13 from the downregulated miRNAs (Figure 6.14). Let-7 was found to be conserved in our upregulated dataset and has been shown to improve cardiac maturation when overexpressed.[140] miR-6538 is a downregulated microRNA across multiple organs(Figure 6.15). It may suppress mRNAs encoding maturation genes. In addition, miR-29c is an example of one that was consistently upregulated in all three organs to different extents. It may degrade transcripts that promote cell

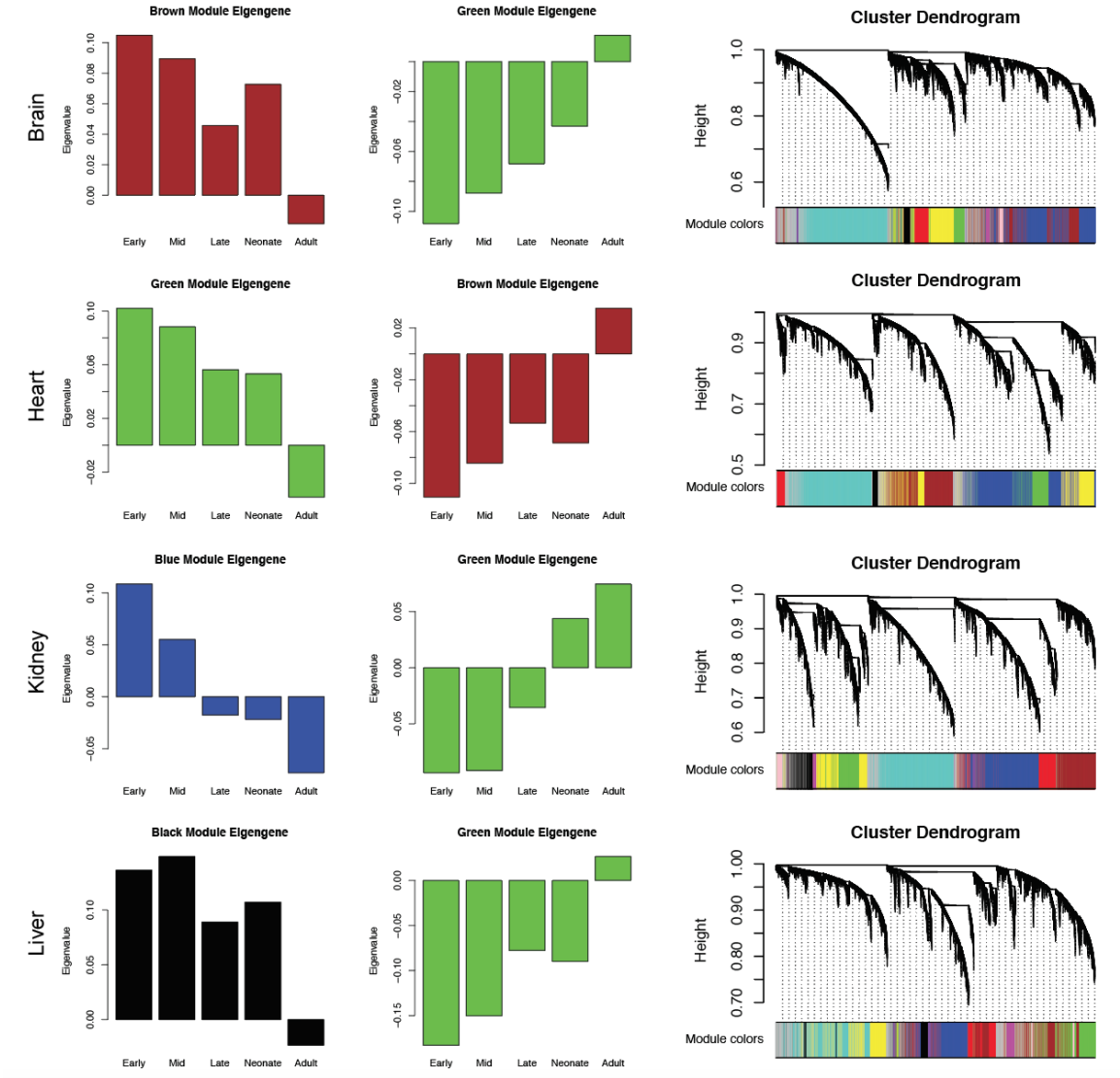

Figure 6-7. WGCNA modules positively and negatively correlated with maturation. Separate GRNs were constructed for each organ.

Figure 6-8. Heatmap showing the IPA activation scores of predicted upstream regulators between stages. This summarizes the top positively enriched transcriptional regulators.

cycle or immature processes.

Discussion

In a massive meta-analysis of publicly available microarray datasets, we developed a map of transcriptomic maturation for the heart, brain, liver, and kidney. We showed that organs progress in their gene expression changes. The maturation transition results in a traceable progression that forms a trajectory in PCA. Since PCA is a linear transformation, the distance between points on the plot is representative of the difference in gene expression. The combined PCA plot showing all organs indicates that they start close together then begin expressing organ specific genes. It is remarkable that they separate, but progress in the same direction. Using fuzzy clustering of gene trends and then interpreting those with GO terms, we discovered that cell cycle genes are commonly downregulated and metabolic genes are upregulated. This is expected since organs reach a steady-state size and cell turnover is reduced to maintaining that

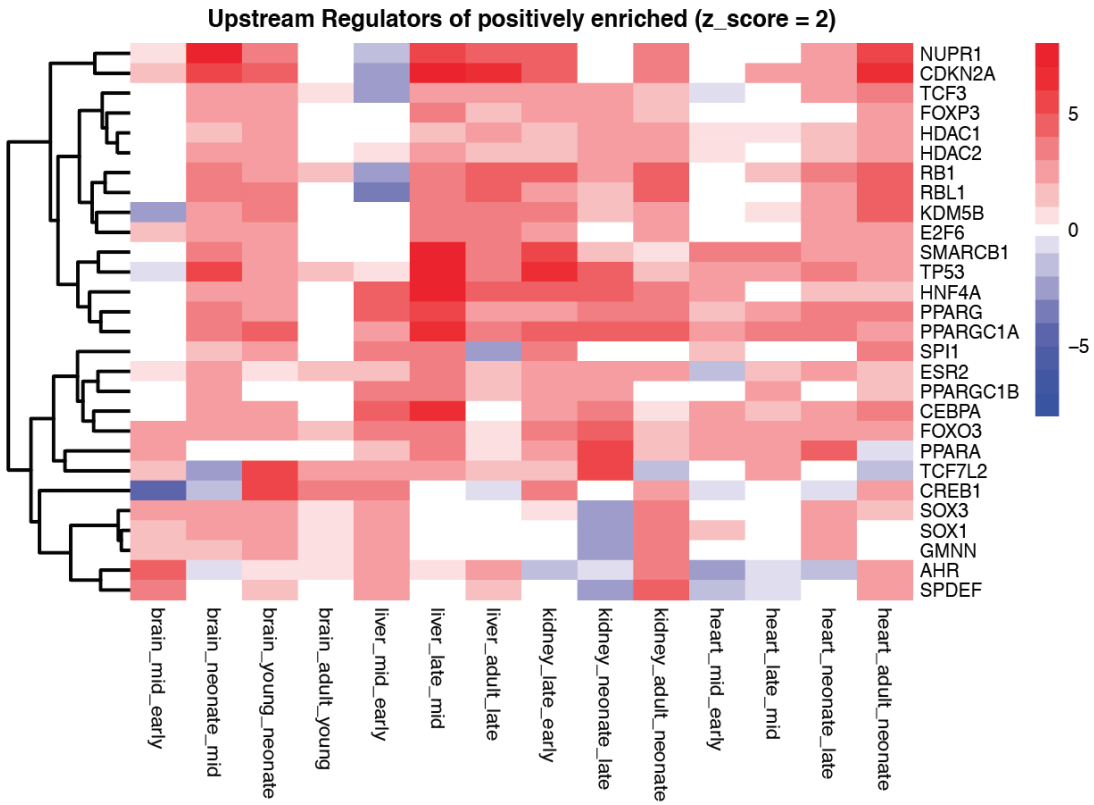

Figure 6-9. Heatmap showing the IPA activation scores of predicted upstream regulators between stages. This summarizes the top negatively enriched transcriptional regulators.

size. The rate of cell cycle differs as cardiomyocytes and neurons are not regenerative, while the liver is regenerative.

Differentially expressed genes that are up and downregulated for each organ were put into IPA to predict upstream regulations. We presented the activation score for top regulators. These matched our GO terms as metabolic and mitochondrial regulators were highly activated in maturation and cell cycle regulators were inactivated. This work was primarily descriptive as it looked for trends and specific genes and miRNAs in maturation that could be important. While we did not find a single pathway that controls all of maturation, we did construct a list of potential regulators that could be tested experimentally in the future.

In the analysis of microRNA trends, we were able to find microRNAs that have

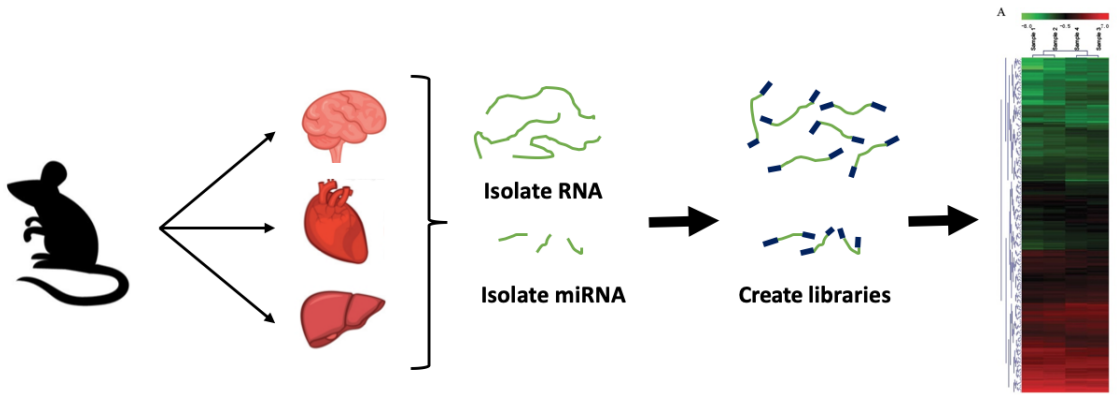

Figure 6-10. Experimental design of microRNA-seq. microRNA was collected from the brain, heart and liver then sequenced.

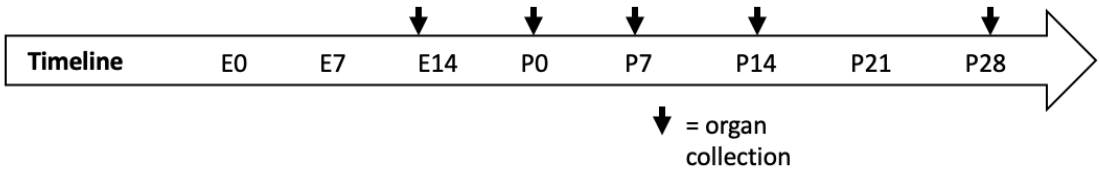

Figure 6-11. Timeline of organ collection for microRNA plots

similar trends. Since microRNAs alone have the ability to reprogram cells, it is possible that they have the ability to regulate maturation.[139] The next step for this work would be to compare the known and predicted targets of each of the top microRNAs. That may provide insight into which genes are suppressed during maturation. This could be combined with the transcriptomic data looking for maturation. Next, we plan on using qPCR to assess the expression levels of each microRNA in PSC-CMs to select dysregulated microRNAs for overexpression. These may promote maturation in PSC-CMs in vitro. In addition, we could run loss of function studies to examine the role they play in vivo. Suppressing miR expression can be challenging because regulation of microRNAs can be located in introns. Therefore antisense microRNAs and CRISPR/Cas9 methods have arisen as possible tools.[154,155]

After this project was completed, RNA-seq datasets became more prevalent. RNA-seq does not require probesets so it can measure the entire transcriptome revealing

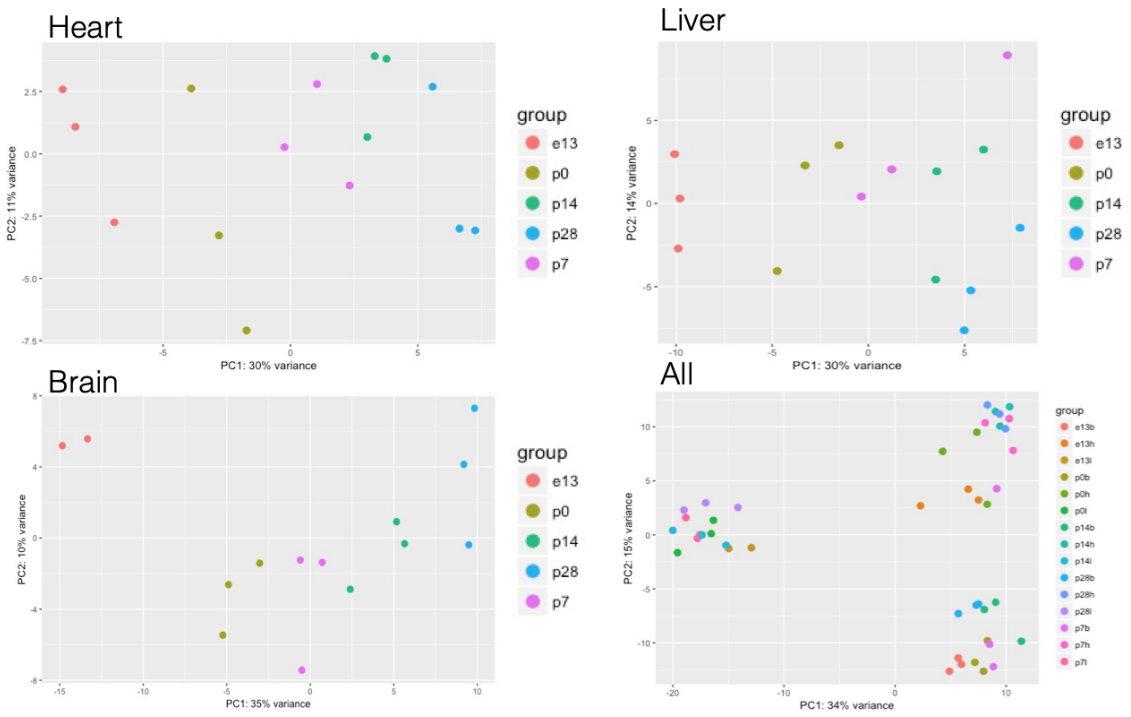

Figure 6-12. Temporal maturation is captured in all individual organ PCA plots. PCA of all combined data shows organ-specific clustering

isoform differences with scalable depth rather than predefined targets. A downside of bulk RNA-seq is that it does not differentiate between cells so it combines many different cell types. At this time, there are single cell atlases of multiple organs, but not time series datasets. Another area of interest has been similarities in different species and the rate of maturation. Mice reach adolescence after 4 weeks, while humans take more than 10 years. It has been shown that CM maturation follows a similar time course.

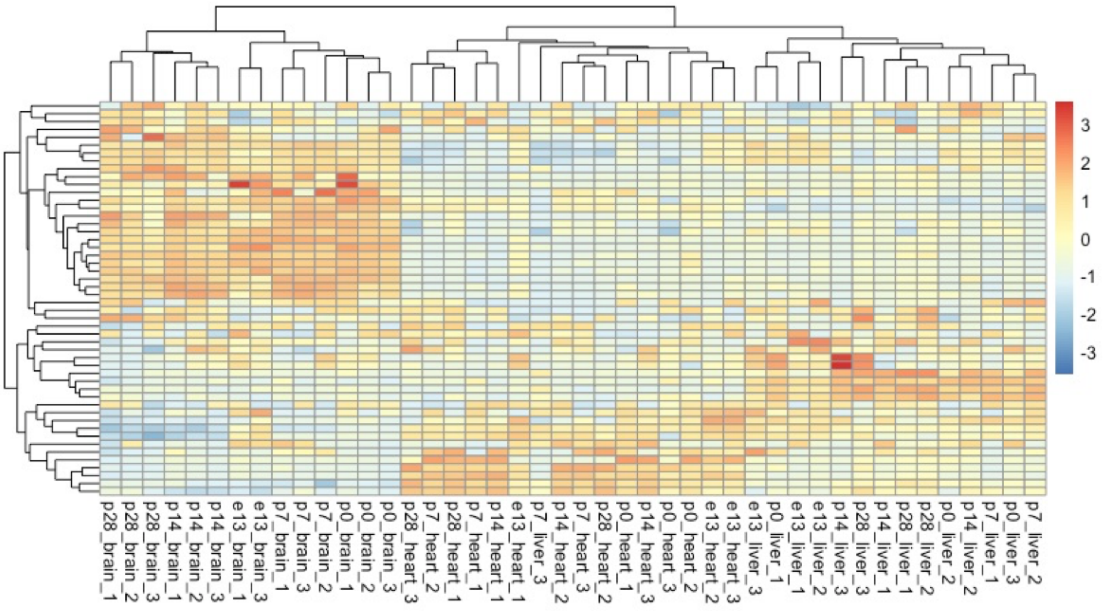

Figure 6-13. Heatmap of top microRNA expression shows organ specific signatures.

P0 vs P28 2 fold change	Heart	Brain	Liver	Conserved
Up-regulated	64	112	64	11
Down-regulated	118	156	86	13

Conserved up

mmu-mir-378a
mmu-let-7c-1
mmu-mir-1843b
mmu-mir-378c
mmu-mir-150
mmu-mir-22
mmu-mir-497a
mmu-mir-143
mmu-mir-34a
mmu-mir-29c
mmu-mir-29a

Conserved down

mmu-mir-1193
mmu-mir-130b
mmu-mir-134
mmu-mir-301b
mmu-mir-335
mmu-mir-450a-1
mmu-mir-466c-1
mmu-mir-466i
mmu-mir-483
mmu-mir-503
mmu-mir-542
mmu-mir-6413
mmu-mir-6538

Figure 6-14. Overlap between microRNAs shows 11 conserved upregulated and 13 conserved downregulated microRNAs, which are listed.

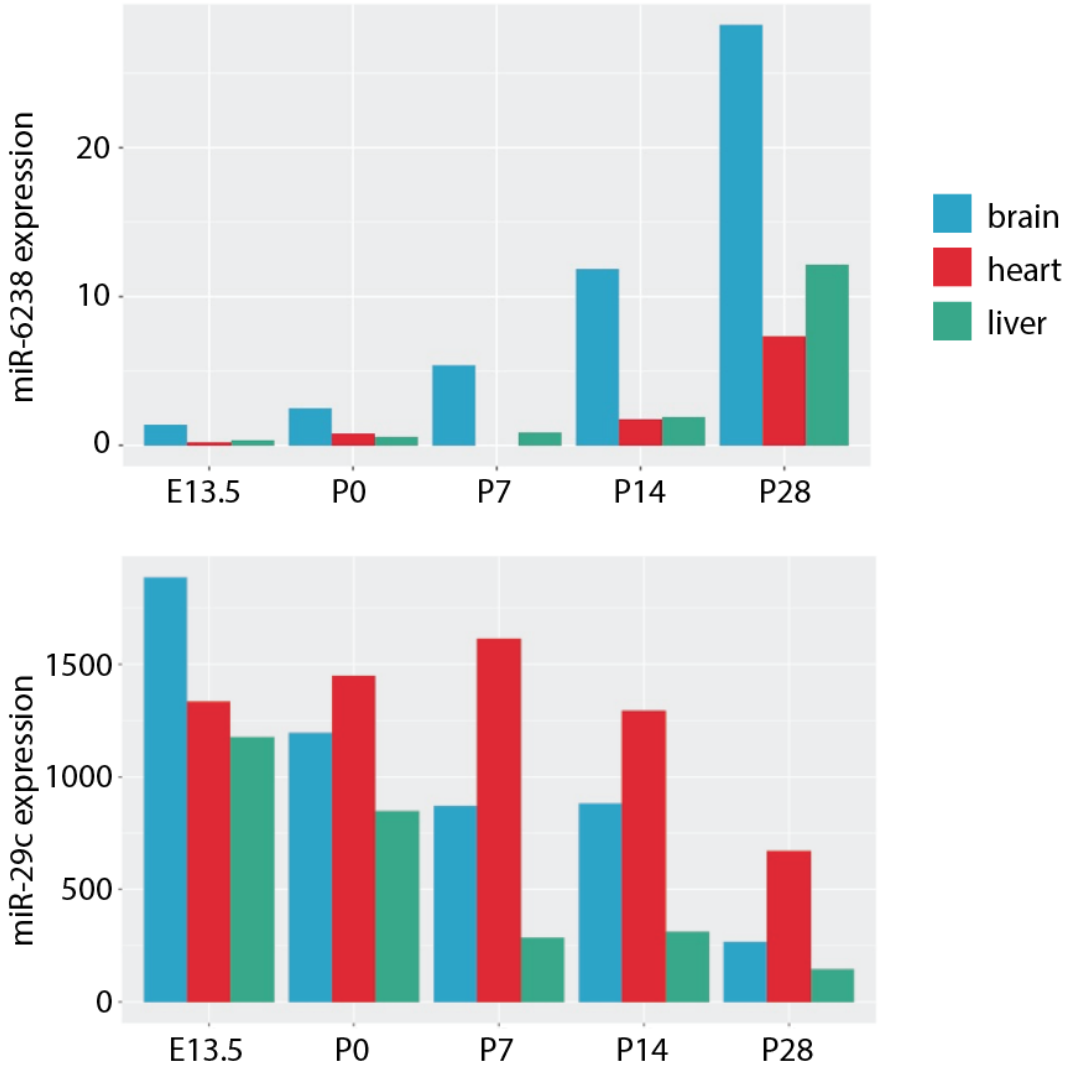

Figure 6-15. microRNA expression patterns for miR-6238 and miR-29c

Chapter 7

Conclusion

Summary

The goal of these experiments was to unveil part of the mechanism of cardiomyocyte maturation. By learning more about the gene regulatory network driving CM maturation, we can alter pathways to generate mature PSC-CMs in the dish. In chapter 1, I laid out the current knowledge of the field and described previous efforts to improve maturation of PSC-CMs. These centered around biomimetic approaches to recreate aspects of the in vivo microenvironment including ECM, mechanical stretching, and electrical stimulation. In chapter 2, I used a meta-analysis of bulk RNA-seq sets to characterize expression trends and predict upstream regulators. We confirmed and identified a novel characteristic of transcriptomic maturation which was the critical window. There appears to be a large shift in gene expression between P7 and P14. We then found that PGC1α was a key predicted upstream regulator and was misregulated in PSC-CMs. Single cell RNA-seq of postnatal maturation supported this conclusion as fatty acid oxidation pathways were consistently activated. In chapter 3, we sought to determine if PGC1α was required for postnatal cardiomyocyte maturation in vivo. We used a conditional mosaic knockout to assess the cell autonomous role using a Cre-lox system with AAV9. After 4 weeks, we measured CM contractility and calcium transients showing that their dynamics resembled immature CMs. The PGC1 null

cells were smaller than control CMs through development and scRNA-seq found that they were consistently less mature.

In chapter 4, we found that these findings could be applied to PSC-CMs. Importantly, PGC1α and PPARα activation following differentiation led to more forceful contraction and hypertrophic growth. These PSC-CMs had nearly 3-fold higher mitochondrial density and significantly higher mitochondrial respiratory capacity. Since PGC1/PPAR are regulators of metabolism and mitochondrial biogenesis, we were interested in how they altered calcium handling, hypertrophy, and contractility and studied this in chapter 5. Using a functional siRNA screen of potential PGC1 targets from the scRNA-seq analysis, we found that SF3B2 was a splicing factor that was required for improvement of calcium handling. SF3B2 has not been studied in the heart and may splice mRNA for proteins involved in the sarcoplasmic reticulum. We also found that YAP1 is required for both postnatal CM hypertrophy and PGC1/PPAR-mediated cell growth.

In chapter 6, we investigated similarities in maturation across multiple organs. Looking into mRNA and microRNA expression, we were able to identify key pathways and potential microRNAs that could promote PSC-CM maturation. These findings could be applied to improving maturation of stem cell derived-hepatocytes, neurons, and other cell types.

Conclusions

We searched for a key regulator of CM maturation. PGC1 was found to control multiple aspects of maturation including hypertrophy, contractility, and gene expression. While our PSC-CMs did not become adult-like in the dish, they did exhibit improved functional parameters, which may make PSC-CMs more useful in disease modeling. Further studies are required to see if PGC1 can be combined with 3D culture and other

small molecule regulators to generate the most mature PSC-CMs developed *in vitro*. However, this would require a better method of comparing matured PSC-CMs between labs. It has been difficult to compare the maturation state of cells as many aspects of maturation must be measured. We did not characterize T-tubule development, multinucleation, elongation, or proliferation, which may have been affected by PGC1 agonist treatment.

Our development of a Cre-lox system for preparation of conditional mosaic knockouts could be impactful as floxed mouse lines exist for many genes. We recommend that other studies of maturation use a cell autonomous approach to rule out feedback loops from altering cellular function. Our siRNA screen of PGC1 targets on calcium handling identified multiple splicing factors. One drawback of this work is that it did not look into the alternative splicing caused by siSF2B2.

Future directions

Our results showed scRNA-seq analysis can identify transcriptional regulators of CM maturation. Multiple other factors were predicted to be upstream regulators of CM maturation. We plan on interrogating these factors in a similar manner. However, we will need to first confirm that they are misregulated in PSC-CMs. Since the qPCR analysis of expression was labor intensive, it will be better to use a time series RNA-seq dataset of PSC-CM maturation to determine the expression trends. One drawback is that signaling pathways could be activated or suppressed by post-translational modifications that do not change mRNA levels.

The first drawback of our study is that PSC-CMs matured, but were still unlike in vivo CMs. With the goal of generating adult-like PSC-CMs, the best approach may be to combine pathway modifications like our PGC1/PPAR agonists with 3D culture systems like an engineered heart tissue. In addition, our PGC1/PPAR agonist

treated-PSC-CMs were cultured in normal media containing high levels of glucose and low levels of fatty acids. Since glucose was shown to inhibit CM maturation, it is possible that these factors are limiting the impact of PGC1/PPAR agonists. Other studies have shown that PGC1 expression is upregulated by culture on microgrooved surfaces. We are interested in determining what upregulates PGC1α in vivo and whether that cue can be added to PSC-CM culture.

The PGC1α activator PQQ is not a specific agonist. It acts by increasing the phosphorylation of CREB at serine 133, which activates PQQ. We did validate some of our results using a PGC1α overexpression plasmid in PSC-CMs, but it would be interesting to see how a physiologically-relevant overexpression could alter maturation.

SF3B2 was shown to be required for calcium handling. This factor has not been studied in cardiomyocytes. We plan on performing loss of function studies using a similar conditional knockout of SF3B2 using a Cre-Lox with an αMHC-Cre. Since these mice do not exist, we will need to generate a floxed SF3B2 mouse line. If a phenotype develops, we will perform postnatal conditional mosaic knockouts of the factor to determine the cell autonomous effects. Our lab has been creating a PSC-CM line expressing dCas9-KRAB to repress gene expression when single guide RNAs are transfected. We can use this system to see if SF3B2 is required for PSC-CM function. Since SF3B2 is a splicing factor, we are interested in finding the mRNAs that are spliced by SF3B2. Using cross linking immunoprecipitation sequencing, we could determine the mRNAs that are bound by SF3B2. Deep sequencing of the transcriptome could also determine alternative splicing by SF3B2 in our knockout mice. Our initial results indicate that SF3B2 plays a critical role in calcium handling so it will be interesting to elucidate this mechanism.

References

1. Kolanowski, T. J., Antos, C. L. & Guan, K. Making human cardiomyocytes up to date: Derivation, maturation state and perspectives. *Int J Cardiol* **241,** 379–386 (2017).

2. Laflamme, M. A. & Murry, C. E. Heart regeneration. *Nature* **473,** 326–35 (2011).

3. Mercola, M., Ruiz-Lozano, P. & Schneider, M. D. Cardiac muscle regeneration: lessons from development. *Genes Dev* **25,** 299–309 (2011).

4. Tan, S. H. & Ye, L. Maturation of Pluripotent Stem Cell-Derived Cardiomyocytes: a Critical Step for Drug Development and Cell Therapy. *J Cardiovasc Transl Res* **11,** 375–392 (2018).

5. Weinberger, F., Mannhardt, I. & Eschenhagen, T. Engineering Cardiac Muscle Tissue: A Maturating Field of Research. *Circ Res* **120,** 1487–1500 (2017).

6. Karbassi, E., Fenix, A., Marchiano, S., Muraoka, N., Nakamura, K., Yang, X. & Murry, C. E. Cardiomyocyte maturation: advances in knowledge and implications for regenerative medicine. *Nat Rev Cardiol* **17,** 341–359 (2020).

7. Sacchetto, C., Vitiello, L., de Windt, L. J., Rampazzo, A. & Calore, M. Modeling Cardiovascular Diseases with hiPSC-Derived Cardiomyocytes in 2D and 3D Cultures. *Int J Mol Sci* **21** (2020).

8. Anzai, T., Yamagata, T. & Uosaki, H. Comparative Transcriptome Landscape of Mouse and Human Hearts. *Front Cell Dev Biol* **8,** 268 (2020).

9. Veerman, C. C., Kosmidis, G., Mummery, C. L., Casini, S., Verkerk, A. O. & Bellin, M. Immaturity of human stem-cell-derived cardiomyocytes in culture: fatal flaw or soluble problem? *Stem Cells Dev* **24,** 1035–52 (2015).

10. Galdos, F. X., Guo, Y., Paige, S. L., VanDusen, N. J., Wu, S. M. & Pu, W. T. Cardiac Regeneration: Lessons From Development. *Circ Res* **120,** 941–959 (2017).

11. Marchiano, S., Bertero, A. & Murry, C. E. Learn from Your Elders: Developmental Biology Lessons to Guide Maturation of Stem Cell-Derived Cardiomyocytes. *Pediatr Cardiol* **40,** 1367–1387 (2019).

12. Ge, F., Wang, Z. & Xi, J. J. Engineered Maturation Approaches of Human Pluripotent Stem Cell-Derived Ventricular Cardiomyocytes. *Cells* **9** (2019).

13. Kannan, S. & Kwon, C. Regulation of cardiomyocyte maturation during critical perinatal window. *J Physiol* **598,** 2941–2956 (2020).

14. Zhu, R., Blazeski, A., Poon, E., Costa, K. D., Tung, L. & Boheler, K. R. Physical developmental cues for the maturation of human pluripotent stem cell-derived cardiomyocytes. *Stem Cell Res Ther* **5,** 117 (2014).

15. Scuderi, G. J. & Butcher, J. Naturally Engineered Maturation of Cardiomyocytes. *Front Cell Dev Biol* **5,** 50 (2017).

16. Bedada, F. B., Wheelwright, M. & Metzger, J. M. Maturation status of sarcomere structure and function in human iPSC-derived cardiac myocytes. *Biochim Biophys Acta* **1863,** 1829–38 (2016).

17. Jiang, Y., Park, P., Hong, S. M. & Ban, K. Maturation of Cardiomyocytes Derived from Human Pluripotent Stem Cells: Current Strategies and Limitations. *Mol Cells* **41,** 613–621 (2018).

18. Kaushik, G. & Engler, A. J. From stem cells to cardiomyocytes: the role of forces in cardiac maturation, aging, and disease. *Prog Mol Biol Transl Sci* **126,** 219–42 (2014).

19. Tallawi, M., Rai, R., Boccaccini, A. R. & Aifantis, K. E. Effect of substrate mechanics on cardiomyocyte maturation and growth. *Tissue Eng Part B Rev* **21,** 157–65 (2015).

20. Besser, R. R., Ishahak, M., Mayo, V., Carbonero, D., Claure, I. & Agarwal, A. Engineered Microenvironments for Maturation of Stem Cell Derived Cardiac Myocytes. *Theranostics* **8,** 124–140 (2018).

21. Feric, N. T. & Radisic, M. Maturing human pluripotent stem cell-derived cardiomyocytes in human engineered cardiac tissues. *Adv Drug Deliv Rev* **96,** 110–34 (2016).

22. Yang, X., Pabon, L. & Murry, C. E. Engineering adolescence: maturation of human pluripotent stem cell-derived cardiomyocytes. *Circ Res* **114,** 511–23 (2014).

23. Blazeski, A., Zhu, R., Hunter, D. W., Weinberg, S. H., Boheler, K. R., Zambidis, E. T. & Tung, L. Electrophysiological and contractile function of cardiomyocytes derived from human embryonic stem cells. *Prog Biophys Mol Biol* **110,** 178–95 (2012).

24. Robertson, C., Tran, D. D. & George, S. C. Concise review: maturation phases of human pluripotent stem cell-derived cardiomyocytes. *Stem Cells* **31,** 829–37 (2013).

25. Ahmed, R. E., Anzai, T., Chanthra, N. & Uosaki, H. A Brief Review of Current Maturation Methods for Human Induced Pluripotent Stem Cells-Derived Cardiomyocytes. *Front Cell Dev Biol* **8,** 178 (2020).

26. Aigha, I. & Raynaud, C. Maturation of pluripotent stem cell derived cardiomyocytes: The new challenge. *Glob Cardiol Sci Pract* **2016,** e201606 (2016).

27. Ronaldson-Bouchard, K., Ma, S. P., Yeager, K., Chen, T., Song, L., Sirabella, D., Morikawa, K., Teles, D., Yazawa, M. & Vunjak-Novakovic, G. Advanced maturation of human cardiac tissue grown from pluripotent stem cells. *Nature* **556,** 239–243 (2018).

28. Machiraju, P. & Greenway, S. C. Current methods for the maturation of induced pluripotent stem cell-derived cardiomyocytes. *World J Stem Cells* **11,** 33–43 (2019).

29. Keung, W., Boheler, K. R. & Li, R. A. Developmental cues for the maturation of metabolic, electrophysiological and calcium handling properties of human pluripotent stem cell-derived cardiomyocytes. *Stem Cell Res Ther* **5,** 17 (2014).

30. Hirose, K., Payumo, A. Y., Cutie, S., Hoang, A., Zhang, H., Guyot, R., Lunn, D., Bigley, R. B., Yu, H., Wang, J., Smith, M., Gillett, E., Muroy, S. E., Schmid, T.,

Wilson, E., Field, K. A., Reeder, D. M., Maden, M., Yartsev, M. M., Wolfgang, M. J., Grutzner, F., Scanlan, T. S., Szweda, L. I., Buffenstein, R., Hu, G., Flamant, F., Olgin, J. E. & Huang, G. N. Evidence for hormonal control of heart regenerative capacity during endothermy acquisition. *Science* **364,** 184–188 (2019).

31. Velayutham, N., Alfieri, C. M., Agnew, E. J., Riggs, K. W., Baker, R. S., Ponny, S. R., Zafar, F. & Yutzey, K. E. Cardiomyocyte cell cycling, maturation, and growth by multinucleation in postnatal swine. *J Mol Cell Cardiol* **146,** 95–108 (2020).

32. Patterson, M., Barske, L., Van Handel, B., Rau, C. D., Gan, P., Sharma, A., Parikh, S., Denholtz, M., Huang, Y., Yamaguchi, Y., Shen, H., Allayee, H., Crump, J. G., Force, T. I., Lien, C. L., Makita, T., Lusis, A. J., Kumar, S. R. & Sucov, H. M. Frequency of mononuclear diploid cardiomyocytes underlies natural variation in heart regeneration. *Nat Genet* **49,** 1346–1353 (2017).

33. Nakada, Y., Canseco, D. C., Thet, S., Abdisalaam, S., Asaithamby, A., Santos, C. X., Shah, A. M., Zhang, H., Faber, J. E., Kinter, M. T., Szweda, L. I., Xing, C., Hu, Z., Deberardinis, R. J., Schiattarella, G., Hill, J. A., Oz, O., Lu, Z., Zhang, C. C., Kimura, W. & Sadek, H. A. Hypoxia induces heart regeneration in adult mice. *Nature* **541,** 222–227 (2017).

34. Mohamed, T. M. A., Ang, Y. S., Radzinsky, E., Zhou, P., Huang, Y., Elfenbein, A., Foley, A., Magnitsky, S. & Srivastava, D. Regulation of Cell Cycle to Stimulate Adult Cardiomyocyte Proliferation and Cardiac Regeneration. *Cell* **173,** 104–116 e12 (2018).

35. Buikema, J. W., Lee, S., Goodyer, W. R., Maas, R. G., Chirikian, O., Li, G., Miao, Y., Paige, S. L., Lee, D., Wu, H., Paik, D. T., Rhee, S., Tian, L., Galdos, F. X., Puluca, N., Beyersdorf, B., Hu, J., Beck, A., Venkamatran, S., Swami, S., Wijnker, P., Schuldt, M., Dorsch, L. M., van Mil, A., Red-Horse, K., Wu, J. Y., Geisen, C., Hesse, M., Serpooshan, V., Jovinge, S., Fleischmann, B. K., Doevendans, P. A., van der Velden, J., Garcia, K. C., Wu, J. C., Sluijter, J. P. G. & Wu, S. M. Wnt Activation and Reduced Cell-Cell Contact Synergistically Induce Massive Expansion of Functional Human iPSC-Derived Cardiomyocytes. *Cell Stem Cell* **27,** 50–63 e5 (2020).

36. Momtahan, N., Crosby, C. O. & Zoldan, J. The Role of Reactive Oxygen Species in In Vitro Cardiac Maturation. *Trends Mol Med* **25,** 482–493 (2019).

37. Ellen Kreipke, R., Wang, Y., Miklas, J. W., Mathieu, J. & Ruohola-Baker, H. Metabolic remodeling in early development and cardiomyocyte maturation. *Semin Cell Dev Biol* **52,** 84–92 (2016).

38. Batho, C. A. P., Mills, R. J. & Hudson, J. E. Metabolic Regulation of Human Pluripotent Stem Cell-Derived Cardiomyocyte Maturation. *Curr Cardiol Rep* **22,** 73 (2020).

39. Slaats, R. H., Schwach, V. & Passier, R. Metabolic environment in vivo as a blueprint for differentiation and maturation of human stem cell-derived cardiomyocytes. *Biochim Biophys Acta Mol Basis Dis* **1866,** 165881 (2020).

40. Sun, X. & Nunes, S. S. Bioengineering Approaches to Mature Human Pluripotent Stem Cell-Derived Cardiomyocytes. *Front Cell Dev Biol* **5,** 19 (2017).

41. Chanthra, N., Abe, T., Miyamoto, M., Sekiguchi, K., Kwon, C., Hanazono, Y. & Uosaki, H. A Novel Fluorescent Reporter System Identifies Laminin-511/521 as Potent Regulators of Cardiomyocyte Maturation. *Sci Rep* **10,** 4249 (2020).

42. Li, J., Zhang, L., Yu, L., Minami, I., Miyagawa, S., Horning, M., Dong, J., Qiao, J., Qu, X., Hua, Y., Fujimoto, N., Shiba, Y., Zhao, Y., Tang, F., Chen, Y., Sawa, Y., Tang, C. & Liu, L. Circulating re-entrant waves promote maturation of hiPSC-derived cardiomyocytes in self-organized tissue ring. *Commun Biol* **3,** 122 (2020).

43. Min, S., Lee, H. J., Jin, Y., Kim, Y. H., Sung, J., Choi, H. J. & Cho, S. W. Biphasic Electrical Pulse by a Micropillar Electrode Array Enhances Maturation and Drug Response of Reprogrammed Cardiac Spheroids. *Nano Lett* **20,** 6947–6956 (2020).

44. Crestani, T., Steichen, C., Neri, E., Rodrigues, M., Fonseca-Alaniz, M. H., Ormrod, B., Holt, M. R., Pandey, P., Harding, S., Ehler, E. & Krieger, J. E. Electrical stimulation applied during differentiation drives the hiPSC-CMs towards a mature cardiac conduction-like cells. *Biochem Biophys Res Commun* (2020).

45. Ye, G., Wen, Z., Wen, F., Song, X., Wang, L., Li, C., He, Y., Prakash, S. & Qiu, X. Mussel-inspired conductive Ti2C-cryogel promotes functional maturation of cardiomyocytes and enhances repair of myocardial infarction. *Theranostics* **10,** 2047–2066 (2020).

46. Madeddu, P. Defective Cardiomyocyte Maturation in the Congenitally Hypoplastic Right Ventricle: A Wrong Molecular Trajectory Leading to Heart Failure? *J Am Heart Assoc* **9,** e019433 (2020).

47. Garry, M. G. & Garry, D. J. Go to the Mattresses: A New Method for Human-Induced Pluripotent Stem Cell-Derived Cardiomyocyte Maturation. *Circ Res* **117,** 982–3 (2015).

48. Yang, X., Rodriguez, M., Pabon, L., Fischer, K. A., Reinecke, H., Regnier, M., Sniadecki, N. J., Ruohola-Baker, H. & Murry, C. E. Tri-iodo-l-thyronine promotes the maturation of human cardiomyocytes-derived from induced pluripotent stem cells. *J Mol Cell Cardiol* **72,** 296–304 (2014).

49. Zhou, R., Li, J., Zhang, L., Cheng, Y., Yan, J., Sun, Y., Wang, J. & Jiang, H. Role of Parkin-mediated mitophagy in glucocorticoid-induced cardiomyocyte maturation. *Life Sci* **255,** 117817 (2020).

50. Miao, S., Zhao, D., Wang, X., Ni, X., Fang, X., Yu, M., Ye, L., Yang, J., Wu, H., Han, X., Qu, L., Li, L., Lan, F., Shen, Z., Lei, W., Zhao, Z. A. & Hu, S. Retinoic acid promotes metabolic maturation of human Embryonic Stem Cell-derived Cardiomyocytes. *Theranostics* **10,** 9686–9701 (2020).

51. Ng, D. C. H., Richards, D. K., Mills, R. J., Ho, U. Y., Perks, H. L., Tucker, C. R., Voges, H. K., Pagan, J. K. & Hudson, J. E. Centrosome Reduction Promotes Terminal Differentiation of Human Cardiomyocytes. *Stem Cell Reports* **15,** 817–826 (2020).

52. Ganguly, E., Spaans, F., Morton, J. S., Kirschenman, R., Aljunaidy, M. M., Phillips, T. E. J., Case, C. P., Cooke, C. M. & Davidge, S. T. Placenta-targeted treatment in hypoxic dams improves maturation and growth of fetal cardiomyocytes in vitro via the release of placental factors. *Exp Physiol* (2020).

53. Guo, Y. & Pu, W. T. Cardiomyocyte Maturation: New Phase in Development. *Circ Res* **126,** 1086–1106 (2020).

54. Wang, Y., Yao, F., Wang, L., Li, Z., Ren, Z., Li, D., Zhang, M., Han, L., Wang, S. Q., Zhou, B. & Wang, L. Single-cell analysis of murine fibroblasts identifies neonatal to adult switching that regulates cardiomyocyte maturation. *Nat Commun* **11,** 2585 (2020).

55. Giacomelli, E., Meraviglia, V., Campostrini, G., Cochrane, A., Cao, X., van Helden, R. W. J., Krotenberg Garcia, A., Mircea, M., Kostidis, S., Davis, R. P., van Meer, B. J., Jost, C. R., Koster, A. J., Mei, H., Miguez, D. G., Mulder, A. A., Ledesma-Terron, M., Pompilio, G., Sala, L., Salvatori, D. C. F., Slieker, R. C., Sommariva, E., de Vries, A. A. F., Giera, M., Semrau, S., Tertoolen, L. G. J., Orlova, V. V., Bellin, M. & Mummery, C. L. Human-iPSC-Derived Cardiac Stromal Cells Enhance Maturation in 3D Cardiac Microtissues and Reveal Non-cardiomyocyte Contributions to Heart Disease. *Cell Stem Cell* **26,** 862–879 e11 (2020).

56. Winbo, A., Ramanan, S., Eugster, E., Jovinge, S., Skinner, J. R. & Montgomery, J. M. Functional coculture of sympathetic neurons and cardiomyocytes derived from human-induced pluripotent stem cells. *Am J Physiol Heart Circ Physiol* **319,** H927–H937 (2020).

57. Vega, R. B., Horton, J. L. & Kelly, D. P. Maintaining ancient organelles: mitochondrial biogenesis and maturation. *Circ Res* **116,** 1820–34 (2015).

58. Isu, G., Robles Diaz, D., Grussenmeyer, T., Gaudiello, E., Eckstein, F., Brink, M. & Marsano, A. Fatty acid-based monolayer culture to promote in vitro neonatal rat cardiomyocyte maturation. *Biochim Biophys Acta Mol Cell Res* **1867,** 118561 (2020).

59. Yang, X., Rodriguez, M. L., Leonard, A., Sun, L., Fischer, K. A., Wang, Y., Ritterhoff, J., Zhao, L., Kolwicz S. C., J., Pabon, L., Reinecke, H., Sniadecki, N. J., Tian, R., Ruohola-Baker, H., Xu, H. & Murry, C. E. Fatty Acids Enhance the Maturation of Cardiomyocytes Derived from Human Pluripotent Stem Cells. *Stem Cell Reports* **13,** 657–668 (2019).

60. Horikoshi, Y., Yan, Y., Terashvili, M., Wells, C., Horikoshi, H., Fujita, S., Bosnjak, Z. J. & Bai, X. Fatty Acid-Treated Induced Pluripotent Stem Cell-Derived Human Cardiomyocytes Exhibit Adult Cardiomyocyte-Like Energy Metabolism Phenotypes. *Cells* **8** (2019).

61. Nakano, H., Minami, I., Braas, D., Pappoe, H., Wu, X., Sagadevan, A., Vergnes, L., Fu, K., Morselli, M., Dunham, C., Ding, X., Stieg, A. Z., Gimzewski, J. K., Pellegrini, M., Clark, P. M., Reue, K., Lusis, A. J., Ribalet, B., Kurdistani, S. K., Christofk, H., Nakatsuji, N. & Nakano, A. Glucose inhibits cardiac muscle maturation through nucleotide biosynthesis. *Elife* **6** (2017).

62. Lingan, J. V., Alanzalon, R. E. & Porter G. A., J. Preventing permeability transition pore opening increases mitochondrial maturation, myocyte differentiation and cardiac function in the neonatal mouse heart. *Pediatr Res* **81,** 932–941 (2017).

63. Feyen, D. A. M., McKeithan, W. L., Bruyneel, A. A. N., Spiering, S., Hormann, L., Ulmer, B., Zhang, H., Briganti, F., Schweizer, M., Hegyi, B., Liao, Z., Polonen, R. P., Ginsburg, K. S., Lam, C. K., Serrano, R., Wahlquist, C., Kreymerman, A., Vu, M., Amatya, P. L., Behrens, C. S., Ranjbarvaziri, S., Maas, R. G. C., Greenhaw, M., Bernstein, D., Wu, J. C., Bers, D. M., Eschenhagen, T., Metallo, C. M. & Mercola, M. Metabolic Maturation Media Improve Physiological Function of Human iPSC-Derived Cardiomyocytes. *Cell Rep* **32,** 107925 (2020).

64. Cho, G. S., Lee, D. I., Tampakakis, E., Murphy, S., Andersen, P., Uosaki, H., Chelko, S., Chakir, K., Hong, I., Seo, K., Chen, H. V., Chen, X., Basso, C., Houser, S. R., Tomaselli, G. F., O'Rourke, B., Judge, D. P., Kass, D. A. & Kwon, C. Neonatal Transplantation Confers Maturation of PSC-Derived Cardiomyocytes Conducive to Modeling Cardiomyopathy. *Cell Rep* **18,** 571–582 (2017).

65. Kadota, S., Pabon, L., Reinecke, H. & Murry, C. E. In Vivo Maturation of Human Induced Pluripotent Stem Cell-Derived Cardiomyocytes in Neonatal and Adult Rat Hearts. *Stem Cell Reports* **8,** 278–289 (2017).

66. Ichimura, H., Kadota, S., Kashihara, T., Yamada, M., Ito, K., Kobayashi, H., Tanaka, Y., Shiba, N., Chuma, S., Tohyama, S., Seto, T., Okada, K., Kuwahara, K. & Shiba, Y. Increased predominance of the matured ventricular subtype in embryonic stem cell-derived cardiomyocytes in vivo. *Sci Rep* **10,** 11883 (2020).

67. Huang, C. Y., Peres Moreno Maia-Joca, R., Ong, C. S., Wilson, I., DiSilvestre, D., Tomaselli, G. F. & Reich, D. H. Enhancement of human iPSC-derived cardiomyocyte

maturation by chemical conditioning in a 3D environment. *J Mol Cell Cardiol* **138,** 1–11 (2020).

68. Wong, A. O., Wong, N., Geng, L., Chow, M. Z., Lee, E. K., Wu, H., Khine, M., Kong, C. W., Costa, K. D., Keung, W., Cheung, Y. F. & Li, R. A. Combinatorial Treatment of Human Cardiac Engineered Tissues With Biomimetic Cues Induces Functional Maturation as Revealed by Optical Mapping of Action Potentials and Calcium Transients. *Front Physiol* **11,** 165 (2020).

69. Silbernagel, N., Korner, A., Balitzki, J., Jaggy, M., Bertels, S., Richter, B., Hippler, M., Hellwig, A., Hecker, M., Bastmeyer, M. & Ullrich, N. D. Shaping the heart: Structural and functional maturation of iPSC-cardiomyocytes in 3D-micro-scaffolds. *Biomaterials* **227,** 119551 (2020).

70. Kolanowski, T. J., Busek, M., Schubert, M., Dmitrieva, A., Binnewerg, B., Poche, J., Fisher, K., Schmieder, F., Grunzner, S., Hansen, S., Richter, A., El-Armouche, A., Sonntag, F. & Guan, K. Enhanced structural maturation of human induced pluripotent stem cell-derived cardiomyocytes under a controlled microenvironment in a microfluidic system. *Acta Biomater* **102,** 273–286 (2020).

71. LaBarge, W., Mattappally, S., Kannappan, R., Fast, V. G., Pretorius, D., Berry, J. L. & Zhang, J. Maturation of three-dimensional, hiPSC-derived cardiomyocyte spheroids utilizing cyclic, uniaxial stretch and electrical stimulation. *PLoS One* **14,** e0219442 (2019).

72. Mills, R. J., Titmarsh, D. M., Koenig, X., Parker, B. L., Ryall, J. G., Quaife-Ryan, G. A., Voges, H. K., Hodson, M. P., Ferguson, C., Drowley, L., Plowright, A. T., Needham, E. J., Wang, Q. D., Gregorevic, P., Xin, M., Thomas, W. G., Parton, R. G., Nielsen, L. K., Launikonis, B. S., James, D. E., Elliott, D. A., Porrello, E. R. & Hudson, J. E. Functional screening in human cardiac organoids reveals a metabolic mechanism for cardiomyocyte cell cycle arrest. *Proc Natl Acad Sci U S A* **114,** E8372–E8381 (2017).

73. Wheelwright, M., Mikkila, J., Bedada, F. B., Mandegar, M. A., Thompson, B. R. & Metzger, J. M. Advancing physiological maturation in human induced pluripotent stem cell-derived cardiac muscle by gene editing an inducible adult troponin isoform switch. *Stem Cells* **38,** 1254–1266 (2020).

74. Uosaki, H., Cahan, P., Lee, D. I., Wang, S., Miyamoto, M., Fernandez, L., Kass, D. A. & Kwon, C. Transcriptional Landscape of Cardiomyocyte Maturation. *Cell Rep* **13,** 1705–16 (2015).

75. Fukuda, R., Gunawan, F., Beisaw, A., Jimenez-Amilburu, V., Maischein, H. M., Kostin, S., Kawakami, K. & Stainier, D. Y. Proteolysis regulates cardiomyocyte maturation and tissue integration. *Nat Commun* **8,** 14495 (2017).

76. Fukuda, R., Gunawan, F., Ramadass, R., Beisaw, A., Konzer, A., Mullapudi, S. T., Gentile, A., Maischein, H. M., Graumann, J. & Stainier, D. Y. R. Mechanical Forces Regulate Cardiomyocyte Myofilament Maturation via the VCL-SSH1-CFL Axis. *Dev Cell* **51,** 62–77 e5 (2019).

77. Garbern, J. C., Helman, A., Sereda, R., Sarikhani, M., Ahmed, A., Escalante, G. O., Ogurlu, R., Kim, S. L., Zimmerman, J. F., Cho, A., MacQueen, L., Bezzerides, V. J., Parker, K. K., Melton, D. A. & Lee, R. T. Inhibition of mTOR Signaling Enhances Maturation of Cardiomyocytes Derived From Human-Induced Pluripotent Stem Cells via p53-Induced Quiescence. *Circulation* **141,** 285–300 (2020).

78. Sakamoto, T., Matsuura, T. R., Wan, S., Ryba, D. M., Kim, J. U., Won, K. J., Lai, L., Petucci, C., Petrenko, N., Musunuru, K., Vega, R. B. & Kelly, D. P. A Critical Role for Estrogen-Related Receptor Signaling in Cardiac Maturation. *Circ Res* **126,** 1685–1702 (2020).

79. Baxter, M., Voronkov, M., Poolman, T., Galli, G., Pinali, C., Goosey, L., Knight, A., Krakowiak, K., Maidstone, R., Iqbal, M., Zi, M., Prehar, S., Cartwright, E. J., Gibbs, J., Matthews, L. C., Adamson, A. D., Humphreys, N. E., Rebelo-Guiomar, P., Minczuk, M., Bechtold, D. A., Loudon, A. & Ray, D. Cardiac mitochondrial function depends on BUD23 mediated ribosome programming. *Elife* **9** (2020).

80. Nguyen, N. U. N., Canseco, D. C., Xiao, F., Nakada, Y., Li, S., Lam, N. T., Muralidhar, S. A., Savla, J. J., Hill, J. A., Le, V., Zidan, K. A., El-Feky, H. W., Wang, Z., Ahmed, M. S., Hubbi, M. E., Menendez-Montes, I., Moon, J., Ali, S. R., Le, V., Villalobos, E., Mohamed, M. S., Elhelaly, W. M., Thet, S., Anene-Nzelu, C. G., Tan, W. L. W., Foo, R. S., Meng, X., Kanchwala, M., Xing, C., Roy, J., Cyert, M. S., Rothermel, B. A. & Sadek, H. A. A calcineurin-Hoxb13 axis regulates growth mode of mammalian cardiomyocytes. *Nature* **582,** 271–276 (2020).

81. VanDusen, N. J., Guo, Y., Gu, W. & Pu, W. T. CASAAV: A CRISPR-Based Platform for Rapid Dissection of Gene Function In Vivo. *Curr Protoc Mol Biol* **120,** 31 11 1–31 11 14 (2017).

82. Guo, Y., Jardin, B. D., Zhou, P., Sethi, I., Akerberg, B. N., Toepfer, C. N., Ai, Y., Li, Y., Ma, Q., Guatimosim, S., Hu, Y., Varuzhanyan, G., VanDusen, N. J., Zhang, D., Chan, D. C., Yuan, G. C., Seidman, C. E., Seidman, J. G. & Pu, W. T. Hierarchical and stage-specific regulation of murine cardiomyocyte maturation by serum response factor. *Nat Commun* **9,** 3837 (2018).

83. Friedman, C. E., Nguyen, Q., Lukowski, S. W., Helfer, A., Chiu, H. S., Miklas, J., Levy, S., Suo, S., Han, J. J., Osteil, P., Peng, G., Jing, N., Baillie, G. J., Senabouth, A., Christ, A. N., Bruxner, T. J., Murry, C. E., Wong, E. S., Ding, J., Wang, Y., Hudson, J., Ruohola-Baker, H., Bar-Joseph, Z., Tam, P. P. L., Powell, J. E. & Palpant, N. J. Single-Cell Transcriptomic Analysis of Cardiac Differentiation from Human PSCs Reveals HOPX-Dependent Cardiomyocyte Maturation. *Cell Stem Cell* **23,** 586–598 e8 (2018).

84. DeLaughter, D. M., Bick, A. G., Wakimoto, H., McKean, D., Gorham, J. M., Kathiriya, I. S., Hinson, J. T., Homsy, J., Gray, J., Pu, W., Bruneau, B. G., Seidman, J. G. & Seidman, C. E. Single-Cell Resolution of Temporal Gene Expression during Heart Development. *Dev Cell* **39,** 480–490 (2016).

85. Cai, W., Zhang, J., de Lange, W. J., Gregorich, Z. R., Karp, H., Farrell, E. T., Mitchell, S. D., Tucholski, T., Lin, Z., Biermann, M., McIlwain, S. J., Ralphe, J. C., Kamp, T. J. & Ge, Y. An Unbiased Proteomics Method to Assess the Maturation

of Human Pluripotent Stem Cell-Derived Cardiomyocytes. *Circ Res* **125,** 936–953 (2019).

86. Poon, E. N., Luo, X. L., Webb, S. E., Yan, B., Zhao, R., Wu, S. C. M., Yang, Y., Zhang, P., Bai, H., Shao, J., Chan, C. M., Chan, G. C., Tsang, S. Y., Gundry, R. L., Yang, H. T. & Boheler, K. R. The cell surface marker CD36 selectively identifies matured, mitochondria-rich hPSC-cardiomyocytes. *Cell Res* **30,** 626–629 (2020).

87. Tabula Muris, C., Overall, c., Logistical, c., Organ, c., processing, Library, p., sequencing, Computational data, a., Cell type, a., Writing, g., Supplemental text writing, g. & Principal, i. Single-cell transcriptomics of 20 mouse organs creates a Tabula Muris. *Nature* **562,** 367–372 (2018).

88. Tabula Muris, C. A single-cell transcriptomic atlas characterizes ageing tissues in the mouse. *Nature* **583,** 590–595 (2020).

89. Kannan, S., Miyamoto, M., Lin, B. L., Zhu, R., Murphy, S., Kass, D. A., Andersen, P. & Kwon, C. Large Particle Fluorescence-Activated Cell Sorting Enables High-Quality Single-Cell RNA Sequencing and Functional Analysis of Adult Cardiomyocytes. *Circ Res* **125,** 567–569 (2019).

90. Brown, J., Pirrung, M. & McCue, L. A. FQC Dashboard: integrates FastQC results into a web-based, interactive, and extensible FASTQ quality control tool. *Bioinformatics* **33,** 3137–3139 (2017).

91. Kim, D., Paggi, J. M., Park, C., Bennett, C. & Salzberg, S. L. Graph-based genome alignment and genotyping with HISAT2 and HISAT-genotype. *Nat Biotechnol* **37,** 907–915 (2019).

92. Liao, Y., Smyth, G. K. & Shi, W. The Subread aligner: fast, accurate and scalable read mapping by seed-and-vote. *Nucleic Acids Res* **41,** e108 (2013).

93. Love, M. I., Huber, W. & Anders, S. Moderated estimation of fold change and dispersion for RNA-seq data with DESeq2. *Genome Biol* **15,** 550 (2014).

94. Kramer, A., Green, J., Pollard J., J. & Tugendreich, S. Causal analysis approaches in Ingenuity Pathway Analysis. *Bioinformatics* **30,** 523–30 (2014).

95. Mi, H., Muruganujan, A., Ebert, D., Huang, X. & Thomas, P. D. PANTHER version 14: more genomes, a new PANTHER GO-slim and improvements in enrichment analysis tools. *Nucleic Acids Res* **47,** D419–D426 (2019).

96. Supek, F., Bosnjak, M., Skunca, N. & Smuc, T. REVIGO summarizes and visualizes long lists of gene ontology terms. *PLoS One* **6,** e21800 (2011).

97. Langfelder, P. & Horvath, S. WGCNA: an R package for weighted correlation network analysis. *BMC Bioinformatics* **9,** 559 (2008).

98. Bagnoli, J. W., Ziegenhain, C., Janjic, A., Wange, L. E., Vieth, B., Parekh, S., Geuder, J., Hellmann, I. & Enard, W. Sensitive and powerful single-cell RNA sequencing using mcSCRB-seq. *Nat Commun* **9,** 2937 (2018).

99. Parekh, S., Ziegenhain, C., Vieth, B., Enard, W. & Hellmann, I. zUMIs - A fast and flexible pipeline to process RNA sequencing data with UMIs. *Gigascience* **7** (2018).

100. Dobin, A., Davis, C. A., Schlesinger, F., Drenkow, J., Zaleski, C., Jha, S., Batut, P., Chaisson, M. & Gingeras, T. R. STAR: ultrafast universal RNA-seq aligner. *Bioinformatics* **29,** 15–21 (2013).

101. Qiu, X., Mao, Q., Tang, Y., Wang, L., Chawla, R., Pliner, H. A. & Trapnell, C. Reversed graph embedding resolves complex single-cell trajectories. *Nat Methods* **14,** 979–982 (2017).

102. Puigserver, P. & Spiegelman, B. M. Peroxisome proliferator-activated receptor-gamma coactivator 1 alpha (PGC-1 alpha): transcriptional coactivator and metabolic regulator. *Endocr Rev* **24,** 78–90 (2003).

103. Ventura-Clapier, R., Garnier, A. & Veksler, V. Transcriptional control of mitochondrial biogenesis: the central role of PGC-1alpha. *Cardiovasc Res* **79,** 208–17 (2008).

104. Finck, B. N. & Kelly, D. P. PGC-1 coactivators: inducible regulators of energy metabolism in health and disease. *J Clin Invest* **116,** 615–22 (2006).

105. Rowe, G. C., Jiang, A. & Arany, Z. PGC-1 coactivators in cardiac development and disease. *Circ Res* **107,** 825–38 (2010).

106. Lehman, J. J., Barger, P. M., Kovacs, A., Saffitz, J. E., Medeiros, D. M. & Kelly, D. P. Peroxisome proliferator-activated receptor gamma coactivator-1 promotes cardiac mitochondrial biogenesis. *J Clin Invest* **106,** 847–56 (2000).

107. Lai, L., Leone, T. C., Zechner, C., Schaeffer, P. J., Kelly, S. M., Flanagan, D. P., Medeiros, D. M., Kovacs, A. & Kelly, D. P. Transcriptional coactivators PGC-1alpha and PGC-lbeta control overlapping programs required for perinatal maturation of the heart. *Genes Dev* **22,** 1948–61 (2008).

108. Birket, M. J., Casini, S., Kosmidis, G., Elliott, D. A., Gerencser, A. A., Baartscheer, A., Schumacher, C., Mastroberardino, P. G., Elefanty, A. G., Stanley, E. G. & Mummery, C. L. PGC-1alpha and reactive oxygen species regulate human embryonic stem cell-derived cardiomyocyte function. *Stem Cell Reports* **1,** 560–74 (2013).

109. Liu, Y., Bai, H., Guo, F., Thai, P. N., Luo, X., Zhang, P., Yang, C., Feng, X., Zhu, D., Guo, J., Liang, P., Xu, Z., Yang, H. & Lu, X. PGC-1alpha activator ZLN005 promotes maturation of cardiomyocytes derived from human embryonic stem cells. *Aging (Albany NY)* **12,** 7411–7430 (2020).

110. Guo, Y., VanDusen, N. J., Zhang, L., Gu, W., Sethi, I., Guatimosim, S., Ma, Q., Jardin, B. D., Ai, Y., Zhang, D., Chen, B., Guo, A., Yuan, G. C., Song, L. S. & Pu, W. T. Analysis of Cardiac Myocyte Maturation Using CASAAV, a Platform for Rapid Dissection of Cardiac Myocyte Gene Function In Vivo. *Circ Res* **120,** 1874–1888 (2017).

111. Yue, P., Xia, S., Wu, G., Liu, L., Zhou, K., Liao, H., Li, J., Zheng, X., Guo, Y., Hua, Y., Zhang, D. & Li, Y. Attenuation of Cardiomyocyte Hypertrophy via Depletion Myh7 using CASAAV. *Cardiovasc Toxicol* (2020).

112. Kumar, L. & M, E. F. Mfuzz: a software package for soft clustering of microarray data. *Bioinformation* **2,** 5–7 (2007).

113. Perez-Gonzalez, N. A., Rochman, N. D., Yao, K., Tao, J., Le, M. T., Flanary, S., Sablich, L., Toler, B., Crentsil, E., Takaesu, F., Lambrus, B., Huang, J., Fu, V., Chengappa, P., Jones, T. M., Holland, A. J., An, S., Wirtz, D., Petrie, R. J., Guan, K. L. & Sun, S. X. YAP and TAZ regulate cell volume. *J Cell Biol* **218,** 3472–3488 (2019).

114. Xiao, Y., Leach, J., Wang, J. & Martin, J. F. Hippo/Yap Signaling in Cardiac Development and Regeneration. *Curr Treat Options Cardiovasc Med* **18,** 38 (2016).

115. Lin, Z., Zhou, P., von Gise, A., Gu, F., Ma, Q., Chen, J., Guo, H., van Gorp, P. R., Wang, D. Z. & Pu, W. T. Pi3kcb links Hippo-YAP and PI3K-AKT signaling pathways to promote cardiomyocyte proliferation and survival. *Circ Res* **116,** 35–45 (2015).

116. Xiao, F., Kimura, W. & Sadek, H. A. A hippo "AKT" regulates cardiomyocyte proliferation. *Circ Res* **116,** 3–5 (2015).

117. Park, S., Choe, M., Yeo, H., Han, H., Kim, J., Chang, W., Yun, S., Lee, H. & Lee, M. Yes-associated protein mediates human embryonic stem cell-derived cardiomyocyte proliferation: Involvement of epidermal growth factor receptor signaling. *J Cell Physiol* **233,** 7016–7025 (2018).

118. Ragni, C. V., Diguet, N., Le Garrec, J. F., Novotova, M., Resende, T. P., Pop, S., Charon, N., Guillemot, L., Kitasato, L., Badouel, C., Dufour, A., Olivo-Marin, J. C., Trouve, A., McNeill, H. & Meilhac, S. M. Amotl1 mediates sequestration of the Hippo

effector Yap1 downstream of Fat4 to restrict heart growth. *Nat Commun* **8,** 14582 (2017).

119. Ikeda, S. & Sadoshima, J. Regulation of Myocardial Cell Growth and Death by the Hippo Pathway. *Circ J* **80,** 1511–9 (2016).

120. Byun, J., Del Re, D. P., Zhai, P., Ikeda, S., Shirakabe, A., Mizushima, W., Miyamoto, S., Brown, J. H. & Sadoshima, J. Yes-associated protein (YAP) mediates adaptive cardiac hypertrophy in response to pressure overload. *J Biol Chem* **294,** 3603–3617 (2019).

121. Ikeda, S., Mukai, R., Mizushima, W., Zhai, P., Oka, S. I., Nakamura, M., Del Re, D. P., Sciarretta, S., Hsu, C. P., Shimokawa, H. & Sadoshima, J. Yes-Associated Protein (YAP) Facilitates Pressure Overload-Induced Dysfunction in the Diabetic Heart. *JACC Basic Transl Sci* **4,** 611–622 (2019).

122. Gholipour, M. & Tabrizi, A. The role of Hippo signaling pathway in physiological cardiac hypertrophy. *Bioimpacts* **10,** 251–257 (2020).

123. Kashihara, T. & Sadoshima, J. Role of YAP/TAZ in Energy Metabolism in the Heart. *J Cardiovasc Pharmacol* **74,** 483–490 (2019).

124. Van den Hoogenhof, M. M., Pinto, Y. M. & Creemers, E. E. RNA Splicing: Regulation and Dysregulation in the Heart. *Circ Res* **118,** 454–68 (2016).

125. Black, A. J., Gamarra, J. R. & Giudice, J. More than a messenger: Alternative splicing as a therapeutic target. *Biochim Biophys Acta Gene Regul Mech* **1862,** 194395 (2019).

126. Beqqali, A. Alternative splicing in cardiomyopathy. *Biophys Rev* **10,** 1061–1071 (2018).

127. Kawamura, N., Nimura, K., Saga, K., Ishibashi, A., Kitamura, K., Nagano, H., Yoshikawa, Y., Ishida, K., Nonomura, N., Arisawa, M., Luo, J. & Kaneda, Y. SF3B2-Mediated RNA Splicing Drives Human Prostate Cancer Progression. *Cancer Res* **79,** 5204–5217 (2019).

128. Hadjikyriacou, A., Yang, Y., Espejo, A., Bedford, M. T. & Clarke, S. G. Unique Features of Human Protein Arginine Methyltransferase 9 (PRMT9) and Its Substrate RNA Splicing Factor SF3B2. *J Biol Chem* **290,** 16723–43 (2015).

129. Terada, Y. & Yasuda, Y. Human immunodeficiency virus type 1 Vpr induces G2 checkpoint activation by interacting with the splicing factor SAP145. *Mol Cell Biol* **26,** 8149–58 (2006).

130. Mirtschink, P., Krishnan, J., Grimm, F., Sarre, A., Horl, M., Kayikci, M., Fankhauser, N., Christinat, Y., Cortijo, C., Feehan, O., Vukolic, A., Sossalla, S., Stehr, S. N., Ule, J., Zamboni, N., Pedrazzini, T. & Krek, W. HIF-driven SF3B1 induces KHK-C to enforce fructolysis and heart disease. *Nature* **522,** 444–449 (2015).

131. Van den Boogaard, M., Wong, L. Y., Christoffels, V. M. & Barnett, P. Acquisition of high quality DNA for massive parallel sequencing by in vivo chromatin immunoprecipitation. *Methods Mol Biol* **977,** 53–64 (2013).

132. Lock, M. C., Tellam, R. L., Botting, K. J., Wang, K. C. W., Selvanayagam, J. B., Brooks, D. A., Seed, M. & Morrison, J. L. The role of miRNA regulation in fetal

cardiomyocytes, cardiac maturation and the risk of heart disease in adults. *J Physiol* **596,** 5625–5640 (2018).

133. White, M. C., Pang, L. & Yang, X. MicroRNA-mediated maturation of human pluripotent stem cell-derived cardiomyocytes: Towards a better model for cardiotoxicity? *Food Chem Toxicol* **98,** 17–24 (2016).

134. Radhakrishnan, B. & Alwin Prem Anand, A. Role of miRNA-9 in Brain Development. *J Exp Neurosci* **10,** 101–120 (2016).

135. Bianchi, N., Zuccato, C., Finotti, A., Lampronti, I., Borgatti, M. & Gambari, R. Involvement of miRNA in erythroid differentiation. *Epigenomics* **4,** 51–65 (2012).

136. Lozano, C., Duroux-Richard, I., Firat, H., Schordan, E. & Apparailly, F. MicroRNAs: Key Regulators to Understand Osteoclast Differentiation? *Front Immunol* **10,** 375 (2019).

137. Reh, T. A. & Hindges, R. MicroRNAs in Retinal Development. *Annu Rev Vis Sci* **4,** 25–44 (2018).

138. Chen, J. F., Murchison, E. P., Tang, R., Callis, T. E., Tatsuguchi, M., Deng, Z., Rojas, M., Hammond, S. M., Schneider, M. D., Selzman, C. H., Meissner, G., Patterson, C., Hannon, G. J. & Wang, D. Z. Targeted deletion of Dicer in the heart leads to dilated cardiomyopathy and heart failure. *Proc Natl Acad Sci U S A* **105,** 2111–6 (2008).

139. Jayawardena, T. M., Finch, E. A., Zhang, L., Zhang, H., Hodgkinson, C. P., Pratt, R. E., Rosenberg, P. B., Mirotsou, M. & Dzau, V. J. MicroRNA induced cardiac

reprogramming in vivo: evidence for mature cardiac myocytes and improved cardiac function. *Circ Res* **116,** 418–24 (2015).

140. Kuppusamy, K. T., Jones, D. C., Sperber, H., Madan, A., Fischer, K. A., Rodriguez, M. L., Pabon, L., Zhu, W. Z., Tulloch, N. L., Yang, X., Sniadecki, N. J., Laflamme, M. A., Ruzzo, W. L., Murry, C. E. & Ruohola-Baker, H. Let-7 family of microRNA is required for maturation and adult-like metabolism in stem cell-derived cardiomyocytes. *Proc Natl Acad Sci U S A* **112,** E2785–94 (2015).

141. Lee, D. S., Chen, J. H., Lundy, D. J., Liu, C. H., Hwang, S. M., Pabon, L., Shieh, R. C., Chen, C. C., Wu, S. N., Yan, Y. T., Lee, S. T., Chiang, P. M., Chien, S., Murry, C. E. & Hsieh, P. C. Defined MicroRNAs Induce Aspects of Maturation in Mouse and Human Embryonic-Stem-Cell-Derived Cardiomyocytes. *Cell Rep* **12,** 1960–7 (2015).

142. Poon, E. N., Hao, B., Guan, D., Jun Li, M., Lu, J., Yang, Y., Wu, B., Wu, S. C., Webb, S. E., Liang, Y., Miller, A. L., Yao, X., Wang, J., Yan, B. & Boheler, K. R. Integrated transcriptomic and regulatory network analyses identify microRNA-200c as a novel repressor of human pluripotent stem cell-derived cardiomyocyte differentiation and maturation. *Cardiovasc Res* **114,** 894–906 (2018).

143. Liu, G., Ding, M., Wang, H., Huang, J., Jing, Q. & Shen, B. Pathway analysis of microRNAs in mouse heart development. *Int J Bioinform Res Appl* **6,** 12–20 (2010).

144. Espinoza-Lewis, R. A. & Wang, D. Z. MicroRNAs in heart development. *Curr Top Dev Biol* **100,** 279–317 (2012).

145. Tao, G. & Martin, J. F. MicroRNAs get to the heart of development. *Elife* **2,** e01710 (2013).

146. Yu, Y., Fuscoe, J. C., Zhao, C., Guo, C., Jia, M., Qing, T., Bannon, D. I., Lancashire, L., Bao, W., Du, T., Luo, H., Su, Z., Jones, W. D., Moland, C. L., Branham, W. S., Qian, F., Ning, B., Li, Y., Hong, H., Guo, L., Mei, N., Shi, T., Wang, K. Y., Wolfinger, R. D., Nikolsky, Y., Walker, S. J., Duerksen-Hughes, P., Mason, C. E., Tong, W., Thierry-Mieg, J., Thierry-Mieg, D., Shi, L. & Wang, C. A rat RNA-Seq transcriptomic BodyMap across 11 organs and 4 developmental stages. *Nat Commun* **5,** 3230 (2014).

147. Xue, L., Yi, H., Huang, Z., Shi, Y. B. & Li, W. X. Global gene expression during the human organogenesis: from transcription profiles to function predictions. *Int J Biol Sci* **7,** 1068–76 (2011).

148. Xue, L., Cai, J. Y., Ma, J., Huang, Z., Guo, M. X., Fu, L. Z., Shi, Y. B. & Li, W. X. Global expression profiling reveals genetic programs underlying the developmental divergence between mouse and human embryogenesis. *BMC Genomics* **14,** 568 (2013).

149. Cardoso-Moreira, M., Halbert, J., Valloton, D., Velten, B., Chen, C., Shao, Y., Liechti, A., Ascencao, K., Rummel, C., Ovchinnikova, S., Mazin, P. V., Xenarios, I., Harshman, K., Mort, M., Cooper, D. N., Sandi, C., Soares, M. J., Ferreira, P. G., Afonso, S., Carneiro, M., Turner, J. M. A., VandeBerg, J. L., Fallahshahroudi, A., Jensen, P., Behr, R., Lisgo, S., Lindsay, S., Khaitovich, P., Huber, W., Baker, J., Anders, S., Zhang, Y. E. & Kaessmann, H. Gene expression across mammalian organ development. *Nature* **571,** 505–509 (2019).

150. Sarropoulos, I., Marin, R., Cardoso-Moreira, M. & Kaessmann, H. Developmental dynamics of lncRNAs across mammalian organs and species. *Nature* **571,** 510–514 (2019).

151. McCall, M. N. & Irizarry, R. A. Thawing Frozen Robust Multi-array Analysis (fRMA). *BMC Bioinformatics* **12,** 369 (2011).

152. Ritchie, M. E., Phipson, B., Wu, D., Hu, Y., Law, C. W., Shi, W. & Smyth, G. K. limma powers differential expression analyses for RNA-sequencing and microarray studies. *Nucleic Acids Res* **43,** e47 (2015).

153. Rueda, A., Barturen, G., Lebron, R., Gomez-Martin, C., Alganza, A., Oliver, J. L. & Hackenberg, M. sRNAtoolbox: an integrated collection of small RNA research tools. *Nucleic Acids Res* **43,** W467–73 (2015).

154. Chang, H., Yi, B., Ma, R., Zhang, X., Zhao, H. & Xi, Y. CRISPR/cas9, a novel genomic tool to knock down microRNA in vitro and in vivo. *Sci Rep* **6,** 22312 (2016).

155. Scherr, M., Venturini, L., Battmer, K., Schaller-Schoenitz, M., Schaefer, D., Dallmann, I., Ganser, A. & Eder, M. Lentivirus-mediated antagomir expression for specific inhibition of miRNA function. *Nucleic Acids Res* **35,** e149 (2007).

Appendix I

Oligonucleotide sequences and Gene Ontology terms

Table I-I. ChIP-qPCR oligonucleotdes

Primer Name	**Sequence**
ESRRA promoter qF	ACTGAACAGCTACGCCCACT
KLB promoter qF	GAGAAAACGCCATTCTCAGG
PSD4 promoter qF	AGCCAGCTGTGTGGAGAGTT
PGC1a promoter qF	CAAGCTGAGTCTGGGGCTAC
PPARA promoter qF	CAGCAGCCAATCAGACACTG
TAZ promoter qF	TTTCCACCAGCCTACGACTT
ESRRA promoter qR	CAGGCCTTGTCGATACACAC
KLB promoter qR	TAGGATGGGGTCATGAGAGC
PSD4 promoter qR	GACGTCAGCCAGCTACAGGT
PGC1a promoter qR	TGTGACTGAAGCCAGCTTTG
PPARA promoter qR	CTGTCGTGGGACCGTAGC
TAZ promoter qR	GTTGTCGCAAAACATGCCTA
CSMD1 promoter qF	AACAAGTCTCCGTGCTCCAG
ZFPM2 promoter qF	TGGAAGAAGTTGCTGGAAGG
LRBA promoter qF	CGTTCTGTGGCAGTAGCATC
ASIC2 promoter qF	AAGAAGGGTCCTGGAGGAAA
TMEM178B promoter qF	GAGAAGAGGGCAGCAGAATG
ACOX1 promoter qF	AACGACAATGAACCGTCTCC
SULT2A1 promoter qF	TCCATGGAAAGGTTCTGTATGA
ACADL promoter qF	AAACAACCATATGCGAGTTCAA
CD36 promoter qF	TGGGCCATTTCCTTTTGTAA
CSMD1 promoter qR	TGGACTCAACCATCCTACCC
ZFPM2 promoter qR	ACTATGCCATCAGCGAAAGG
LRBA promoter qR	GAGAAAGGTCAAGGCACCTG
ASIC2 promoter qR	CCACTAGTCTGGCCCTTAGC
TMEM178B promoter qR	TTTGCTCCCTTGGTGATAGC
ACOX1 promoter qR	GTGGGACTCACCTCCTTTCA
SULT2A1 promoter qR	CCAAGTTCATGACCCCAAAT
ACADL promoter qR	TGCTGATTTGGTTTGGGTTT
CD36 promoter qR	GTCCCAACAAAGCCTGAAAA
GAPDH promoter qF	TCCGCAGCCTTTTCAATAAT
HPCAL1 promoter qF	CTGGCCATTGGGACTGTACT
GAPDH promoter qR	GAGGAGTCCTTGGAGTGTGC
HPCAL1 promoter qR	GATGGGTGTTAAGGCCACTG
ESRRA intron qF	TCCAGGACGGACAGAAAAAG
SP7 intron qF	CCCCTTCCTCTCCCTCTATG
ESRRA intron qR	AGAAATCCGCCTGCCTCT
SP7 intron qR	CTGCCAGAGGTCCTGAGTTC

Table I-II. Knockout validation primers

Primer Name	**Sequence**
PGC1a exon 2-7 qF	TCGGAAATCATATCCAACCAG
PGC1a exon 2-7 qR	TGCAGTTCCAGAGAGTTCCA
PGC1a exon 2-3 qF	AACAATGAGCCTGCGAACAT
PGC1a exon 2-3 qR	ACTGGCCTCGTTGTCAGTG
PGCb exon 3-4 qF	GGACGCCAGTGACTTTGACT
PGCb exon 3-4 qR	TTCATCCAGTTCTGGGAAGG
PGCb exon 3-8 qF	ACAGCTGTGTGCTGACTTGC
PGCb exon 3-8 qR	CCAAGAGAGTCGCTTTGTGA
PGCb exon 3-9 qF	GGACGCCAGTGACTTTGACT
PGCb exon 3-9 qR	GGCTTGTATGGAGGTGTGGT

Table I-III. PGC1 cmKO differentially expressed genes

	GO Term	P-value	FDR
GO:0051179	localization	1.44E-12	0.00%
GO:0055114	oxidation-reduction process	1.53E-12	0.00%
GO:0046034	ATP metabolic process	3.10E-12	0.00%
GO:0060048	cardiac muscle contraction	5.50E-12	0.00%
GO:0008152	metabolic process	1.33E-11	0.00%
GO:0051234	establishment of localization	1.59E-11	0.00%
GO:0009205	purine ribonucleoside triphosphate metabolic process	2.09E-11	0.00%
GO:0009199	ribonucleoside triphosphate metabolic process	2.82E-11	0.00%
GO:0009167	purine ribonucleoside monophosphate metabolic process	4.17E-11	0.00%
GO:0009126	purine nucleoside monophosphate metabolic process	4.59E-11	0.00%
GO:0009144	purine nucleoside triphosphate metabolic process	4.59E-11	0.00%
GO:0006941	striated muscle contraction	4.76E-11	0.00%
GO:0009161	ribonucleoside monophosphate metabolic process	5.56E-11	0.00%
GO:0006810	transport	6.26E-11	0.00%
GO:0044237	cellular metabolic process	8.32E-11	0.00%
GO:0009123	nucleoside monophosphate metabolic process	1.18E-10	0.00%
GO:0045333	cellular respiration	1.53E-10	0.00%
GO:0009141	nucleoside triphosphate metabolic process	2.64E-10	0.00%
GO:0055008	cardiac muscle tissue morphogenesis	5.93E-10	0.00%
GO:0022900	electron transport chain	1.34E-09	0.00%
GO:0060047	heart contraction	1.36E-09	0.00%
GO:0003015	heart process	1.83E-09	0.00%
GO:0044699	single-organism process	2.81E-09	0.00%
GO:0046128	purine ribonucleoside metabolic process	2.83E-09	0.00%
GO:0042278	purine nucleoside metabolic process	3.84E-09	0.00%
GO:0060415	muscle tissue morphogenesis	5.88E-09	0.00%
GO:0006091	generation of precursor metabolites and energy	6.49E-09	0.00%
GO:0006807	nitrogen compound metabolic process	9.95E-09	0.00%
GO:0006936	muscle contraction	1.02E-08	0.00%
GO:0003012	muscle system process	1.02E-08	0.00%
GO:0009119	ribonucleoside metabolic process	1.07E-08	0.00%
GO:0022904	respiratory electron transport chain	1.17E-08	0.00%

Continued on next page

Table I-III – *Continued from previous page*

	GO Term	**P-value**	**FDR**
GO:0034641	cellular nitrogen compound metabolic process	1.25E-08	0.00%
GO:1901657	glycosyl compound metabolic process	1.55E-08	0.00%
GO:0048644	muscle organ morphogenesis	2.20E-08	0.00%
GO:0016043	cellular component organization	2.70E-08	0.00%
GO:0009116	nucleoside metabolic process	3.20E-08	0.00%
GO:0007507	heart development	3.63E-08	0.00%
GO:0003007	heart morphogenesis	3.65E-08	0.00%
GO:0048738	cardiac muscle tissue development	3.76E-08	0.00%
GO:0006725	cellular aromatic compound metabolic process	5.42E-08	0.00%
GO:0006139	nucleobase-containing compound metabolic process	5.87E-08	0.00%
GO:0046483	heterocycle metabolic process	5.98E-08	0.00%
GO:0071704	organic substance metabolic process	1.46E-07	0.00%
GO:0044238	primary metabolic process	1.46E-07	0.00%
GO:0071840	cellular component organization or biogenesis	1.88E-07	0.00%
GO:1901360	organic cyclic compound metabolic process	2.33E-07	0.00%
GO:0043933	macromolecular complex subunit organization	5.13E-07	0.00%
GO:0015980	energy derivation by oxidation of organic compounds	5.37E-07	0.00%
GO:0009987	cellular process	5.53E-07	0.00%
GO:0044763	single-organism cellular process	7.93E-07	0.00%
GO:0042775	mitochondrial ATP synthesis coupled electron transport	8.34E-07	0.00%
GO:0009150	purine ribonucleotide metabolic process	1.09E-06	0.00%
GO:0048523	negative regulation of cellular process	1.19E-06	0.00%
GO:0009259	ribonucleotide metabolic process	1.60E-06	0.00%
GO:0042773	ATP synthesis coupled electron transport	1.97E-06	0.00%
GO:0006163	purine nucleotide metabolic process	2.02E-06	0.00%
GO:0048519	negative regulation of biological process	2.04E-06	0.00%
GO:0009117	nucleotide metabolic process	2.16E-06	0.00%
GO:0019693	ribose phosphate metabolic process	2.78E-06	0.00%
GO:0055010	ventricular cardiac muscle tissue morphogenesis	2.93E-06	0.00%
GO:0072521	purine-containing compound metabolic process	3.08E-06	0.00%
GO:0006753	nucleoside phosphate metabolic process	3.34E-06	0.00%
GO:0060537	muscle tissue development	3.48E-06	0.00%
GO:0003205	cardiac chamber development	5.35E-06	0.00%

Continued on next page

Table I-III – *Continued from previous page*

	GO Term	**P-value**	**FDR**
GO:0008015	blood circulation	5.77E-06	0.00%
GO:0014706	striated muscle tissue development	6.87E-06	0.00%
GO:0003013	circulatory system process	6.91E-06	0.00%
GO:0030239	myofibril assembly	7.41E-06	0.00%
GO:1902589	single-organism organelle organization	8.36E-06	0.00%
GO:0003229	ventricular cardiac muscle tissue development	1.05E-05	0.00%
GO:0003231	cardiac ventricle development	1.07E-05	0.00%
GO:0003208	cardiac ventricle morphogenesis	1.27E-05	0.00%
GO:0044710	single-organism metabolic process	1.82E-05	0.00%
GO:0055086	nucleobase-containing small molecule metabolic process	1.98E-05	0.00%
GO:0019637	organophosphate metabolic process	2.07E-05	0.00%
GO:0015985	energy coupled proton transport, down electrochemical gradient	3.54E-05	0.00%
GO:0015986	ATP synthesis coupled proton transport	3.54E-05	0.00%
GO:0015992	proton transport	4.58E-05	0.00%
GO:0006818	hydrogen transport	5.16E-05	0.00%
GO:0007517	muscle organ development	5.90E-05	0.00%
GO:1902600	hydrogen ion transmembrane transport	6.26E-05	0.00%
GO:0006119	oxidative phosphorylation	6.50E-05	0.00%
GO:0006996	organelle organization	7.08E-05	0.00%
GO:0072359	circulatory system development	8.69E-05	0.00%
GO:0061061	muscle structure development	0.0001197	0.00%
GO:0022607	cellular component assembly	0.0001423	0.00%
GO:1901576	organic substance biosynthetic process	0.00019825	0.00%
GO:0051171	regulation of nitrogen compound metabolic process	0.00020217	0.00%
GO:0008016	regulation of heart contraction	0.00020908	0.00%
GO:0009058	biosynthetic process	0.00023073	0.00%
GO:0044057	regulation of system process	0.000274	0.00%
GO:0044249	cellular biosynthetic process	0.00027699	0.00%
GO:0065008	regulation of biological quality	0.00037452	0.00%
GO:0006754	ATP biosynthetic process	0.00037544	0.00%
GO:0009127	purine nucleoside monophosphate biosynthetic process	0.00049528	0.00%
GO:0009168	purine ribonucleoside monophosphate biosynthetic process	0.00049528	0.00%
GO:0010468	regulation of gene expression	0.00052977	0.00%

Continued on next page

Table I-III – *Continued from previous page*

	GO Term	**P-value**	**FDR**
GO:0006123	mitochondrial electron transport, cytochrome c to oxygen	0.00056503	0.00%
GO:0003206	cardiac chamber morphogenesis	0.00059131	0.00%
GO:0006793	phosphorus metabolic process	0.00063471	0.00%
GO:0009156	ribonucleoside monophosphate biosynthetic process	0.00072357	0.00%
GO:0065003	macromolecular complex assembly	0.0007811	0.00%
GO:0009142	nucleoside triphosphate biosynthetic process	0.00092218	0.00%
GO:0010927	cellular component assembly involved in morphogenesis	0.0010402	0.00%
GO:0044281	small molecule metabolic process	0.00117409	0.00%
GO:1901564	organonitrogen compound metabolic process	0.00121963	0.00%
GO:0019219	regulation of nucleobase-containing compound metabolic process	0.0012365	0.00%
GO:0044085	cellular component biogenesis	0.00128161	0.00%
GO:0006796	phosphate-containing compound metabolic process	0.00128443	0.00%
GO:0009124	nucleoside monophosphate biosynthetic process	0.00130824	0.00%
GO:0009206	purine ribonucleoside triphosphate biosynthetic process	0.00195086	0.00%
GO:0009145	purine nucleoside triphosphate biosynthetic process	0.00222598	0.00%
GO:0009201	ribonucleoside triphosphate biosynthetic process	0.0025335	0.00%
GO:0009653	anatomical structure morphogenesis	0.00265502	0.00%
GO:0055002	striated muscle cell development	0.00306339	0.00%
GO:0043462	regulation of ATPase activity	0.00314238	0.00%
GO:0010467	gene expression	0.00323753	0.00%
GO:0009060	aerobic respiration	0.0032583	0.00%
GO:0098662	inorganic cation transmembrane transport	0.00346989	0.00%
GO:0051239	regulation of multicellular organismal process	0.00365692	0.00%
GO:0010605	negative regulation of macromolecule metabolic process	0.00405621	0.00%
GO:0042451	purine nucleoside biosynthetic process	0.00416063	0.00%
GO:0046129	purine ribonucleoside biosynthetic process	0.00416063	0.00%
GO:0031032	actomyosin structure organization	0.00421994	0.00%
GO:2000112	regulation of cellular macromolecule biosynthetic process	0.00424466	0.00%
GO:0060255	regulation of macromolecule metabolic process	0.00463497	0.00%
GO:0009892	negative regulation of metabolic process	0.00604075	0.02%
GO:0030048	actin filament-based movement	0.00607754	0.02%
GO:0030029	actin filament-based process	0.00633614	0.02%
GO:1903522	regulation of blood circulation	0.00641667	0.02%

Continued on next page

Table I-III – *Continued from previous page*

	GO Term	**P-value**	**FDR**
GO:0048729	tissue morphogenesis	0.0065094	0.02%
GO:0080090	regulation of primary metabolic process	0.00652219	0.02%
GO:0070252	actin-mediated cell contraction	0.00657864	0.03%
GO:0010629	negative regulation of gene expression	0.00763574	0.03%
GO:0055001	muscle cell development	0.00869612	0.03%
GO:0034654	nucleobase-containing compound biosynthetic process	0.0087891	0.03%
GO:0051641	cellular localization	0.00906754	0.03%
GO:0031323	regulation of cellular metabolic process	0.00962081	0.03%
GO:0019438	aromatic compound biosynthetic process	0.00964853	0.03%
GO:0009889	regulation of biosynthetic process	0.00971462	0.03%

Appendix II

Code repository

A. Bash script

```
cd /Users/CKlab/Documents/HISAT2_HOME

for file in *.fastq
do
       java -jar trimmomatic-0.36.jar SE -phred33 ~/Documents/HISAT2_HOME/"$file"
           ~/Documents/HISAT2_HOME/"t2$file" ILLUMINACLIP:NexteraPE-PE.fa:2:30:10
           LEADING:38 TRAILING:35 SLIDINGWINDOW:4:20 MINLEN:36
done


for file2 in ps*.fastq
do
       ./hisat2 -q -x ~/Documents/HISAT2_HOME/genome -U ~/Documents/HISAT2_HOME/"
           $file2" -S "$file2".sam
done


cd /Users/CKlab/Documents/subread/bin
./featureCounts -t exon -g gene_id -a refFlat.gtf -o counts.txt ~/Documents/
    HISAT2_HOME/ps*.sam
```

B. R script

```
library(Seurat) #this uses Seurat v2.4

#barcodes for cells
wt_cells <- pbmc@cell.names[pbmc@meta.data$rfp == "RFP-"]

#timepoints
tps <- pbmc@meta.data$timepoint[pbmc@meta.data$rfp == "RFP-"]
```

```
#greate a new seurat object that is a subset of pbmc input
wild_type_cells <- CreateSeuratObject(raw.data = data[,wt_cells])

wild_type_cells <- NormalizeData(object = wild_type_cells, normalization.method =
    "LogNormalize",
                  scale.factor = 10000)

mito.genes <- grep(pattern = "^MT-", x = rownames(x = pbmc@data), value = TRUE)
percent.mito <- Matrix::colSums(pbmc@raw.data[mito.genes, ])/Matrix::colSums(wild_
    type_cells@raw.data)

wild_type_cells <- AddMetaData(object = wild_type_cells, metadata = percent.mito,
    col.name = "percent.mito")

wild_type_cells <- AddMetaData(object = wild_type_cells, metadata = tps, col.name
    = "timepoint")

wild_type_cells <- ScaleData(object = wild_type_cells, vars.to.regress = c("nUMI",
     "percent.mito"))

wild_type_cells <- FindVariableGenes(object = wild_type_cells, mean.function =
    ExpMean, dispersion.function = LogVMR,
                       x.low.cutoff = 0.0125, x.high.cutoff = 3, y.cutoff = 0.5)

wild_type_cells <- RunPCA(object = wild_type_cells, pc.genes = wild_type_cells@var.
    genes, do.print = TRUE, pcs.print = 1:5,
            genes.print = 5)

wild_type_cells <- RunTSNE(object = wild_type_cells, dims.use = 1:10, do.fast =
    TRUE)
TSNEPlot(object = wild_type_cells, pt.size = 2)

wild_type_cells <- RunUMAP(object = wild_type_cells, dims.use = 1:10, do.fast =
    TRUE)
UMAPPlot(object = wild_type_cells, pt.size = 2)
#tsne data


svg(filename = "umap_plot.svg",height=5, width = 6.15, pointsize = 12)
UMAPPlot(object = wild_type_cells, group.by = "condition", pt.size = 1.6)
dev.off()


# calculate size normalization

#select expression data from monocle object
unnormexp <- as.matrix(HSMM@assayData$exprs)

#select size factors
sizef <- as.matrix(HSMM@phenoData@data$Size_Factor)

# normalize expression
normexp <- sweep(unnormexp, 2, sizef, "/")
```

```
#add to monocle object
HSMM@assayData$exprs_sfnorm <- normexp


library(monocle)
#run monocle size factor and dispersion functios
CMdata <- estimateSizeFactors(CMdata)
CMdata <- estimateDispersions(CMdata)
CMdata <- detectGenes(CMdata, min_expr = 0.1)

#run differential expression gene test
diff_test_res <- differentialGeneTest(CMdata, fullModelFormulaStr = "~timepoint")
#
ordering_genes <- row.names (subset(diff_test_res, qval < 0.01))
CMdata <- setOrderingFilter(CMdata, ordering_genes)
plot_ordering_genes(CMdata)

#reduce dimension
CMdata <- reduceDimension(CMdata, max_components = 2,
                      method = 'DDRTree')

#order cells
CMdata <- orderCells(CMdata)

#plot trajectory
plot_cell_trajectory(CMdata, color_by = "matt", size=2)

## diff exp for P7

diff_test_res_P7 <- differentialGeneTest(CMdata[, pData(CMdata)$condition %in% c("
    P07␣RFP-","P07␣RFP+")], fullModelFormulaStr = "~matt")
sig_genes <- subset(diff_test_res_P7, qval < 0.1)

## Select
sig_genes <- sig_genes[,c("gene_short_name", "pval", "qval")]

#calculate fold change

CMdata_p7 <- CMdata[, pData(CMdata)$condition %in% c("P07␣RFP-","P07␣RFP+")]
# get average expression for each group
P00wt <- as.matrix(rowMeans(as.matrix(CMdata_new[, pData(CMdata_new)$condition %in
    % c("P00␣RFP-")]@assayData$exprs_sfnorm)))



### plotting genexp vs pseudotime
plotgene_exp <- function(gene) { #gene is a string eg "Myh6"

#select pseudotime vecetor
pst <- as.matrix(HSMM_wtsub2@phenoData@data$Pseudotime)
#convert to normalized expression to log2
expv <- log2(as.matrix(HSMM_wtsub2@assayData$exprs_sfnorm[gene,])+1)

#merge pseudotime and expressoin
```

```
p_exp <- as.data.frame(cbind(as.numeric(pst), as.numeric(expv)))
colnames(p_exp) <- c("pst","expv") #set column names

#plot using ggplot2
library(ggplot2)
ggplot(data = p_exp, aes(x= pst, y = expv)) +
  geom_point() +
  geom_smooth() +
  ggtitle(gene) +
  ylab("Log2 Expression") +
  xlab("Pseudotime") +
  title(gene) +
  theme_bw(base_size = 20) +
  theme(panel.grid.major = element_blank(),
        panel.grid.minor = element_blank(),
        panel.background = element_rect(colour = "black", size=4),
        axis.text.x = element_text(colour = "black"),
        axis.text.y = element_text(colour = "black")
  )
}


goi <- "Yap1" #gene of interest
HSMM_p7 <- HSMM[,HSMM@phenoData@data$timepoint == "P07"] #subset to p7
expd <- HSMM_p7@assayData$exprs_sfnorm[goi,] #select the size factor normalized
    data for the gene of interest
rfpstat <- HSMM_p7@phenoData@data$rfp #
timepointstat <- HSMM_p7@phenoData@data$timepoint
df2 <- as.data.frame(cbind(as.numeric(expd),rfpstat,timepointstat))

Yap1-plot <- ggplot(data = df2, aes(x=timepointstat,y=expd,fill=rfpstat))+
  geom_bar(stat = "summary", fun.y="mean", position = position_dodge(1.1), colour
      = "black") +
  stat_summary(fun.data = mean_se,geom="errorbar",width=0.15, position = position_
      dodge(1.1)) +
  theme_classic(base_size = 20) +
  scale_y_continuous(expand=c(0,0))

yexp_rfp <- expd[rfpstat == "RFP+"]
yexp_con <- expd[rfpstat == "RFP-"]

t.test(yexp_con,yexp_rfp)

ggsave("yap1_p7_expression.svg",plot=Yap1_plot,width=4.5,height=5)
```

Appendix III

Abbreviations

Abbreviation	Definition
AAV	adeno-associated virus
ADP	adenosine di-phosphate
AMP	adenosine monophosphate
ATP	adenosine tri-phosphate
bFGF	basic fibroblast growth factor
CASAAV	CRISPR/Cas9-AAV-based somatic mutagenesis
ChIP	chromatin immunoprecipitation
CM	cardiomyocyte
cmKO	conditional mosaic knock out
CTD	calcium transient duration
DAPI	4',6-diamidino-2-phenylindole
DAVID	Database for Annotation Visualization and Integrated Discovery
DNA	deoxyribonucleic acid
dNTP	deoxynucleoside triphosphate
ECM	extracellular matrix
EDTA	ethylenediaminetetraacetic acid
EHT	engineered heart tissue
ERR	estrogen related receptor
ESC	embryonic stem cell
FACS	fluorescent activated cell sorting

fRMA frozen robust multi-array
GC genome copy
GEO gene expression omnibus
GFP green fluorescent protein
GO gene ontology
GRN gene regulatory network
HCN4 hyperpolarization activated cyclic nucleotide gated potassium channel 4
HIF1a hypoxia-inducible factor 1a
IPA ingenuity pathway analysis
iPSC induced pluripotent stem cell
KD-D Kolmogorov-Smirnov distance
KEGG Kyoto Encyclopedia of Genes and Genomes
KHK ketohexokinase
lncRNA long noncoding RNAs
LP-FACS large particle fluorscent activated cell sorting
MACS model-based analysis of ChIP-seq
mcSCRB-seq molecular crowding single cell RNA-barcoding and sequencing
miRNA microRNA
NCBI National Center for Biotechnology Information (NCBI)
NES normalized enrichment score
OCR oxygen consumption rate
PAR-CLIP photoactivatable ribonucleoside-enhanced crosslinking immunoprecipitation
PBS phosphate-buffered saline
PCA principal component analysis
PCR polymerase chain reaction
PDMS polydimethylsiloxane
PGC1a PPAR gamma coactivator 1 alpha
PPAR Peroxisome proliferator activation receptor
PSC pluripotent stem cell

PSC-CM pluripotent stem cell-derived cardiomyocyte

qPCR quantitative polymerase chain reaction

RFP red fluorescent protein

RNA ribonucleic acid

ROS reactive oxygen species

RPM Revolutions Per Minute

SERCA sarco/endoplasmi reticulum calcium ATPase

SF3B2 splicing factor 3 B2

siRNA small interferring ribonucleic acid

snRNP small nuclear ribonucleoprotein

SRA sequence read archive

SRF serum response factor

T3 tri-iodothryonine

TAC transverse aortic constriction

TEM transmisison electron microscopy

t-SNE t-distributed stochastic neighbor embedding

UMAP uniform manifold approximation and projection for dimension reduction

UMI unique molecular identifier

VEGF vascular endothelial growth factor

WGA wheat germ agglutinin

WGCNA weighted gene co-expression analysis

WT wild type

YAP YES-associated protein

3D three dimensional

Sean Murphy

521 Saint Paul St Baltimore, MD 21202
smurph50@jhu.edu | 206-724-2818

EDUCATION

Johns Hopkins University, Baltimore, MD — Anticipated Nov 2020
PhD Biomedical Engineering — GPA: 4.0

University of Washington, Seattle, WA — Graduated June 2015
B.S. Bioengineering, B.A. Economics, Minor in Applied Mathematics, *Magna Cum Laude* — GPA: 3.84

Inglemoor High School, Kenmore, WA — Graduated June 2011
International Baccalaureate Diploma — GPA: 3.97

RESEARCH EXPERIENCE

Heart Generation and Regeneration Lab, Johns Hopkins University — Baltimore, MD
Graduate Research Assistant, PI: Dr. Chulan Kwon — Jan 2016- Present

- Designed a research study to predict key transcriptional regulators of cardiomyocyte maturation and test their efficacy in promoting engineered heart tissue function.
- Analyzed single cell RNA-seq using custom pipeline and R to build a temporal transcriptome map of mouse heart development.
- Generated a genetic engineering system using adeno-associated virus to achieve a conditional mosaic knockout so to understand the cell autonomous role of PGC-1a.
- Collaborated with researchers at UCSD to analyze ChIP-seq and ATAC-seq of fibroblast reprogramming into cardiomyocytes, yielding insights into reprogramming mechanism.
- Trained and supervised undergraduate students in cell culture, flow cytometry, and coding.

Cardiac Biosystems Lab, Johns Hopkins University — Baltimore, MD
Graduate Research Assistant, PI: Dr. Leslie Tung — Aug 2015-Dec 2015

- Synthesized decellularizied porcine ECM hydrogel for stem cell-derived cardiomyocyte culture, providing a consistent method for generating 3D culture constructs.
- Wrote a grant proposal to fund graduate studies, allowing me to devote more time to higher risk projects that were not a central focus of the lab.

Laflamme Lab, University of Washington — Seattle, WA
Undergraduate Researcher, PI: Dr. Michael Laflamme — Apr 2012-Jun 2015

- Developed immunohistochemistry protocols for GFP in paraffin-embedded tissue samples to visualize distribution of cell therapy graft in rat hearts.
- Localized Ribonucleotide Reductase in human pluripotent stem cell-derived cardiomyocytes grafted into rat hearts using immunostaining.
- Identified off-target effects of antiarrhythmic peptide rotigaptide on hPSC-CMs, showing viability of peptide to improve excitation contraction coupling of stem cell graft.

WORK EXPERIENCE

Seattle Genetics — Bothell, WA
Chemistry Research Intern — Jun 2014 – Sep 2014

- Adapted protocol to magnetically isolate endosomes and lysosomes to characterize tumor microenvironment.
- Evaluated cytotoxicity and intracellular drug concentration of antibody drug conjugates across multiple cell lines and cancer indications.
- Investigated mechanism of action of novel antibody drug conjugates.

Knotis Jun 2012 – Sep 2012
Business Development Intern Seattle, WA

- Worked at Seattle tech start up to improve product design of online small business tools and presented mobile strategy to leadership team.
- Designed marketing materials to increase client use of product following one-on-one meetings with local small businesses.

Microsoft Aug 2010 – Aug 2011
Intern Redmond, WA

- Developed metric scorecards, interpreting business intelligence to management.
- Prepared and presented a competitive analysis presentation to the consumer engagement team.

TEACHING EXPERIENCE

ViaX Oct 2018 – Present
Instructor of Regenerative Medicine

Systems Bioengineering II Lab Course (BME 580.424) Jan 2019 – May 2019
Head Teaching Assistant

Cell and Tissue Engineering Lab Course (BME 580.451) Aug 2017 – Dec 2017
Teaching Assistant

HONORS

Turock Award – Travel Scholarship	2019
American Heart Association Pre-Doctoral Fellowship	2018
First Place – T Rowe Price Biotech Stock Pitch Competition	2017
NSF Graduate Research Fellowship	2016
Dean's List	2011-2015
Outstanding Scholar in Economics Award	2015
Levinson Emerging Scholars Award	2014
Mary Gates Research Scholarship	2014
Phi Beta Kappa	2014
Finalist at Rice University National Undergraduate Global Health Design Competition	2014
William P. Wood Bioengineering Scholarship	2013
Mary Gates Research Scholarship	2013
Bruno Strauss Business and Engineering Scholarship	2012
Mac Williams IB Student of the Year	2011
Washington Scholar	2011
Knopp Aerospace Scholarship	2011
Rusty Young Community Leader Scholarship	2011
Seattle ACE Engineering Scholarship	2011
First Place in DECA International Business Case Study Competition	2010
Eagle Scout	2010

PUBLICATIONS

Sean Murphy, Sandeep Kambhampati, Suraj Kannan, Hideki Uosaki, Chulan Kwon. "Multi-organ in vivo maturation comparison identifies transcriptomic similarities." In Preparation. 2020.

Maria Missinato, **Sean Murphy**, Anais Kervadec, Michaela Lynott, Mafalda Loreti, Michael Yu, Suraj Kannan, Christopher Lee, Prashila Amatya, Chung-Teng Huang, Chulan Kwon, Pier Lorenzo Puri, Li Quan, Peter Adams, Alessandra Sacco, Peter Andersen, Alexandre Colas. "Transcription factor-mediated control of barriers to cell fate reprogramming." In preparation. 2020.

Sean Murphy, Matthew Miyamoto, Anais Kervadec, Suraj Kannan, Sandeep Kambhampati, Brian Lin, Emmanouil Tampakakis, Sam Paek, Peter Andersen, Dong Lee, Steven An, David Kass, Hideki Uosaki, Alexandre Colas, Chulan Kwon. "PGC1/PPAR drive cardiomyocyte maturation through regulation of Yap1 and SF3B2". *Biorxiv.* 2020.

Kannan S, Miyamoto M, B Lin, Zhu R, **Murphy S**, Kass D, Andersen P, Kwon C. "Large particle fluorescence-activated cell sorting enables high quality single cell RNA-sequencing and functional analysis of adult cardiomyocytes." *Circulation Research.* 2019. 125: 567–569.

Andersen P, Tampakakis E, Jimenez D, Kannan S, Miyamoto M, Shin HK, **Murphy S**, Sulistio E, Chelko S, Kwon C. "Precardiac organoids form two heart fields via Bmp/Wnt signaling." *Nature Communications*. 2018. 9(1), 3140.

Cho GS, Lee DI, Tampakakis E, **Murphy SA**, Andersen P, Chelko S, Chakir K, Hong I, Seo K, Chen HV, Chen X, Basso C, Houser SR, Tomaselli GF, O'Rourke B, Judge DP, Kass DA, Kwon C. "Neonatal transplantation confers maturation of PSC-derived cardiomyocytes conducive to modeling cardiomyopathy." *Cell Reports*. 2017. 18(2):571-582.

Lundy SD, **Murphy SA**, Dupras SK, Dai J, Murry CE, Laflamme MA, Regnier M. "Cell-based delivery of dATP via gap junctions enhances cardiac contractility." *Journal of Molecular and Cellular Cardiology*. 2014. 72: 350-9.

PRESENTATIONS AND POSTERS

Sean Murphy. "The role of PGC1a/PPAR in in vivo heart maturation and applications to stem cell therapy." Institute for Cardioscience at Johns Hopkins University. November 2019.

Murphy SA, Sandeep Kambhampati, Chulan Kwon. "Profiling microRNA expression during organ maturation." Weinstein Cardiovascular Development and Regeneration Conference in Indianapolis, IN. May 2019.

Sean Murphy, Suraj Kannan, Chulan Kwon. "Overcoming obstacles toward heart regeneration: maturing stem cells into cardiac tissue." Partnering Towards Discovery Initiative at Johns Hopkins University. March 2019.

Murphy SA, Miyamoto MK, Kannan S, Andersen P, Uosaki, H, Kwon C. "PPAR/PGC1a activation promotes pluripotent stem cell-derived cardiomyocyte maturation." Weinstein Cardiovascular Development and Regeneration Conference in Nara, Japan. May 2018.

Andersen, Peter, Dennisse Jimenez-Cyrus, Stephen P. Chelko, Suraj Kannan, Emmanouil Tampakakis, Amir Saberi, **Sean Murphy**, Matthew Miyamoto, and Chulan Kwon. "Heart Fields Are Induced by Coordinated Activity of Wnt and Bmp Signaling and Identified by

CD184 and EphA2 in PSC-Derived Organoids." Circulation 136, no. suppl1 (2017): A24063-A24063.

Kannan S, Saberi A, **Murphy SA**, Kwon C. “De novo reconstructed developmental trajectory of embryonic and post-natal hearts.”” Weinstein Cardiovascular Development and Regeneration Conference. May 2017.

Murphy SA, Filice D, Zhu WZ, MA Laflamme. “Rotigaptide modulation of human pluripotent stem cell-derived cardiomyocyte maturation and proliferation.” National Council on Undergraduate Research Conference, April 2015.

Murphy SA, SD Lundy, M Regnier, MA Laflamme. “Quantification of Ribonucleotide Reductase in human embryonic stem cell derived cardiomyocyte cell therapy.” University of Washington Undergraduate Research Symposium, May 2013.

SKILLS

Laboratory: Single cell RNA seq, ChIP-seq, scATAC-Seq, qPCR, stem cell culture, flow cytometry, FACS, tissue culture, mouse colony management, western blotting, fluorescent microscopy, paraffin embedded histology, RNA isolation, signal processing, liquid chromatography-mass spectrometry, hydrogel synthesis, tissue decellularization.

Computer: Proficient in R, Python, Bash
Familiar with LabView, ImageJ, IPA, Matlab, Solidworks, COMSOL, IGV

LEADERSHIP, SERVICE AND ACTIVITIES

Johns Hopkins Ultimate, *Coach* 2019 – Present
- Led competitive ultimate team in training and tournament play.

JH Biotech Investment Group 2017 – Present
- Analyzed biotech companies and attended seminars on biotech investment.

Thread, *Head of Family* 2015 – Present
- Mentored and tutored one student from an urban Baltimore high school.

P-TECH *Steering Committee* 2016 – Present
- Designed mentor program for advanced career training program.

Modern Board Game Society, *President* 2016 – Present
- Led student group that organizes events to play strategic board games.

BME PhD Council, *Vice President of Communications* 2016 – 2017
- Manage communications for the BME PhD student organization.

Graduate Student Association, *BME representative* 2015 – 2017
- Served as liaison between BME PhD Council and JHU School of Medicine Graduate Student Association.

Book Thing of Baltimore, *Volunteer* 2015 – 2016
- Organized used books for distribution to the Baltimore community.

Bioengineers Without Borders, *Vice President and Project Lead* 2011 – 2015
- Developed ultrasound hydration monitor for use in low resource settings.
- Finalist at Rice 360 Institute for Global Health Technology Design Competition.

STEM Mentors, *Co-founder and President* 2013 – 2015

- Identified need for and built STEM mentoring program at Seattle area high schools
- Planned collaborative design activities and presentations on STEM fields.

Roots Youth Shelter, *Volunteer* 2013 – 2015

- 100+ hours of volunteer work in day-to-day operations at local youth shelter.

Engineering Ambassadors, *K-12 Outreach Coordinator* 2012 – 2015

- Set up outreach events and represented UW College of Engineering at local events.

Bioengineering Outreach 2013 – 2015

- Organized and contributed to outreach events in Cardiovascular Engineering module at Seattle area high schools to generate interest in bioengineering careers.

Vita

Sean was born November 21, 1992 in Los Angeles, California to Michael and Annette Murphy. He graduated from Inglemoor High School in Kenmore, Washington in 2011 with an International Baccalaureate Diploma. He earned his Bachelor of Science in Biomedical Engineering with honors and Bachelor of Arts in Economics at the University of Washington in 2015. He worked in the lab of Dr. Michael Laflamme on the use of stem cell derived cardiomyocytes for cell therapy. He then enrolled in the Biomedical Engineering PhD program at Johns Hopkins University in 2015. He rotated in the lab of Dr. Leslie Tung and worked in the lab of Dr. Chulan Kwon. He was supported by a National Science Foundation Graduate Research Fellowship and an American Heart Association predoctoral fellowship.